

**PERFORMANCE ANALYSIS OF THE
CARRIER-SENSE MULTIPLE ACCESS
PROTOCOL FOR FUTURE GENERATION
WIRELESS NETWORKS**

A DISSERTATION SUBMITTED TO
THE DEPARTMENT OF ELECTRICAL AND ELECTRONICS
ENGINEERING
AND THE GRADUATE SCHOOL OF ENGINEERING AND SCIENCE
OF BILKENT UNIVERSITY
IN PARTIAL FULFILLMENT OF THE REQUIREMENTS
FOR THE DEGREE OF
DOCTOR OF PHILOSOPHY

By
Mehmet Köseoğlu
June, 2013

I certify that I have read this thesis and that in my opinion it is fully adequate, in scope and in quality, as a dissertation for the degree of Doctor of Philosophy.

Prof. Dr. Ezhan KARAŞAN(Advisor)

I certify that I have read this thesis and that in my opinion it is fully adequate, in scope and in quality, as a dissertation for the degree of Doctor of Philosophy.

Assoc. Prof. Dr. Nail AKAR

I certify that I have read this thesis and that in my opinion it is fully adequate, in scope and in quality, as a dissertation for the degree of Doctor of Philosophy.

Assoc. Prof. Dr. İbrahim KÖRPEOĞLU

I certify that I have read this thesis and that in my opinion it is fully adequate, in scope and in quality, as a dissertation for the degree of Doctor of Philosophy.

Prof. Dr. Tolga DUMAN

I certify that I have read this thesis and that in my opinion it is fully adequate, in scope and in quality, as a dissertation for the degree of Doctor of Philosophy.

Assoc. Prof. Dr. Murat ALANYALI

Approved for the Graduate School of Engineering and Science:

Prof. Dr. Levent Onural
Director of the Graduate School

ABSTRACT

PERFORMANCE ANALYSIS OF THE CARRIER-SENSE MULTIPLE ACCESS PROTOCOL FOR FUTURE GENERATION WIRELESS NETWORKS

Mehmet Köseoğlu

PhD. in Electrical and Electronics Engineering

Supervisor: Prof. Dr. Ezhan KARAŞAN

June, 2013

Variants of the carrier-sense multiple access (CSMA) protocol has been employed in many communications protocols such as the IEEE 802.11 and Ethernet standards. CSMA based medium access control (MAC) mechanisms have been recently proposed for other communications scenarios such as sensor networks and acoustical underwater networks. Despite its widespread use, the performance of the CSMA protocol is not well-studied from the perspective of these newly encountered networking scenarios. We here investigate the performance of the CSMA protocol from the point of three different aspects: throughput in networks with large propagation delay, short-term fairness for delay sensitive applications in large networks and energy efficiency-throughput trade-off in networks with battery operated devices.

Firstly, we investigate the performance of the CSMA protocol for channels with large propagation delay. Such channels are recently encountered in underwater acoustic networks and in terrestrial wireless networks covering larger areas. However, a mathematical model of CSMA performance in such networks is not known. We propose a semi-Markov model for a 2-node CSMA channel and then extend this model for arbitrary number of users. Using this model, we obtain the optimum symmetric probing rate that achieves the maximum network throughput as a function of the average propagation delay, \bar{d} , and the number of nodes sharing the channel, N . The proposed model predicts that the total capacity decreases with \bar{d}^{-1} as N goes to infinity when all nodes probe the channel at the optimum rate. The optimum probing rate for each node decreases with $1/N$ and the total optimum probing rate decreases faster than \bar{d}^{-1} as N goes to infinity.

Secondly, we investigate whether the short-term fairness of a large CSMA

network degrades with the network size and density. Our results suggest that (a) the throughput region that can be achieved within the acceptable limits of short-term fairness reduces as the number of contending neighboring nodes increases for random regular conflict graphs, (b) short-term fair capacity weakly depends on the network size for a random regular conflict graph but a stronger dependence is observed for a grid topology. We also present related results from the statistical physics literature on long-range correlations in large systems and point out the relation between these results and short-term fairness of CSMA systems.

Thirdly, we investigate the energy efficiency of a CSMA network proposing a model for the energy consumption of a node as a function of its throughput. We show that operating the CSMA network at a very high or at a very low throughput is energy inefficient because of increasing carrier-sensing and sleeping costs, respectively. Achieving a balance between these two opposite operating regimes, we derive the energy-optimum carrier-sensing rate and the energy-optimum throughput which maximize the number of transmitted bits for a given energy budget. For the single-hop case, we show that the energy-optimum total throughput increases as the number of nodes sharing the channel increases. For the multi-hop case, we show that the energy-optimum throughput decreases as the degree of the conflict graph of the network increases. For both cases, the energy-optimum throughput reduces as the power required for carrier-sensing increases. The energy-optimum throughput is also shown to be substantially lower than the maximum throughput and the gap increases as the degree of the conflict graph increases for multi-hop networks.

Keywords: Wireless Networking, Wireless Multiple Access, Carrier-sense Multiple Access, Energy Efficiency, Underwater Networks, Short-term Fairness, Propagation Delay.

ÖZET

TAŞIYICI DİNLEYEN ÇOKLU ERİŞİM PROTOKOLÜNÜN GELECEK NESİL KABLOSUZ AĞLAR İÇİN PERFORMANS ANALİZİ

Mehmet Köseoğlu

Elektrik ve Elektronik Mühendisliği, Doktora

Tez Yöneticisi: Prof. Dr. Ezhan KARAŞAN

Haziran, 2013

Taşıyıcı dinleyen çoklu erişim (CSMA) protokolünün farklı biçimleri IEEE 802.11 ve Ethernet standardı gibi pek çok haberleşme protokolünde kullanılmıştır. Bunlara ek olarak, son zamanlarda, CSMA tabanlı çoklu erişim kontrolü mekanizmalarının algılama ağları ve akustik su altı ağları gibi farklı haberleşme senaryolarında kullanılması önerilmiştir. Günümüze kadar olan yaygın kullanımına rağmen, CSMA protokolünün performansı bu yeni karşılaşılan ağ senaryoları açısından derinlemesine incelenmemiştir. Biz bu tezde CSMA protokolünün performansını üç farklı açıdan inceliyoruz: yüksek yayılım gecikmeli ağlarda veri iletim performansı, büyük ağlarda gecikmelere hassas uygulamalar açısından kısa dönemli denkserlik ve pil ile çalışan cihazlar açısından veri iletim hızı ile enerji verimliliği arasındaki ödünleşim.

İlk olarak, CSMA protokolünün performansı yüksek yayılım gecikmeli ağlar açısından incelenmiştir. Son zamanlarda bu tip kanallarla su altı akustik ağlarda ve geniş alanları kapsayan yer üstü kablosuz ağlarda karşılaşılmaktadır. Fakat, bu tip kanallarda CSMA performansının matematiksel modeli bilinmemektedir. Biz önce iki birimli bir CSMA kanalı için bir yarı-Markov modeli önerip daha sonra bu modeli her hangi sayıda birim için genişlettik. Bu modeli kullanarak, maksimum ağ veri iletim hızını ortalama yayılım gecikmesinin, \bar{d} , ve ağdaki birim sayısının, N , bir fonksiyonu olarak elde ettik. Önerdiğimiz model N sonsuza giderken toplam ağ kapasitesinin ile azaldığını göstermektedir. Her birim için optimum yoklama kanal sıklığı $1/N$ ile azalmakta ve N sonsuza giderken toplam optimum yoklama hızı \bar{d}^{-1} den hızlı azalmaktadır.

İkinci olarak, büyük bir CSMA ağının kısa dönemli denkserliğinin ağ büyüklüğü ve yoğunluğuyla azalıp azalmadığını inceliyoruz. Elde ettiğimiz

sonuçlar şöyle sıralanabilir: (a) kısa dönemli denkserliğin kabul edilebilir sınırları içerisinde kalarak elde edilebilen maksimum veri hızı (kısa dönemli denkser kapasite) bir birimin komşularının sayısının artmasıyla azalmaktadır. (b) kısa dönemli denkser kapasite rastgele bir ağ grafiği için ağ büyüklüğüne zayıf bir şekilde bağlıyken ızgara grafiğinde daha kuvvetli bir bağlılık gözlenmektedir. Bunlara ek olarak istatistiksel fizik literatüründen büyük sistemlerde uzun mesafeli ilintiler üzerine olan ilgili sonuçları sunduk ve bu sonuçlarla CSMA sistemlerinin kısa dönemli denkserliği arasındaki ilişkiye işaret ettik.

Üçüncü olarak, bir CSMA ağının enerji verimliliğini bir birimin enerji harcamasını veri hızının bir fonksiyonu olarak modelleyerek inceledik. CSMA ağını çok yüksek ya da çok düşük veri hızlarında işletmenin artan kanal dinleme veya uyku maliyetleri yüzünden enerji açısından verimsiz olduğunu gösterdik. Bu iki zıt durum arasında dengeyi bularak sınırlı bir enerji bütçesi için gönderilen bit sayısını en büyük yapan enerji-optimum kanal dinleme hızını ve enerji-optimum veri hızını türettik. Tek atlamalı durum için, enerji-optimum toplam veri hızının kanalı paylaşan birim sayısı ile beraber arttığını gösterdik. Çok atlamalı durum için, enerji-optimum veri hızının ağın çakışma grafiğinin derecesiyle azaldığını gösterdik. Her iki durumda da enerji-optimum kanal dinleme için gereken güç miktarı arttıkça azalmaktadır. Ayrıca, enerji-optimum veri hızının maksimum veri hızına kıyasla oldukça küçük olduğu ve çok atlamalı durumda bu farkın çakışma grafiğinin derecesi arttıkça arttığı gösterilmiştir.

Anahtar sözcükler: Kablosuz ağlar, kablosuz çoklu erişim, taşıyıcı dinleyen çoklu erişim, enerji verimliliği, su altı ağları, kısa dönemli denkserlik, yayılım gecikmesi.

Acknowledgement

I would like to express my sincere thanks to my thesis advisor Prof. Ezhan Karasan not only for his academic guidance but also for being a mentor for all aspects of the graduate student life. He was genuinely interested in the problems that I encountered and was always eager to help during the nine years that we have worked together. I would especially like to express my gratitude to him for his understanding during the course of my father's illness.

I would like to thank Prof. Nail Akar and Prof. Ibrahim Korpeoglu for accepting to be a member of my thesis monitoring committee and for their comments and recommendations throughout my studies. I would also like to thank Prof. Tolga Duman and Prof. Murat Alanyali for accepting to read and comment on this thesis. I would especially like to thank Prof. Murat Alanyali for his suggestions at the beginning of my PhD studies and for hosting me at the Boston University during the summer of 2010.

I would like to thank my office mate Ayca Ozcelikkale for endless discussions about graduate life and academia in general.

I would also especially like to thank Kivanc Kose, Alican Bozkurt, Asli Unlugedik and Alexander Suhre for their friendship, especially at lunch.

Thanks to my friends Ahmet Serdar Tan, Gokhan Bora Esmer, Yigitcan Eryaman, Namik Sengezer, Avsar Polat Ay, Sami Ezercan, Bilge Kasli, Elif Aydogdu, Volkan Hunerli, Ali Ozgur Yontem, Erdem Ulusoy and Erdem Sahin for their friendship and support.

I would also like to thank my parents for their encouragement and my little daughter Asli for changing my life forever.

Last but not least, I would like to thank my dear wife Hande for her support during my PhD studies. Without her encouragement and love, my PhD life would be much less bearable.

Contents

1	Introduction	1
1.1	Contributions	6
2	Literature Review	9
2.1	An overview of random access protocols	9
2.2	Performance of Random Access under Large Propagation Delay .	11
2.2.1	Outdoor 802.11 networks	11
2.2.2	Underwater Acoustic Networks	12
2.3	Fairness of Large Scale CSMA Systems	15
2.3.1	Long-term fairness	16
2.3.2	Short-term Fairness	19
2.4	Energy Efficiency of the CSMA Protocol	21
2.4.1	Sources of Energy Inefficiency	22
2.4.2	Energy efficient random access protocols	22

3	Throughput Modeling of Single Hop CSMA Networks with Non-Negligible Propagation Delay	25
3.1	Scenario Description	27
3.2	Semi-Markov Model for the 2-Node CSMA channel	28
3.2.1	State Definitions	28
3.2.2	Accuracy of the Model	37
3.2.3	The Capacity Region of the CSMA Channel for $N = 2$. . .	38
3.3	Asymptotic Capacity and Optimum Probing Rate	41
3.3.1	Throughput Reduction Caused by a Single Neighbor . . .	42
3.3.2	Derivation of the Asymptotic Capacity and Optimum Probing Rate	44
3.4	Improving Short-term Fairness in a CSMA channel with non-negligible propagation delay	47
3.5	Comparison of the proposed CSMA model with IEEE 802.11b channel access	50
3.6	Conclusions	53
4	Effect of Network Density and Size on the Short-term Fairness Performance of CSMA Systems	55
4.1	System Model and Studied Topologies	57
4.1.1	System Model	57
4.1.2	Studied Conflict Graph Topologies	58
4.2	Short-term Fairness Metrics	59

4.2.1	Short-term Fairness Horizon	59
4.2.2	Short-term Fair Capacity Region	60
4.2.3	Number of successive transmissions	60
4.3	Mathematical Analysis for a Tree	61
4.4	Simulation Study	63
4.4.1	Simulation Method	64
4.4.2	Tree Topology	65
4.4.3	Grid Topology	70
4.4.4	Random Topology	71
4.4.5	Comparison of Different Topologies	73
4.5	Practical Implications on the Deployment of Wi-Fi Networks	75
4.6	Analogy with the hard-core model	79
4.6.1	Uniqueness of a Gibbs Measure	80
4.6.2	Reconstruction Threshold	81
4.6.3	Short-term Fairness and Mixing Time	82
4.6.4	Simulations	82
4.7	Conclusions	83
5	Energy-optimum Carrier Sensing Rate and Throughput in CSMA-based Wireless Networks	85
5.1	Single-hop Network	88

5.1.1	System Model	89
5.1.2	Energy Consumption Model	90
5.2	Multi-hop Network	92
5.2.1	System Model	92
5.2.2	Energy Consumption Model	93
5.3	Bounds on the energy-optimum throughput and maximum throughput	96
5.3.1	Lower bounds on the maximum throughput, σ_d^{\max}	97
5.3.2	Upper bound on the maximum throughput, σ_d^{\max}	97
5.3.3	Lower bound on the energy-optimum throughput, σ_d^*	98
5.3.4	Upper bound on the energy-optimum throughput, σ_d^*	98
5.3.5	Lower bound on $\sigma_d^*/\sigma_d^{\max}$	99
5.3.6	Upper bound on $\sigma_d^*/\sigma_d^{\max}$	100
5.4	Numerical Results	100
5.4.1	Single-hop Network	100
5.4.2	Multi-hop Network	103
5.4.3	Bounds on the σ_d^{\max} and σ_d^* for the multi-hop network.	106
5.5	Conclusions	109
6	Conclusions	112

List of Figures

3.1	The state diagram for the semi-Markov model.	29
3.2	(a) Idle channel period after a successful transmission. Duration of this period is $2d$. (b) If a transmission starts in this idle period, it continues free from collisions for a duration of a and enters into a vulnerable period. The duration a equals to the starting transmission time after the successful transmission.	31
3.3	(a) Busy and idle channel periods after an unsuccessful transmission. (b) If a transmission starts in the idle period, it continues free from collisions for a while and enters into a vulnerable period.	33
3.4	Performance of the semi-Markov model and the simplified model as R_1 changes for $d = 0.4$	38
3.5	(a) The capacity region of a CSMA channel with two-nodes for different propagation delays. (b) Probing rates of nodes required to achieve the limits of the capacity region.	40
3.6	Total throughput of two nodes sharing a channel as the propagation delay increases for different $R_1 = R_2 = R$ values.	40
3.7	$g_1(R_1, R_2, d)$ with changing R_1 and R_2	42
3.8	Comparison of the total network throughput as a function of \bar{d} for different values of N along with the lower and upper bounds.	46

3.9	The capacity of the network as \bar{d} increases. The asymptotic capacity is plotted using (3.42).	47
3.10	Total optimum probing rate in the network as \bar{d} increases. Asymptotic total optimum probing rate is plotted using (3.40).	48
3.11	Maximum throughput achieved by the back-off scheme.	50
3.12	Mean number of successive transmission achieved by the back-off scheme.	50
3.13	Throughput of the IEEE 802.11 MAC and the optimum throughput of the pure CSMA model.	52
3.14	Mean waiting times between transmissions of the IEEE 802.11 MAC and the pure CSMA model operating at the optimum probing rate.	53
4.1	Studied Topologies. (a) The tree topology that we study. Each node has b children except leaf nodes. (b) The N by N grid. (c) A sample regular random topology with a degree of 3.	58
4.2	States of nodes in a line topology. Node 0 is transmitting, Node -1 and 1 are therefore idle and Node -2 and 2 are active with probability p	62
4.3	Short-term fairness horizon of the tree topology with different degrees. (a) as the probing rate increases (b) as the average throughput increases. Short-term fairness thresholds of $Th=50$ and 100 transmissions per node are also shown as horizontal dashed lines.	66
4.4	Short-term fair capacity of the tree topology as the degree increases.	67
4.5	Short-term fairness horizon of the tree topology as the height of the tree increases. Internal nodes in all trees have $d = 4$	68

4.6	Mean number of successive transmissions as the average throughput increases. Dashed lines plot the results of the proposed model.	69
4.7	Short-term fairness horizon of the grid topology for three different dimensions.	70
4.8	Average short-term fairness horizon of randomly generated topologies with different degrees as the average throughput increases. Short-term fairness thresholds of Th=50 and 100 transmissions per node are also shown as horizontal dashed lines.	71
4.9	Short-term fair capacity of the randomly generated topologies as the degree increases with short-term fairness thresholds of Th=50 and 100.	72
4.10	Average short-term fairness horizons for the randomly generated topologies with different network sizes.	73
4.11	Short-term fairness horizons for the tree, grid and random topologies as the throughput increases. All three topologies have $d = 4$.	74
4.12	Short-term fair capacities for tree and random topologies as the degree increases with short-term fairness threshold Th=50.	75
4.13	A 5 km by 5 km area is covered by Wi-Fi access points which are located in a mesh pattern where (a) $l = 300m$ and (b) $l = 450m$. The interference relationship between nodes are denoted by lines between interfering nodes.	77
4.14	Short-term fairness horizon of the simulated Wi-Fi deployment for different internodal distances. Higher density of deployment results in higher short-term fairness horizon at the same throughput.	78
4.15	Coverage of the simulated Wi-Fi deployment for different internodal distances.	78

4.16	The uniqueness threshold, non-reconstruction bound and the short-term fairness horizon for tree topologies with (a) $d = 4$ (b) $d = 10$ (c) $d = 18$	83
5.1	A sample timeline of two nodes in a single-hop scenario.	88
5.2	Markov chain for the single-hop case. The stationary probabilities of the states except the initial state gives the throughput of each node.	88
5.3	A wireless network topology and the conflict graph of its links. Lines with arrows indicate the links in the network topology and dashed lines indicate that two nodes are within the interference range of each other without having a link between them.	93
5.4	Energy consumption per node in the single-hop network. (a) Total energy consumption (b) Energy consumed while sleeping (c) Energy consumed while carrier sensing	101
5.5	Change of energy-optimum total throughput as the number of nodes increases for the single-hop network.	102
5.6	Energy-optimum carrier-sensing rate per node as the number of nodes increases for the single-hop network.	102
5.7	Energy-optimum carrier-sensing rate per node as P_c/P_s increases for the single-hop network.	103
5.8	Energy-optimum total throughput as P_c/P_s increases for the single-hop network.	104
5.9	Relationship between the throughput and the carrier sensing rate for tree conflict graphs and random regular conflict graphs with $d = 2, 3$ and 4.	105

5.10	Energy consumption per node in the multi-hop network. (a) Total energy consumption (b) Energy consumed while sleeping (c) Energy consumed while carrier sensing	105
5.11	The energy-optimum carrier sensing rate as a function of $\frac{P_c}{P_s}$ for the multi-hop network.	106
5.12	The energy-optimum throughput as a function of $\frac{P_c}{P_s}$ for the multi-hop network.	107
5.13	Maximum throughput as a function of d for the multi-hop network for a) $\frac{t_c}{t_l} \approx 0.02$ b) $\frac{t_c}{t_l} = 0.001$	108
5.14	Energy-optimum throughput as a function of d for the multi-hop network for a) $\frac{t_c}{t_l} \approx 0.02$ b) $\frac{t_c}{t_l} = 0.001$	108
5.15	Ratio of energy-optimum throughput to maximum throughput as a function of d for the multi-hop network for a) $\frac{t_c}{t_l} \approx 0.02$ b) $\frac{t_c}{t_l} = 0.001$	109

List of Tables

5.1 List of Notations	111
---------------------------------	-----

Chapter 1

Introduction

The most basic method of providing communication between two nodes is to deploy a point-to-point link between the nodes such as connecting them with a cable. In point-to-point channels, there is no interference between nodes and resource sharing is not required. Establishing point-to-point links, however, are not always possible. For example, wireless medium is naturally a broadcast channel where transmissions of nearby nodes interfere with each other. Even for a wired topology, deploying new links when a node is added is not economical.

When a shared transmission medium is used, the channel has to be divided between users so that the interference is prevented. The policies that determine the rules of channel sharing is called as the multiple access methods. There are two main types of multiple access methods: Reservation-based multiple access schemes and random multiple access schemes.

Reservation-based multiple access methods *channelize* the transmission medium over various dimensions and allocate a separate channel to each user. This allocation can be done by a fixed assignment of frequencies (FDMA), time slots (TDMA) or orthogonal codes (OFDM) to different nodes. These methods provide low access delay to users and are efficient when the users have stable traffic demands. On the other hand, these methods are not scalable: If the number of users increases too much, the number of channels may not be enough. Moreover,

these methods inefficiently utilize the channel when the user demand is low or fluctuating.

Another way of sharing the channel between nodes is to use random access methods where the nodes do not access the channel in a particular order. The channel is shared between nodes in the time domain but not in a structured manner. Instead, the nodes attempt to access the channel at random points in time. Depending on the success of the transmission attempt, nodes determine the timing of their next channel access attempt.

Random access is suitable for scalable and distributed operation. In contrast to fixed channel assignment mechanisms, addition of new nodes are easier and remaining nodes can adapt to the addition of new nodes. The random access mechanism can be run without a centralized controller in contrast to reservation-based assignment schemes. Also, random access mechanisms multiplex the traffic of different users so that temporal variations in the traffic patterns of individual nodes do not result in inefficiency.

The earliest form of the random access mechanism is the ALOHA protocol [1] which was proposed to enable communications of terminals located in the different islands of Hawaii with a central computer. In the ALOHA protocol, the nodes transmit whenever they have a data to transmit. If transmissions of different terminals collide which happens when two terminals transmit at the same time, the terminals retransmit after a random amount of time. In the ALOHA protocol, probability of collisions is very high due to the lack of any collision prevention mechanism.

Carrier Sense Multiple Access (CSMA) [2] is a simple improvement over the ALOHA protocol. In this protocol, the nodes listen to the channel before transmitting and they abstain from transmitting if the channel is busy. With the addition of the carrier sensing, collision probability is reduced in comparison to ALOHA. CSMA is the basis of many currently used wireless protocols such as the IEEE 802.11 and 802.15.4 standards and several MAC proposals for sensor networks such as BMAC [3].

CSMA is also proposed for newer communication protocols due to its simple and distributed nature, however, its performance has not been investigated for several previously unconsidered scenarios. We investigate three of these new scenarios in this thesis which may be critical for future wireless networks. First, we analyze the effect of non-negligible propagation delay on the performance of the CSMA protocol. Such channels are typically encountered in underwater acoustic networks and large terrestrial networks. Second, we analyze the self-organization phenomenon which appears in large-scale CSMA networks. Such networks form naturally due to high penetration of wireless network in residential areas and self-organization in such networks may dramatically reduce the quality of service in terms of short-term fairness. Third, we analyze the energy consumption of the CSMA protocol at various traffic loads. This analysis is important due to the widespread use battery powered wireless devices and environmental considerations.

The first issue that we investigate is the performance of CSMA in channels with large propagation delay. Due to the propagation delay of wireless signals, a node hears the transmission of another node with some delay so transmissions of these two nodes may collide in spite of using carrier-sensing. Propagation delay is not considered as a significant problem in the current wireless configurations because it is negligible in comparison to the transmission times. For example, propagation delay in a typical indoor WiFi network is smaller than 1% of the packet transmission duration.

On the other hand, larger propagation delays should be considered in the performance modeling of future wireless networks. First of all, there is an emerging need for underwater acoustic networks [4] which experience very large propagation delays due to low propagation speed of acoustic waves. The effect of the propagation delay on the underwater acoustic networks is dramatic: The propagation delay of a packet over a distance of 1 km is 670 ms which is larger than the transmission delay of a 2000 byte packet at rates exceeding 24 Kbps. So, propagation delay must be a major consideration for terrestrial wireless networks covering large distances and for underwater networks even for short distances and low transmission rates.

Second, new high-speed wireless networks are developed for covering larger areas to provide Internet access in rural regions. For example, IEEE 802.22 standard [5] envisions a coverage distance of 100 km. The propagation delay of radio waves over a distance of 100 km equals to $334 \mu s$ which is larger than the transmission delay of a 2000 byte packet at rates exceeding 48 Mbps. Although the IEEE 802.22 standard specifies a centralized access mechanism, propagation delay has to be taken into account if future regional wireless networks using a random access based MAC scheme are to be deployed.

At high propagation delays, the channel access rate of the nodes in a CSMA network becomes crucial. If the nodes attempt to access the channel very frequently, collision probability is increased. On the other hand, attempting to access the channel rarely may result in under-utilization of the medium. We propose a performance model for CSMA under large propagation delay which gives the throughput of a CSMA channel as a function of propagation delay. Using this model, we also obtain channel access rates which achieve this capacity.

Another problem associated with the CSMA protocol is the short-term fairness problems that may arise due to the distributed nature of random access. Short-term fairness is essential for network performance especially if the traffic is delay-sensitive. Delay-sensitive applications cannot tolerate long periods of starvation such as the audio traffic. Since delay-sensitive multimedia applications constitute a significant portion of the Internet traffic, short-term fairness is an important attribute of a multiple-access protocol. Since most of the random access schemes run without the centralized controller, providing fairness among nodes is a challenging problem and short-term fairness of a network may be impaired even the throughput distribution between nodes is fair on the average.

In this thesis, we investigate a specific cause of unfairness in a CSMA network which is associated with the increasing deployment density and system size. As the penetration of wireless networks increases, the density of deployment of wireless networks increase. This increased density results in many local interactions between wireless networks deployed in nearby locations. These locally interacting networks form a large-scale system of loosely interacting networks. Using

the insights from statistical physics literature on large-scale locally interacting networks, we investigate how such interactions affect the fairness of the system. We show that the density affects the quality of service of wireless networks which becomes apparent in the short-term fairness of the CSMA protocol.

The third problem that we investigate is the energy efficiency of the CSMA protocol. Energy efficiency is a well-known problem for energy constrained devices such as hand-held devices and sensor networks. Although energy consumption of various CSMA-based standards have been evaluated previously, we propose a general energy consumption model which can be generalized to any CSMA-based MAC proposal. In the proposed model, we consider the energy consumed for carrier-sensing and energy consumed while sleeping which are usually ignored or omitted in the previous literature.

Energy consumption due to carrier sensing may become significant as the throughputs increase. Recently, several throughput-optimal CSMA algorithms are proposed which can theoretically achieve the feasible throughput region using an adaptive CSMA protocol. In these algorithms, the carrier sensing rates need to approach to infinity to achieve the maximum throughput. If the energy consumption due to carrier sensing is taken into account, achieving maximum throughput may be very energy-inefficient.

On the other hand, low carrier sensing rates may underutilize the medium and cause energy inefficiency. In this case, nodes spend most of their lifetimes in a sleep state which also reduces the amount of data transferred for a given energy budget. We find the energy-optimum carrier sensing rate and the corresponding energy-optimum throughput which minimizes the energy consumption per transmitted bit.

In the next section, we detail the contributions of this thesis to each of these three issues.

1.1 Contributions

In Chapter 3, we model the throughputs of nodes sharing a single CSMA channel under non-negligible propagation delay by using a semi-Markov model. We obtain the capacity region of the CSMA channel with non-zero propagation delay. Our results suggest that the capacity reduces to 40% of the zero-delay capacity for the 2-node case when the propagation delay is 10% of the packet transmission time demonstrating the importance of propagation delay in the performance of CSMA.

We determine how aggressive nodes should be in order to optimize the trade-off between the channel utilization and the collision probability so that the maximum throughput is achieved. We first extend the 2-node to an arbitrary number of nodes and, then, we derive the optimum probing rates as a function of the average propagation delay, \bar{d} , and the number of nodes, N . The optimum probing rate maximizes the channel utilization by exploiting the balance between the collision probability and the channel utilization.

We also investigate the asymptotic behavior of the capacity region as the propagation delay and the number of nodes increase. In the limit as $N \rightarrow \infty$, the model predicts that the total capacity changes in proportional to \bar{d}^{-1} . The optimum node probing rate decreases with $1/N$ as $N \rightarrow \infty$. Moreover, the total optimum network probing rate achieved by all nodes decreases faster than \bar{d}^{-1} for large N according to the proposed model.

We also compare the performance of the 802.11 channel access scheme with the proposed capacity and optimum probing rate analysis. For a simple two-node scenario, the 802.11 channel access scheme behaves closely similar with the proposed analysis for the pure CSMA as the propagation delay increases despite the discrepancies between the studied CSMA model and the 802.11 MAC protocol.

In Chapter 4, we analyze which portion of the capacity region of the CSMA protocol can be utilized in a short-term fair manner. We call this throughput

region as *the short-term fair capacity region*. We present a mathematical analysis of the short-term fairness of the tree topology and a comprehensive simulation-based study of tree, grid and randomly generated networks investigating the effects of network topology, nodal degree and network size on short-term fairness. We demonstrate the implications of degree dependence of short-term fairness on a Wi-Fi deployment scenario.

We claim that the short-term fairness among the interacting wireless transmitters is affected by the degree of the conflict graph of these transmitters. A denser deployment results in an increase in the number of contending neighbors of a network and our results suggest that the practically useful portion of the throughput region reduces as the number of neighboring networks increases.

We demonstrate the implications of our study on a practical city-wide Wi-Fi deployment scenario. Our results indicate that short-term fairness has to be sacrificed to improve coverage in such a system. To improve coverage, the density of the deployment has to be increased which causes the nodal degree of the system to increase. This, in turn, reduces short-term fairness.

We discuss if there is a reduction in the performance of interacting networks as the system size increases. Our results suggest that there is a weak dependence on the system size for a random placement of networks if the density of deployment is kept unchanged. On the other hand, the performance of networks with a grid conflict graph may severely degrade with system size if all networks operate at high throughputs.

We highlight the results from the statistical physics and theoretical computer science literatures on the long-range dependence in physical systems and identify a relationship between CSMA networks and physical systems. Despite the discrepancies between the physical models and the practical networking scenarios, we point out similarities between the short-term fair capacity region and the phase transition thresholds of the physical models.

In Chapter 5, we first provide an analytical model for the energy consumption

of a single-hop CSMA network and, then, for a multi-hop network with a random regular conflict graph. For both scenarios, we analyze the energy consumed in various states such as sleeping and carrier-sensing. We derive the energy-optimum carrier sensing rate and the corresponding energy-optimum throughput which minimize the energy consumption per transmitted bit. The energy-optimum throughput finds a balance between the energy consumed in the states of sleeping and carrier sensing per transmitted bit.

For the single-hop network, we show that the energy-optimum throughput is higher for larger networks because sleeping costs increase dramatically at a low throughput with the number of nodes. Also, the energy-optimum throughput increases as the power required for carrier-sensing reduces in proportion to the power required for sleeping. As sensing becomes less expensive, the nodes should attempt to transmit packets more frequently to minimize energy consumed per bit.

For the multi-hop case, we show that the energy-optimum throughput depends on the degree of the conflict of graph of the network and on the power consumption of carrier sensing. We find that the energy-optimum throughput reduces as the degree of the conflict graph increases, i.e., as the interference increases. Similar to the single-hop case, the energy-optimum carrier sensing rate and the energy-optimum throughput increase as the power required for carrier sensing reduces.

In the next chapter, we review the relevant literature on the performance of the CSMA protocol. Performance analysis of CSMA for channels with large propagation delay is given in Chapter 3. We discuss the implications of this thesis and possible lines of future work in Chapter 6.

Chapter 2

Literature Review

In this section, we review the relevant literature on random access protocols and, in particular, CSMA. First, we provide an overview of early random access research. Next, we summarize the research on random access for channels with large propagation delay. Then, relevant literature on fairness of random access protocols are presented. We also provide an overview of the throughput-optimal CSMA research and energy efficiency of CSMA protocols.

2.1 An overview of random access protocols

In this part, we provide a brief overview of history of random access protocols up to date. More comprehensive reviews can be found in [6] and [7].

The first random access protocol proposed is the ALOHA protocol [1] which is developed to enable the communication of the terminals located in the islands of Hawaii with a central computer. Since the nodes send packets whenever they have data, the probability of collisions is high. A performance improvement over this protocol is achieved by dividing the time into slots and only allowing each packet transmission to start at the beginnings of slots which is called as Slotted ALOHA [8].

An advancement over the ALOHA is the carrier sense multiple access (CSMA) protocol [2]. In CSMA, each node senses the channel before transmitting and refrain from transmitting if the channel is busy. So, some of the collisions are avoided. The CSMA protocol is divided into three types according to the actions that the nodes take after sensing the channel busy. In 1-persistent CSMA, a node continuously sense the channel and transmit immediately when it finds the channel idle. In p-persistent CSMA, a node transmits a packet with probability p at each idle slot. In the non-persistent CSMA, the packet transmission is rescheduled according to a stochastic distribution when the channel is sensed busy. 1-persistent CSMA has a high collision probability and p-persistent CSMA has no important advantages of non-persistent CSMA [6].

CSMA protocol is employed in the Ethernet standard with the addition of collision detection. When transmissions of the two nodes collide, it is possible the nodes to detect the collision over a wireline. When they detect collision, the nodes stop their transmissions and schedule a new transmission after a random amount. The duration is selected from a window which size is doubled when a collision occurs. Such an adaptation slows the traffic injection into the network, thereby reducing collisions. Performance of CSMA/CD is analyzed in [9].

CSMA protocol is also implemented in the wireless IEEE 802.11 standard with additional mechanisms. Additional mechanisms are required because wireless medium introduces some challenges in comparison to the wired media. In the wireless environment, collision detection is not feasible, so the standard does not employ a similar mechanism to the Ethernet protocol. Also, transmissions of some interfering nodes may not be sensed which is called as the hidden node problem. To alleviate this problem, a handshaking mechanism is introduced [10, 11] which is called as the RTS/CTS (Request to Send/Clear to Send) mechanism. This mechanism is an optional mechanism which is used for large packets by the IEEE 802.11 standard.

2.2 Performance of Random Access under Large Propagation Delay

Classic analyses of the CSMA protocol rely on some important assumptions which may not always correlate with the practical applications. For example, performance analysis of unslotted CSMA was given by Kleinrock and Tobagi [12] is based on the infinite number of users assumption [6]. So, the throughput expression does not provide accurate results for a small number of users. For finite number of users, Takagi and Kleinrock analyzed persistent CSMA [13]. This analysis, however, is valid only for persistent CSMA and relies on the assumption that each user has independent and exponentially distributed idle periods.

The effect propagation delay on CSMA has been studied in two main contexts: The first one is the long-distance deployment of 802.11 networks and the second one is the underwater acoustic networks. Long-distance WiFi links are proposed to be deployed as a low cost communications alternative for suburban areas. However, the 802.11 is not designed for outdoors and several modifications have to be made in the protocol. For underwater networks, the propagation speed of acoustic waves is very low so that the performance severely suffers from propagation delay. In the following parts, we survey the studies which investigate the influence of propagation delay in these two contexts.

2.2.1 Outdoor 802.11 networks

The performance of the 802.11 protocol has not been initially studied for channels with large propagation delay because of the short communication range for which the standard is designed. However, because of its low operating cost and its operation in the unlicensed band, 802.11 was considered as a possible alternative for rural internet access when deployed in a multicell setting. The feasibility of such an outdoor deployment was investigated in several studies.

The outdoor performance of 802.11 is first emulated in [14] suggesting minor

modifications to use 802.11 in an outdoor environment. The effects multipath dispersion and path loss on the IEEE 802.11 protocol is investigated in [15] and the authors concluded that the 802.11b protocols radio performance is suitable for outdoor cellular networks despite the fact that the wireless range is smaller than that of CDMA networks. Same research group also investigated the multiple access performance of the 802.11 standard for outdoor networks [16] and showed that multiple access performance of the 802.11 protocol is satisfactory for a cell size of 6 km.

Technical challenges in deploying an 802.11 for multi-hop long distance links is investigated using a testbed in [17] and the authors note that the ACK timeout duration of the 802.11 is short and RTS/CTS mechanism is inefficient for long-distance links. [18] also investigates a deployment of long distance links for different channel conditions. A characterization of causes of packet loss for WiFi long-distance links are given in [19] and a TDMA based protocol is designed in [20].

There are also several studies aiming to modify the Bianchi's 802.11 analysis [21] including the consideration of large propagation delays. In [22], the authors propose an extended model and specifically investigate the effect of slot time on the performance of the 802.11 protocol. Another extended analysis of 802.11 which does not assume slot synchronization is given in [23]. Another analytical model of 802.11 for long distances is given in [24] which offers adjustments for 802.11 parameters such as ACKTimeout, CTSTimeout, SlotTime, and CWmin.

2.2.2 Underwater Acoustic Networks

There is a relatively larger body of literature on analyzing propagation delay for acoustic networks since the effect of the propagation delay is more critical for underwater networks because of the relatively slow propagation speed of acoustic waves [25].

Several studies investigated if the traditional way of collision avoidance shows

good performance under large propagation delay. The performance of the CSMA protocol with the RTS/CTS mechanism under large propagation delays is investigated in [26, 27, 28]. These studies demonstrate that the use of RTS/CTS does not improve the performance of CSMA under large propagation delays due to the increased overhead of handshaking with propagation delay. In [28], the authors propose a method which aims to fix the time between the transmission of an RTS and the reception of the CTS. So, the node transmitting the RTS can utilize the intermediate time to transmit other packets and receive CTS at an expected time. Same authors used a similar method to improve utilization in [29]. In [30], the authors defined a configurable handshaking method where the handshaking duration is minimized using the tolerance to interference from long distance nodes.

There are several studies investigating the performance of the ALOHA protocol without handshaking in underwater settings and offering modifications. The performance of the ALOHA protocol for underwater sensor networks with large propagation delays is analyzed in [31, 32]. Both studies state that the performance of slotted ALOHA reduces to the performance of unslotted ALOHA under large propagation delays. Adapting slot lengths according to the propagation delay is proposed [33, 34], but using larger slot lengths reduces efficiency when the propagation delay is comparable with packet transmission times. Addition of a guard band to transmissions is proposed in [32] and an additional synchronization mechanism for slotted ALOHA is suggested in [35]. A variant of ALOHA called p-persistent ALOHA is analyzed for multi-hop networks in [36]. In p-persistent ALOHA, the nodes reduce their probability of channel access to prevent collisions. This idea is similar to the earlier works on ALOHA and CSMA which aims to adapt the channel access rate to operate the network in the optimal operating load [37].

The literature on the underwater MAC protocols generally focuses on the ALOHA protocol instead of CSMA. The rationale behind this approach is that the carrier-sensing operation may give the wrong information about the channel state: First, an idle channel does not certainly indicate a transmission will be completed without collisions: As the propagation delay increases, the probability that a

collision occurs increases. Second, a busy channel does not certainly indicate that a collision will occur at the receiver side. If the receiver is out of range of the sensed transmission, it can successfully receive packets. Despite the unreliability of the sensing operation, the carrier sensing operation provides an information about the channel state and if this information is utilized in an intelligent manner, it can improve throughput.

There are some proposals which utilize overhearing in an underwater setting to learn about the ongoing transmissions in the network. For example, two MAC algorithms based on overhearing are proposed in [38]. The first method, ALOHA-CA, overhears about the transmissions that are going on in the channel and use that information to schedule transmissions. In ALOHA-CA, a node may transmit even if there is an ongoing transmission in the channel if its transmission will not collide at the intended receiver. In the second method, ALOHA-AN, a node notifies the intended recipient with a small packet before its transmission. So, all nodes in the network can become aware of the upcoming transmission. Both methods require the propagation delay information of every node pair has to be known by each node in the network. However, time synchronization is not needed.

Another method based on overhearing is proposed in [39]. In this method, each node keeps a delay map of the network and keeps a record of ongoing transmissions which are learned by overhearing. The method employs RTS/CTS like handshaking and requires clock synchronization. The main idea is to utilize the channel better by allowing concurrent transmissions. The proposed algorithm, however, performs worse than ALOHA with carrier sensing in terms of throughput for a random deployment of sensors. The authors argue that the fairness and energy consumption of ALOHA with carrier sensing is impaired in comparison to the proposed algorithm.

In contrast to sender initiated handshaking proposals, a receiver initiated reservation protocol is proposed in [40]. In this protocol, the receiver sends a retrieve request to its neighbors and collect their packet transmission requests. The receiver, then, replies with an ordered list of transmissions for the sender to schedule transmissions accordingly. The transmitters know the propagation delay

map so they can arrange their transmissions to arrive at the requested time. In this method, a handshaking procedure is used to transmit more than one packet so it is more efficient than handshaking before each packet. This method is shown to outperform ALOHA-AN but it increases complexity significantly.

Apart from these methods, there are several MAC proposals for underwater networks implementing different forms of random access. A combination of round robing scheduling and CSMA is investigated in [41] but this method requires a central network coordinator to keep the scheduling of transmitters which may not be feasible in an underwater environment. A periodic wake-up and sleep scheduling is proposed during which the data is transmitted in bursts and cumulative acknowledgments are used [42]. A slotted MAC protocol is proposed in [43]. A low power wake-up radio is implemented to reserve the channel and to minimize idle listening in T-Lohi [44].

The results of an at-sea testing of three MAC protocols is given in [45]. This paper compares CSMA, DACAP [30] and T-Lohi [44]. The results show significant discrepancies between the simulations and sea experiments. Especially DACAP performs worse than the simulations because possible ACK losses causes inefficiency due to repeated handshaking. This result show that the resilience of underwater multiple access methods has to be investigated under channel losses because most of the studies assume that the channel is lossless.

2.3 Fairness of Large Scale CSMA Systems

Throughput is generally the main consideration in evaluating the performance of wireless protocols. However, fairness of a wireless protocol is also crucial because unfairness between nodes or flows in a wireless network may result in poor user experience.

Fairness of a wireless system can be measured in two different time scales: Long-term unfairness of the transmitters is the discrepancy between throughputs of nodes in the long-run. Short-term unfairness, on the other hand, is the inequity

between throughputs of nodes when they are monitored for a short-duration. Short-term fairness is only possible for a long-term fair network since it is not possible for a network to be short-term fair when it is unfair in the long-term.

The fairness problem of wireless networks has been investigated in different contexts. The first line of study is in the context of multi-hop networking applications of the IEEE 802.11 protocol. The second line of study is the investigation of an idealized version of CSMA where only the essential features of a multiple access protocol is studied. Studies in the latter category omit some practical aspects of wireless networking protocols but may lead to deeper insights about the underlying dynamics of CSMA networks. Our study falls into the second category but we also provide an overview of fairness studies of 802.11 in a multi-hop setting.

2.3.1 Long-term fairness

2.3.1.1 Measurement

To quantify the fairness of a network, measurement metrics are needed. The following are several long-term fairness metrics from the literature:

- Jain’s fairness index: Jain’s fairness index is the most common fairness index around the networking community. If N is the number of nodes, Jain’s index for throughputs is given by [46]

$$I_{Jain} = \frac{(\sum_{i=1}^N T_i)^2}{N \sum_{i=1}^N T_i^2} \quad (2.1)$$

where T_i is the throughput of node i . In the case of equal throughputs, the Jain’s index equals to 1 and it equals to 0 if only one of the nodes can transmit.

- Gini index: This index is widely used in economics literature and it is sometimes used in wireless network fairness measurement [47, 48] although it is not as common as the Jain’s index. It is derived from the Lorenz curve

which plots the share of cumulative aggregate throughput of nodes or flows. In the ideal situation where all nodes get equal share, the Lorenz curve is a line with a 45-degree angle. Gini index is ratio of the area between the Lorenz curve and the diagonal line to the area of the triangle limited by the diagonal line. In the perfectly fair case, the Gini index is 0. Its formal expression for a communications scenario is given by

$$I_{Gini} = \frac{1}{2N^2\bar{T}} \sum_i \sum_j |T_i - T_j|. \quad (2.2)$$

where \bar{T} is defined as the average throughput.

There are also several other fairness index proposals specific to communication resource allocation [49, 50] but we do not elaborate these studies. For a more theoretical discussion of fairness measurement, the readers may refer to [51].

2.3.1.2 802.11 Networks

The success of 802.11 in single-hop networks lead to investigations of its feasibility for multi-hop networks. Unfortunately, these studies demonstrated that its performance is not very efficient. Per node throughputs are shown to decay dramatically in a multi-hop scenario [52] and some researchers assert that 802.11 is not suitable for multi-hop networks [53].

Fairness problems associated with the 802.11 protocol is one of the reasons which makes its adaptation for a multihop network difficult. Several causes of long-term and short-term unfairness in multi-hop 802.11 networks are presented in [54]. Examples of these causes are hidden terminals, geographical disadvantage of some nodes and unsuitability of some protocol parameters for a multi-hop scenario. Starvation of an intermediate node in a multi-hop system topology was first noted in [55] and analyzed using a Markov model. The unfairness problem is analyzed for small topologies in [56] and for larger topologies in [48]. Optimization of the value of CWmin of the 802.11 protocol is suggested in [57] to achieve desired fairness-throughput threshold. A multi-channel coordination method is devised to solve the starvation problem in [58].

More recently, a more theoretical approach to the fairness of CSMA networks has been developed using an idealized model of CSMA.

2.3.1.3 Idealized CSMA

The idealized model of CSMA is used in the analysis of fundamental reasons of unfairness in CSMA networks. This idealized model ignores collisions and, hence, does not employ an exponential back-off. The nodes sense the channel at exponentially distributed intervals and capture the channel when they find the channel idle. The studies that investigate the fairness of an idealized CSMA system can be roughly categorized into two: First class of studies deal with the fairness of fixed rate CSMA systems where each transmitter sense the channel at the same rate. Second class of studies investigates the fairness of CSMA systems where the transmitters adapt their sensing rates according to recently proposed distributed CSMA algorithms.

For fixed-rate CSMA systems, unfairness in the long-term average throughputs of transmitters has been investigated. A fundamental cause of the long-term unfairness of CSMA was shown to be the self-organization of transmission patterns [59]. Unfairness in a large CSMA system caused by the unfair advantage of border nodes at high access rates was analyzed in [60]. To eliminate border effects, channel access rates which equalize throughputs are proposed for linear networks and $2 \times N$ grids [61, 62]. Determination of channel access rates which achieves target throughputs is investigated in [63]. In an earlier study, throughput equalizing rates for a tandem network is also investigated [64]. A back-of-the-envelope method for computing throughputs in a CSMA network is presented in [65].

Recently, adaptive CSMA algorithms that can achieve throughput optimality have been proposed [66, 67, 68, 69]. These algorithms solve the long-term fairness problem of CSMA systems by adapting the channel access rate of nodes according to their demands. In these algorithms, nodes in an unfair position will increase their channel access probability as their queue lengths grow. This mechanism

balances the average throughputs of transmitters in the long-run. The main drawback of these methods is that they ignore collisions, so the performance of these methods in the case of collisions are not clear.

Another major problem with the adaptive CSMA algorithms is that their short-term fairness performance is not as desirable as their long-term fairness performance especially for high throughputs. This problem will be elaborated in the next section.

2.3.2 Short-term Fairness

2.3.2.1 Measurement

Measurement of short-term fairness is different from the measurement of long term fairness. The average values of resource allocation such as throughput, number of packets transmitted does not give enough information about short-term fairness. In this case, the temporal behavior of the system has to be investigated. The following are several measures of short-term fairness proposed in the literature.

- Short-term fairness horizon: Short-term fairness horizon is measured by sliding a window over the transmission history of the network and computing a fairness index for each window. The average of these values for a given window size is the fairness index associated with that window size. Short-term fairness horizon is the minimum window size over which the fairness index exceeds some predefined value [70]. Originally, the authors used two different fairness measures, the first is the Jain's index and the second one is the Kullback-Leibler distance. In [70], the minimum window size which gives a Jain's fairness index of 0.95 or a Kullback-Liebler distance of 0.05 is selected as the short-term fairness horizon. In our study, We use a Jain's fairness index of 0.95 as the short-term fairness threshold.

- Number of inter-transmissions: This metric measures the number of transmissions that other node's perform between the transmissions of a given node. It measures how much a node starves once it loses its access to the channel. It is used in [71, 72].
- Number of successive transmissions: This metric measures the number of successive transmissions that a node makes once it captures the channel [72]. The number of successive transmissions and the number of inter-transmissions are related because the number of inter-transmissions of a node can be considered as the sum of mean number of successive transmissions of all other nodes. Since the number of inter-transmissions is inherently dependent on the number of nodes in the network, we use the number of successive transmissions in this study.

2.3.2.2 802.11 Networks

The first analysis of short-term fairness of CSMA/CA and ALOHA are proposed in [70]. In [71], the authors demonstrated that 802.11 exhibits good short-term fairness for a two-node scenario. An analysis of short-term fairness in a multi-hop scenario is given in [73] including higher protocol layers. An analytical model of short-term unfairness in the presence of for a 3-node hidden terminal case is given in [72].

2.3.2.3 Idealized CSMA

Despite the studies that investigate long-term fairness of a fixed rate CSMA system, there are not many studies that deal with the short-term fairness problem. Short-term fairness of long-term fair grid and line topologies were analyzed briefly in [60]. For a given topology, a method of analysis is proposed using the Markov chain of independent sets [74] but this analysis requires enumeration of all independent sets which is computationally difficult.

Recently proposed throughput-optimal CSMA algorithms ensures the fair allocation of throughput in the long-run according to the demands of nodes. However, throughput allocation among transmitters may be unfair in the short-term even when the average throughput distribution is fair in the long-run. Short-term unfairness becomes more apparent as throughputs increase and, as a result, variation in the channel access delay of transmitters increases. Degradation in the short-term fairness as the throughput-optimality is achieved is investigated in [75]. Several bounds for delay are proposed [76, 77, 78, 79, 80] and methods for minimizing the delay are devised [81, 82, 83]. To reduce delay, appropriate selection of the rate adaptation function is also investigated [84, 85, 86].

In this thesis, we investigate the short-term fairness of a fixed rate CSMA system and investigate the effect of system size, density and topology on the short-term fairness. Previous studies on fixed-rate CSMA systems are often limited to linear and grid topologies. In this thesis, we also study random regular topologies that demonstrate very different short-term fairness characteristics from the grid topology. Besides, to the best of our knowledge, the relationship between the degree of a network and its short-term fairness has not been shown before. We demonstrate that this relationship may result in a trade-off between the coverage and the short-term fairness of a Wi-Fi based access network.

2.4 Energy Efficiency of the CSMA Protocol

As the wireless mobile devices gets widespread and with the gaining popularity of sensor networks, the energy efficiency of wireless devices become a major concern. In wireless devices, especially in sensor networks, communication consumes much more power than processing. Transmitting one bit of information consumes as much energy of executing several hundred instructions [87]. For that reason, minimizing communication overhead is crucial.

2.4.1 Sources of Energy Inefficiency

We here list some of the sources of energy inefficiency in the context of sensor networks [87]:

- Collisions: When the two transmissions collide at the receiver, none of the packets can be decoded so energy consumed for these transmissions are wasted.
- Idle listening: The receiver listens the channel while waiting a transmission. Although a node consumes less energy while receiving than transmitting, the energy consumption becomes significant when the node listens the channel for long periods.
- Overhearing: A node may receive messages that are not destined to itself which increases energy consumption. A node should better turn off its radio when it detects such a transmission.
- Protocol overhead: The control packets such as RTS/CTS and the protocol headers increases the energy consumption per transmitted data. However, the use of control packets may reduce overall energy consumption if they help to reduce other energy consuming causes such as collisions or idle listening.

2.4.2 Energy efficient random access protocols

Multiple channel systems such as frequency-division multiple access (FDMA) and code-division multiple access (CDMA) ensures collision free transmissions. However, they need complex radios which may have high energy consumption so energy efficient MAC protocols generally use single channel radios. However, it is possible to employ a second very low power radio to signal the start of a transmission to the recipients [88].

Another method to eliminate collisions is to use time-division multiple access

(TDMA). TDMA is also suitable for lowering idle listening since nodes may receive only during predetermined time intervals so that they can shut down their radios in other intervals. On the other hand, the strict synchronization requirement of TDMA makes it harder to implement in a distributed scenario. Besides, TDMA is not scalable and inefficient in a variable rate scenario.

A less strict method is to use a slotted system where the nodes start their transmissions only at the beginnings of a global slot. This method also requires synchronization between nodes but it is less strict than TDMA. In SMAC [89], nodes turn their radios on and off in synchronization. Beginning of each slot is used for synchronization purposes and the nodes perform their transmissions in first part of the remaining time and, then, sleep until the start of the next slot. It uses the RTS/CTS mechanism to avoid the hidden terminal problem. In T-MAC, the authors employ a similar mechanism to SMAC but they adaptively select the active period in each cycle: A node stays in the active state until no activity is detected for a predefined time. After this point, the node sleeps and wakes up at the beginning of the next slot. In DMAC, the duty cycling schedules of nodes are arranged according to their hop count to the sink node, so it is possible to transmit a packet from a node to the sink node with low latency. In Crankshaft [90], the authors proposed a MAC protocol for dense sensor networks. Different nodes wake up at different times so that the overhearing problem is reduced.

Our main focus here is to investigate the energy efficiency of random access protocols where no synchronization between nodes is assumed. The main challenge with such mechanisms is to reduce the idle listening duration.

One of the methods to reduce idle listening is using a preamble transmitted by the sender [91, 92]. In this method, the sender adds a preamble to the beginning of its transmission. The receiver periodically turns on its radio and listens to the channel. If it detects a preamble, it starts to receive the packet. Here, the length of the preamble must be longer than the periods of duty cycling. ALOHA and CSMA with preamble sampling is analyzed in [92]. The authors showed that ALOHA with preamble sampling allows much longer lifetimes at low traffic loads whereas it does not have an advantage at higher traffic loads. B-MAC [3]

and X-MAC [93] are other examples of MAC protocols employing preambles. A wiser preamble sampling method, WiseMAC, built on [92] is proposed in [94]. In this method, a node learns the sampling schedule of its neighbors so it starts to transmit the preamble just before their wake-up so a shorter preamble is sufficient.

In contrast to sender initiated preambuling methods, there is also a receiver initiated MAC protocol called RI-MAC [95]. In this method, when a sender has a packet to send, it wakes up and start to listen for a beacon signal from the receiver. Receivers periodically wake-up and transmit a beacon signal and wait for a transmission. If the sender receives a beacon signal from its destination, it transmits the packet. The receivers sleep again if a transmission does not arrive after transmitting the beacon signal. Instead of long preambles transmitted by the senders, short beacon signals are transmitted which improves utilization.

Another method is to use second low power radio. This secondary radio is not used for data transmission, it only transmits wake-up signals. In [88], the authors proposed such a system where the sender transmits a wake-up signal after buffering a predefined amount of packets in its transmissions queue. Receiving the wake-up signal, all receivers wake up. First, a filtering packet is transmitted to indicate the destination node. Hearing this signal, all nodes but the destined node return to sleep.

A different approach to duty cycling is proposed in PW-MAC [96]. In this predictive wake-up method, each node uses a pseudo-random number generator to determine its wake-up times. If the sender knows the seed of the pseudo-number generators of its neighbors, it can transmit a packet at the precise time of the wake-up of its neighbor. This method is also receiver-initiated, the receiver transmits a beacon when it wakes-up and the sender who has just awoke transmits the packet after the reception of this beacon signal.

Chapter 3

Throughput Modeling of Single Hop CSMA Networks with Non-Negligible Propagation Delay

One of the main drawbacks of the CSMA protocol is the collisions which may occur as a result of the propagation delay between nodes. In the current wireless configurations, however, propagation delay is not considered as a significant problem because it is negligible in comparison to the transmission times. On the other hand, larger propagation delays should be considered in the performance modeling of future wireless networks for several reasons: First, there are new wireless networks developed for covering larger areas to provide Internet access in rural areas [5] where the propagation delay is larger. Second, there is an emerging need for underwater acoustic networks [4] which experience very large propagation delays due to low propagation speed of acoustic waves. Finally, as the transmission rates increase, packet durations decrease, consequently, ratio of the propagation delay to the transmission time increases.

We here model the throughputs of nodes sharing a single CSMA channel under

non-negligible propagation delays. We determine how aggressive nodes should be in order to optimize the trade-off between the channel utilization and the collision probability. We also investigate the asymptotic behavior of the capacity region as the propagation delay and the number of nodes increase. The contributions of this chapter are:

- a semi-Markov model for the throughput of the two saturated nodes sharing a CSMA channel. Using this model, we present the capacity region of the CSMA channel with non-zero propagation delay. When the propagation delay is 10% of the packet transmission time, the capacity reduces to 40% of the zero-delay capacity for the 2-node case.
- derivation of the optimum probing rates as a function of the average propagation delay, \bar{d} , and the number of nodes, N , by extending the 2-node model. The optimum probing rate maximizes the channel utilization by exploiting the balance between the collision probability and the channel utilization.
- an investigation of the asymptotic total capacity for large N . In the limit as $N \rightarrow \infty$, the model predicts that the total capacity changes in proportional to \bar{d}^{-1} . The optimum node probing rate decreases with $1/N$ as $N \rightarrow \infty$. Moreover, the total optimum network probing rate achieved by all nodes decreases faster than \bar{d}^{-1} for large N according to the proposed model.
- an investigation of a back-off mechanism which is employed in order to mitigate the the short-term unfairness problem in CSMA. When the propagation delay increases, the capture effect in CSMA becomes more significant especially when a small number of nodes are sharing the channel. Using a back-off after each transmission, this unfairness becomes much less significant without having a throughput penalty.
- a comparison of the performance of the 802.11 channel access scheme with the proposed capacity and optimum probing rate analysis. For a simple two-node scenario, the 802.11 channel access scheme behaves closely similar with the proposed analysis for the pure CSMA as the propagation delay increases

despite the discrepancies between the studied CSMA model and the 802.11 MAC protocol.

In the next section, we describe the scenario on which we built our study. The semi-Markov model for the 2-node case and the capacity region of the CSMA link are presented in Section 3.2. Derivation of the asymptotic optimum probing rate and the total channel capacity along with the performance evaluation of these expressions are discussed in Section 3.3. We investigate a back-off mechanism for improving the fairness of CSMA under large propagation delay in Section 3.4. Section 3.5 compares the 802.11 channel access scheme with the proposed capacity and optimum probing rate analysis.

3.1 Scenario Description

In this section, we present the assumptions of this study and explain the motivations behind these assumptions.

- All nodes can hear each other, i.e., all transmissions are single hop.
- Nodes employ an unslotted CSMA protocol. We model a CSMA network where the largest one-way propagation delay can be as much as half of the packet transmission time.
- Nodes do not employ collision detection since collision detection is not feasible for wireless networks.
- Nodes do not employ any handshaking mechanism to avoid collisions. Although a handshaking mechanism may reduce packet collisions, it brings a significant overhead when the propagation delay is high. Besides, control packets used in handshaking may also collide when the propagation delay is large.
- We assume that the back-off intervals are exponentially distributed. Since the exponential distribution supports infinite back-off intervals, it is not

used in real-life protocols. However, it is more suitable for the performance analysis because of its memoryless behavior. Similarly, geometric distribution is used in IEEE 802.11 performance analysis in the literature because of its memoryless nature, and it is shown to perform similar to the uniform back-off length distribution [97].

- We assume a fixed packet transmission time. Although some studies show that the throughput can be increased by increasing packet transmission times, we do not follow that approach in order to avoid degradation in the short-term fairness.

3.2 Semi-Markov Model for the 2-Node CSMA channel

In this section, we first present a throughput model for the CSMA channel for 2 nodes. Then, we compare the performance of this model with the simulation results and present the capacity region of the 2-node CSMA channel to demonstrate the effect of propagation delay on the capacity of the CSMA protocol.

3.2.1 State Definitions

The semi-Markov model for the 2-node case is built from the point of the view of one of the nodes where states represent the phases that a node visits as time evolves. The state diagram of the chain is depicted in Fig. 3.1.

Assume that node 1 started a transmission after a long idle period and node 1 is sharing the channel with node 2. This transmission is vulnerable to collisions until node 2 hears this transmission (State 2). If the transmission survives this period, it is certain that the transmission will safely complete (State 3). After the end of this transmission, node 2 will still be exposed to the transmission of node 1 for a period time because of the propagation delay. During this period,

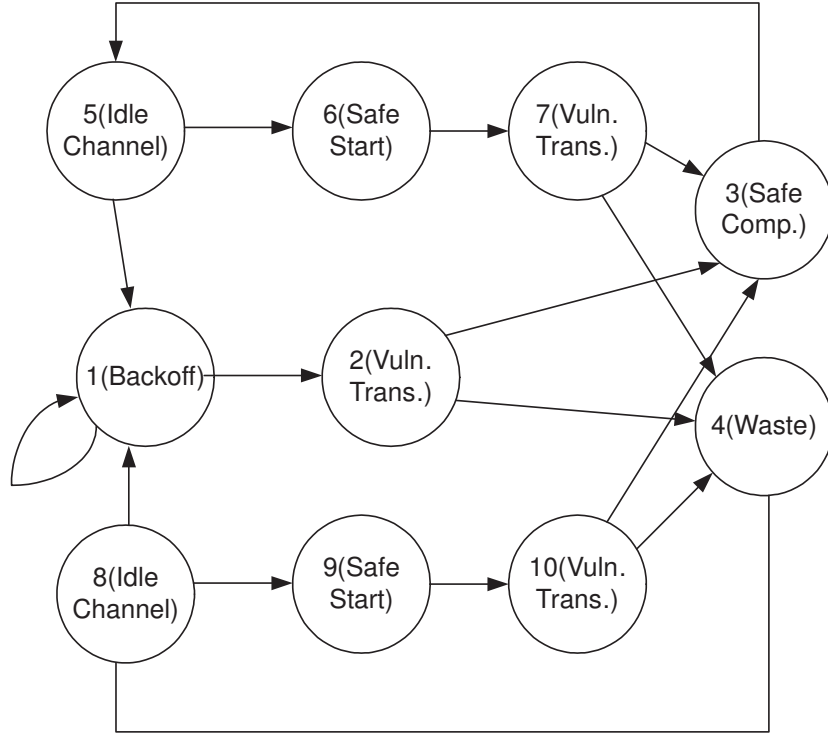


Figure 3.1: The state diagram for the semi-Markov model.

node 1 is advantageous to start another transmission (State 5). If node 1 starts a transmission while node 2 is still exposed to its previous transmission, new transmission can be safe from collisions for a period of time (State 6). When this period ends, it becomes vulnerable again (State 7) but it can safely complete after node 2 hears this transmission (State 3). If a collision occurs, transmission is wasted (State 4). At the end of this collided transmission, node 2 will still be exposed to the collided transmission so a shorter period of successful probing exists (State 8). New transmission will pass through safe (State 9) and vulnerable states (State 10).

Below we present the holding time distributions and the transition probabilities between these states. We normalize the time such that each packet has a fixed transmission time of unit duration. Note that d denotes the one-way propagation delay between nodes and we assume $2d < 1$. Nodes 1 and 2 independently sense the channel at exponentially distributed intervals with mean $1/R_1$ and $1/R_2$, respectively, and transmit their packets if the channel is idle. R_1 and R_2 refer to the probing rates of Nodes 1 and 2, respectively. S_i denotes the holding time

in state i . Probability distribution function (PDF) and cumulative distribution function (CDF) of S_i are denoted by f_{S_i} and F_{S_i} , respectively. We define $p_{i,j}$ as the transition probability from state i to state j .

State 3 (Safe Completion): After a transmission starts, a colliding transmission can only arrive within $2d$ period because node 2 becomes aware of the transmission of node 1 at d . Since node 2 will not start a transmission after this point, it is certain that a colliding transmission will not arrive after $2d$ and the transmission will be safely completed. The holding time in this state is deterministic and equal to $1 - 2d$:

$$f_{S_3}(t) = \begin{cases} 1 & \text{if } t = 1 - 2d, \\ 0 & \text{o.w.} \end{cases} \quad (3.1)$$

After a successful transmission, there is an idle channel period which is the next state described. In our model, that period is denoted as State 5 and the transition probability from State 3 to State 5 is 1, i.e.,

$$p_{3,5} = 1. \quad (3.2)$$

State 5 (Idle Channel): After a successful transmission, it is certain that node 1 will not receive a transmission from node 2 for a duration of $2d$ because node 2 is still exposed to node 1's successful transmission as shown in Fig. 3.2a. After the successful completion, if node 1 performs channel probing within the $2d$ duration, it will find the channel idle and start transmission and enter State 6 (Safe Start). If it does not probe the channel within the $2d$ period, the system will enter State 1 (Backoff). Hence, the transition probabilities from State 5 are given by

$$p_{5,1} = e^{-R_1 2d} \quad p_{5,6} = 1 - e^{-R_1 2d} \quad (3.3)$$

and the holding time distribution in State 5 is given by

$$f_{S_5}(t) = \begin{cases} R_1 e^{-R_1 t} & \text{if } t < 2d, \\ e^{-R_1 2d} & \text{if } t = 2d, \\ 0 & \text{o.w.} \end{cases} \quad (3.4)$$

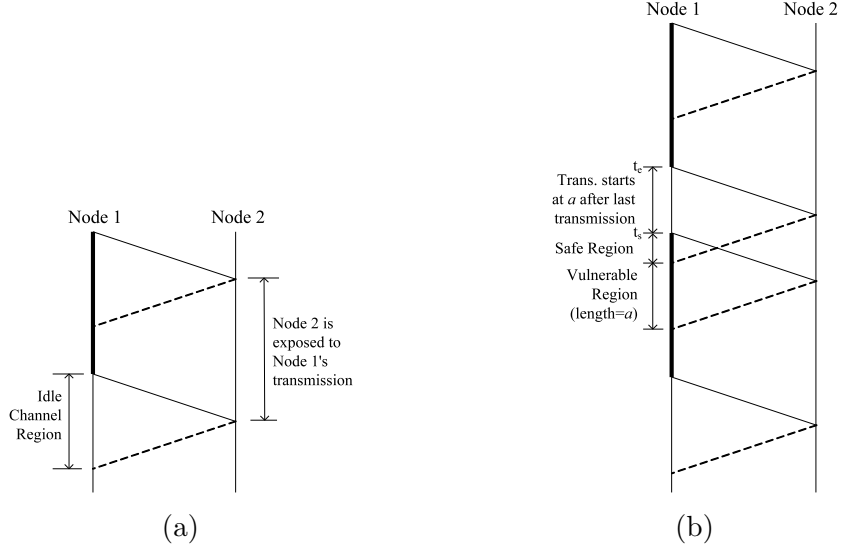


Figure 3.2: (a) Idle channel period after a successful transmission. Duration of this period is $2d$. (b) If a transmission starts in this idle period, it continues free from collisions for a duration of a and enters into a vulnerable period. The duration a equals to the starting transmission time after the successful transmission.

Then, the expected holding time at State 5 can be written as

$$E[S_5] = \int_0^{2d} tR_1e^{-R_1t}dt + 2de^{-R_12d} = \frac{1 - e^{-R_12d}}{R_1}. \quad (3.5)$$

State 6 (Safe Start): If node 1 starts transmission within the $2d$ period, it is certain that this transmission will safely continue until time $t_e + 2d$, where t_e is the end of last packet transmission as it can be observed from Fig. 3.2b. After this state, the transmission will enter a vulnerable state (State 7):

$$p_{6,7} = 1. \quad (3.6)$$

The holding time distribution in this state is given by

$$f_{S_6}(t) = \begin{cases} \frac{R_1e^{-R_1(2d-t)}}{1 - e^{-R_12d}} & \text{if } t < 2d \\ 0 & \text{o.w.} \end{cases} \quad (3.7)$$

Then,

$$E[S_6] = \int_0^{2d} t \frac{R_1e^{-R_1(2d-t)}}{1 - e^{-R_12d}} dt = -\frac{1}{R_1} + d + d \coth(R_1d). \quad (3.8)$$

State 7 (Vulnerable Transmission): After State 6, the transmission becomes vulnerable in $[t_e + 2d, t_s + 2d]$ as shown in Fig. 3.2b, where t_s is the starting time of the transmission of the current packet. As noted in the figure, the length of the vulnerable period is equal to the starting time of the transmission after the last transmission. For that reason, the length of this period is exponentially distributed truncated at $2d$. Then, the probability of successful completion of the transmission, which corresponds to the probability of transition to State 3, is expressed as

$$p_{7,3} = \int_0^{2d} \frac{R_1 e^{-R_1 t}}{1 - e^{-R_1 2d}} e^{-R_2 t} dt = \frac{e^{-R_2 d} R_1 \operatorname{csch}(R_1 d) \sinh((R_1 + R_2)d)}{R_1 + R_2}. \quad (3.9)$$

Consequently,

$$p_{7,4} = 1 - p_{7,3}. \quad (3.10)$$

In order to obtain the holding time distribution of this state, the distribution of the minimum of two random variables has to be found. Either the vulnerable period will end without collisions and the system will enter State 3 or a colliding transmission will arrive and the system will enter State 4. The first distribution which denotes the length of the vulnerable period, V , is exponentially distributed truncated at $2d$. The second distribution is the distribution of the arrival of the other node's transmission, C , which is exponentially distributed with mean $1/R_2$.

$$F_{S_7}(t) = \begin{cases} 1 - \left(\int_t^{2d} \frac{R_1 e^{-R_1 x}}{1 - e^{-R_1 2d}} dx \right) e^{-R_2 t} & t < 2d \\ 1 & \text{o.w.} \end{cases} \quad (3.11)$$

Taking the derivative, $f_{S_7}(t)$ can be obtained:

$$f_{S_7}(t) = \begin{cases} -\frac{e^{-aR_1 - aR_2 + 2R_1 d} R_1}{1 - e^{2R_1 d}} + \frac{e^{-aR_2} (1 - e^{-aR_1 + 2R_1 d}) R_2}{1 - e^{2R_1 d}} & t < 2d \\ 0 & \text{o.w.} \end{cases} \quad (3.12)$$

The expected length of this period is given by

$$E[S_7] = \int_0^{2d} t f_{S_7}(t) dt = \frac{(-1 + e^{-2R_2 d}) R_1 + (-1 + e^{2R_1 d}) R_2}{(-1 + e^{2R_1 d}) R_2 (R_1 + R_2)}. \quad (3.13)$$

State 4 (Waste): If a colliding transmission arrives during the vulnerable period of a transmission, the system will enter State 4. The duration of this period

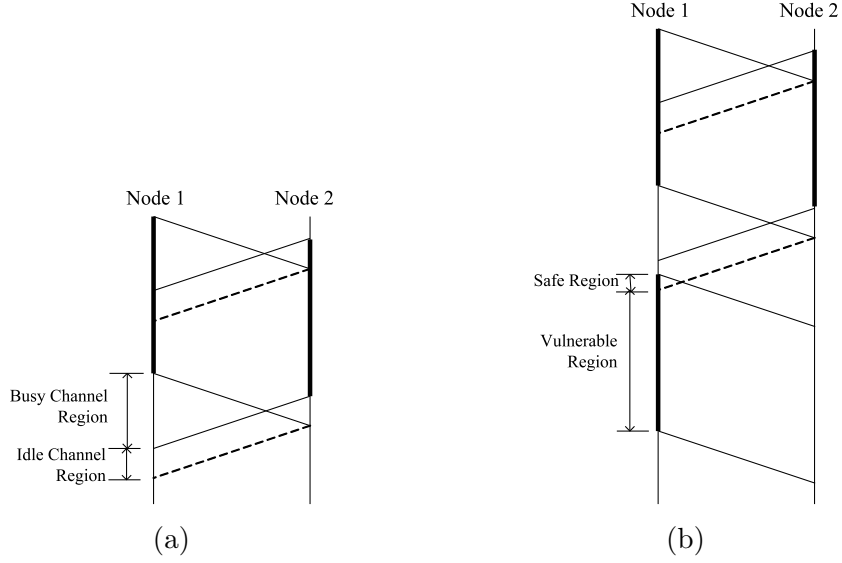


Figure 3.3: (a) Busy and idle channel periods after an unsuccessful transmission. (b) If a transmission starts in the idle period, it continues free from collisions for a while and enters into a vulnerable period.

equals 1 which is the length of the colliding transmission, hence $E[S_4] = 1$. After State 4, the system will enter an idle waiting state (State 8): $p_{4,8} = 1$.

State 8 (Idle Channel): After State 4, there is still an idle period during which a probe will be successful as it can be observed in Fig. 3.3a. However, this period will be shorter than $2d$ in contrast to State 5. The length of this period is given by $2d - t_c$ where t_c is the duration of the collision after the previous transmission. We assume that the collision duration is uniformly distributed in $[0, 2d]$. Then, the probability that the node probes the channel before the end of the idle period, i.e., the transition probability from State 8 to State 9, can be expressed as

$$p_{8,9} = \int_0^{2d} \frac{1}{2d} \int_0^u R_1 e^{-xR_1} dx du = 1 - \frac{1 - e^{-R_1 2d}}{2R_1 d} \quad (3.14)$$

and $p_{8,1} = 1 - p_{8,9}$. The distribution of the holding time in State 8 is the minimum of two random variables. The first one is the length of the idle period which is uniformly distributed between 0 and $2d$. The other one is the probing time which

is exponentially distributed with mean $1/R_1$.

$$F_{S_8}(t) = \begin{cases} (1 - e^{-R_1 t \frac{2d-t}{2d}}) & t < 2d \\ 1 & \text{o.w.} \end{cases} \quad (3.15)$$

Taking the derivative, $f_{S_8}(t)$ can be written as

$$f_{S_8}(t) = \begin{cases} \frac{e^{-R_1 t}}{2d} + \frac{e^{-R_1 t} R_1 (-t+2d)}{2d} & t < 2d \\ 0 & \text{o.w.} \end{cases} \quad (3.16)$$

The expected holding time at State 8 is given by

$$E[S_8] = \int_0^{2d} t f_{S_8}(t) dt = -\frac{1 - e^{-2R_1 d} - 2R_1 d}{2R_1^2 d}. \quad (3.17)$$

State 9 (Safe Start): If the node probes the channel in the idle period after an unsuccessful transmission, the started transmission will continue safely for a while as shown in Fig. 3.3b. Let U denote the length of the idle period which is uniformly distributed between 0 and $2d$ and E is the starting time of the transmission which is exponentially distributed with mean $1/R_1$. Since the length of the idle period is $U - E$, the CDF of S_9 can be written as

$$\begin{aligned} F_{S_9}(t) &= Pr(U - E < t | E < U) \\ &= Pr(U - E < t | E < U, U < t) + Pr(U - E < t | E < U, U > t) \\ &= Pr(U < t) + Pr(U - E < t | E < U, U > t) \\ &= \frac{t}{2d} + \int_0^{2d} \frac{1}{2d} \int_{u-t}^u R_1 e^{-R_1 t} dt du \\ &= \frac{t + \frac{1 - e^{-R_1 t} - e^{R_1(t-2d)} + e^{-R_1 2d}}{R_1}}{2d} \end{aligned} \quad (3.18)$$

Then, $f_{S_9}(t)$ is given by

$$f_{S_9}(t) = \frac{1 + e^{-R_1 t} - e^{R_1(t-2d)}}{2d} \quad (3.19)$$

and the expected holding time is expressed as

$$E[S_9] = \int_0^{2d} t f_{S_9}(t) dt = \frac{1 + R_1 d(-1 + R_1 d) - e^{-R_1 2d}(1 + R_1 d)}{R_1^2 d}. \quad (3.20)$$

After visiting State 9, the system will enter State 10: $p_{9,10} = 1$.

State 10 (Vulnerable Period): After State 9, there is a vulnerable period during which a collision may occur as it can be observed from Fig. 3.3b. Distribution of the holding time of State 10 is the minimum of two distributions: The first one is the maximum duration of this period which is the subtraction of the holding time in State 9 from $2d$ and the second one is exponentially distributed with mean $1/R_2$ which corresponds to the duration until the start of a colliding transmission. Probability that a colliding transmission arrives during a transmission can be written as

$$\begin{aligned}
p_{10,4} &= \int_0^{2d} \frac{1 + e^{-(2d-u)R_1} - e^{R_1(-u)}}{2d} \int_0^u R_2 e^{-R_2 t} dt du \\
&= 1 + \frac{e^{-2dR_1}}{2d(R_1 - R_2)} + \frac{e^{-2dR_2}}{2dR_2} + \frac{e^{-2dR_2}}{2d(-R_1 + R_2)} - \frac{e^{-2d(R_1+R_2)}}{2d(R_1 + R_2)} - \frac{R_1}{2d(R_1R_2 + R_2^2)}
\end{aligned} \tag{3.21}$$

and $p_{10,3} = 1 - p_{10,4}$. The holding time cumulative distribution function, $F_{S_{10}}(t)$, is given by

$$\begin{aligned}
F_{S_{10}}(t) &= 1 - e^{-R_2 t} \int_t^{2d} \frac{1 + e^{-R_1(2d-t)} - e^{R_1(-t)}}{2d} \\
&= 1 - e^{-R_2 t} - \frac{e^{-R_2 t}}{2dR_1} - \frac{e^{-2dR_1 - R_2 t}}{2dR_1} + \frac{e^{-R_1 t - R_2 t}}{2dR_1} + \frac{e^{-R_2 t + R_1(-2d+t)}}{2dR_1} + \frac{e^{-R_2 t} t}{2d}
\end{aligned} \tag{3.22}$$

Then, the expected holding time is given by

$$\begin{aligned}
E[S_{10}] &= \int_0^{2d} t f_{S_{10}}(t) dt \\
&= \frac{1}{2dR_2^2(-R_1^2 + R_2^2)} e^{-2d(R_1+R_2)} ((R_1 - R_2)R_2 - e^{2dR_1}(R_1 - 2R_2)(R_1 + R_2) \\
&\quad - e^{2dR_2}R_2(R_1 + R_2) + e^{2d(R_1+R_2)}(R_1^2 - R_1(1 + 2dR_1)R_2 + 2dR_2^3)).
\end{aligned} \tag{3.23}$$

State 1 (Backoff): If the node does not probe the channel in the idle periods after successful or unsuccessful transmissions, the system will enter the backoff state. In this state, the successful probing probability (i.e. the probability of

finding the channel idle at the time of probing) is reduced because the other node's transmission could have been already started before the node probes the channel. If the node finds the channel busy, the system will make a self-transition to this state. Although the probability of finding the channel idle depends on the previous state, we assume it is independent of the previous states and express the successful probing probability as

$$p_{1,2} = \frac{\frac{1}{R_2}}{\frac{1}{R_2} + 1} \quad (3.24)$$

which is the ratio of the expected waiting time over whole time. The expected holding time in this state is

$$E[S_1] = \frac{1}{R_1} \quad (3.25)$$

and $p_{1,1} = 1 - p_{1,2}$.

State 2 (Vulnerable Transmission): If the node finds the channel idle at State 1, it starts a transmission. This transmission will be vulnerable to other node's transmission from the beginning since it does not start immediately after a transmission. So, probability of transition from State 2 to State 3 and 4 can be written as

$$p_{2,3} = e^{-R_2 2d} \quad p_{2,4} = 1 - e^{-R_2 2d}. \quad (3.26)$$

Then, the holding time distribution in State 2 is given by

$$f_{S_2}(t) = \begin{cases} R_2 e^{-R_2 t} & \text{if } t < 2d, \\ e^{-R_2 2d} & \text{if } t = 2d, \\ 0 & \text{o.w.} \end{cases} \quad (3.27)$$

Then, the expected holding time at State 2 can be written as

$$E[S_2] = \int_0^{2d} t R_2 e^{-R_2 t} dt + 2d e^{-R_2 2d} = \frac{1 - e^{-R_2 2d}}{R_2}. \quad (3.28)$$

Throughput Expression: The transition matrix of the jump-chain of the

semi-Markov model shown in Fig. 3.1 is given by

$$P = \begin{pmatrix} p_{1,1} & p_{1,2} & 0 & 0 & 0 & 0 & 0 & 0 & 0 & 0 \\ 0 & 0 & p_{2,3} & p_{2,4} & 0 & 0 & 0 & 0 & 0 & 0 \\ 0 & 0 & 0 & 0 & 1 & 0 & 0 & 0 & 0 & 0 \\ 0 & 0 & 0 & 0 & 0 & 0 & 0 & 1 & 0 & 0 \\ p_{5,1} & 0 & 0 & 0 & 0 & p_{5,6} & 0 & 0 & 0 & 0 \\ 0 & 0 & 0 & 0 & 0 & 0 & 1 & 0 & 0 & 0 \\ 0 & 0 & p_{7,3} & p_{7,4} & 0 & 0 & 0 & 0 & 0 & 0 \\ p_{8,1} & 0 & 0 & 0 & 0 & 0 & 0 & 0 & p_{8,9} & 0 \\ 0 & 0 & 0 & 0 & 0 & 0 & 0 & 0 & 0 & 1 \\ 0 & 0 & p_{10,3} & p_{10,4} & 0 & 0 & 0 & 0 & 0 & 0 \end{pmatrix}. \quad (3.29)$$

The steady-state probability distribution of the jump chain with a transition matrix P is a 1x10 vector, π , and it can be obtained by solving

$$\begin{aligned} \pi &= \pi P \\ \sum_i \pi_i &= 1. \end{aligned} \quad (3.30)$$

since the stationary probability vector, π , remains same despite the multiplication of the transition matrix. Let T_1 and T_2 denote throughputs of node 1 and node 2, respectively. Since the duration of a successful transmission is 1 and π_3 gives the successful transmission probability, T_1 can be written as

$$T_1(R_1, R_2, d) = \frac{\pi_3}{\sum_i \pi_i E[S_i]}. \quad (3.31)$$

Although the throughput has a closed-form expression, space limitations prevent us from presenting the full expression. The model computes the throughput very accurately as it will be shown next through numerical examples.

3.2.2 Accuracy of the Model

We evaluate the performance of the semi-Markov model for the 2-node case. The simulations are performed by a self-developed simulation software based on Java for a duration of 10^6 time units where a transmission lasts for 1 time unit.

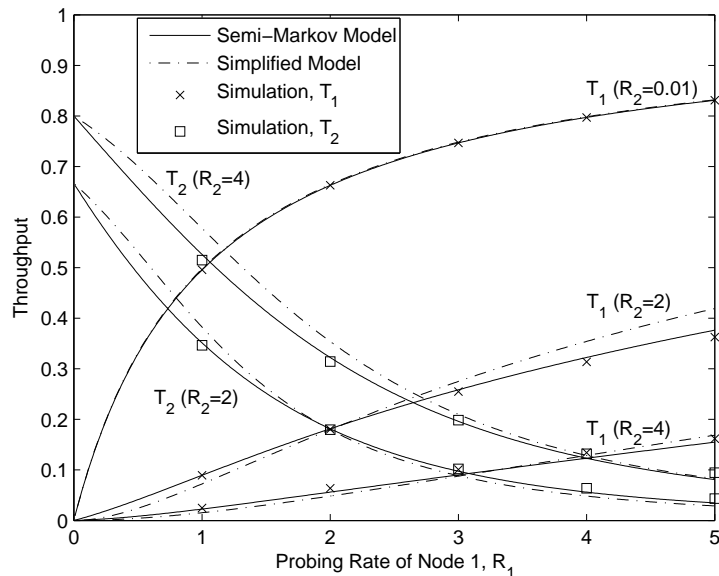


Figure 3.4: Performance of the semi-Markov model and the simplified model as R_1 changes for $d = 0.4$.

Fig. 3.4 depicts the throughputs of nodes in a 2-node network as a function of R_1 for $d = 0.4$. Different plots on the graph correspond to different values of R_2 . As it can be observed, the semi-Markov model accurately predicts the throughput. Maximum absolute error in throughput between the model and the simulations is 0.02, which shows that the assumptions made in deriving the holding time distributions of State 1 and 8 have minor effects on the accuracy of the model.

3.2.3 The Capacity Region of the CSMA Channel for $N = 2$

In this part, we provide the capacity region of the CSMA channel under non-zero propagation delay. Fig. 3.5a shows the maximum achievable throughputs of the two nodes sharing a CSMA channel as d increases. This graph is obtained by numerical maximization of the throughput function obtained by the semi-Markov model.

It is theoretically possible to achieve the full capacity region for the zero-delay channel by probing the channel at an infinite rate. In the zero-delay case, all throughput pairs $T_1 + T_2 \leq 1$ can be achieved. However, the capacity region shrinks as d increases. This reduction is more apparent if nodes probe the channel at similar rates as the wasted capacity increases due to collisions. On the contrary, total achievable throughput increases if one of the nodes dominates the channel because the dominant node experiences fewer collisions.

Fig. 3.5b shows the optimum probing rates of nodes that achieve the maximum capacity as the propagation delay changes. The graph shows that nodes should probe the channel less aggressively if the propagation delay is large because of higher collision probability. Also, it can be seen that the optimum probing rate of a node is dependent on the probing rate of the other node. Nodes should be less aggressive if both nodes try to achieve similar throughputs. On the other hand, an increase in the probing rate is beneficial only if the other node probes the channel at a low rate.

The effect of the propagation delay on the throughput can be seen in Fig. 3.6 for symmetric probing rate values. As the propagation delay increases, probing at a lower rate yields larger throughputs by reducing the collision probability. Probing at a higher rate, however, increases the throughput at low propagation delays by decreasing the channel access delay.

These results show the importance of network-awareness and probing rate adaptation when the propagation delay is non-negligible. If several nodes sharing a channel have high throughput demands, they must be cautious not to probe the channel too frequently in order not to increase collisions. The distributed probing rate adaptation algorithm proposed in [66] allows arbitrarily large probing rates because of the zero-delay assumption but simulations show that this approach is not optimal especially when the propagation delay is large.

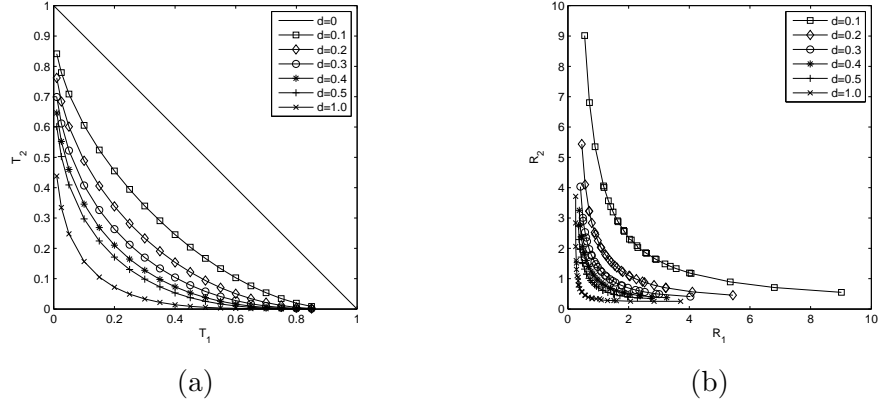


Figure 3.5: (a) The capacity region of a CSMA channel with two-nodes for different propagation delays. (b) Probing rates of nodes required to achieve the limits of the capacity region.

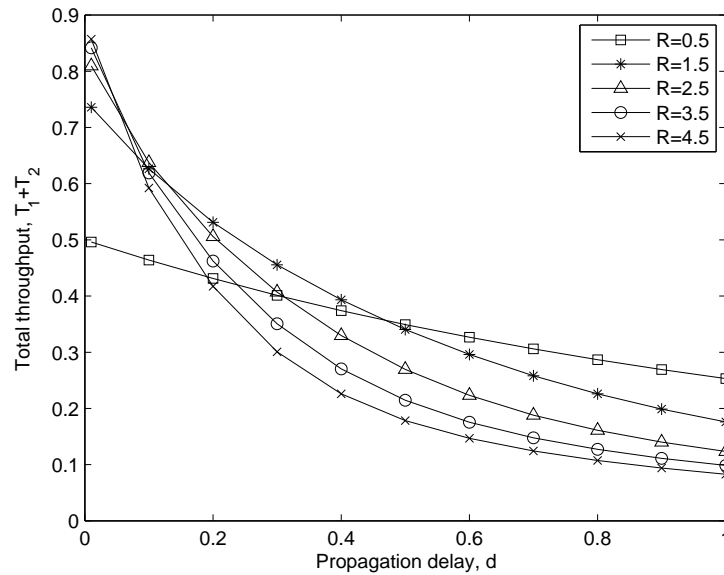


Figure 3.6: Total throughput of two nodes sharing a channel as the propagation delay increases for different $R_1 = R_2 = R$ values.

3.3 Asymptotic Capacity and Optimum Probing Rate

In this section, we obtain the optimum probing rate which achieves the maximum throughput for a CSMA channel with N nodes. We investigate how this optimum rate and maximum throughput changes as the average propagation delay, \bar{d} , and the number of nodes sharing the CSMA channel, N , increase.

For $N > 2$, modeling interactions between nodes sharing a single channel in an asynchronous fashion becomes highly complex. Each node is exposed to the transmissions of all other nodes in the channel which are also affected by the transmissions of the remaining nodes in the channel. Considering that the distances between nodes differ from each other and transmissions may start at any time, some simplifying assumptions are needed to obtain results for $N > 2$. For that reason, we assume that the throughput reduction of a node caused by each neighbor is independent of other neighbors and total throughput reduction of a node can be found by multiplying individual throughput reductions stemming from each neighbor. Despite a reduction in accuracy, this approximation allows us to derive a simple expression for the channel throughput which describes how total maximum throughput and the optimum probing rate scales with \bar{d} and N . Numerical results given at the end of this section show that the inaccuracy resulting from the above independence assumption is small and the proposed asymptotic throughput and optimum probing rate functions accurately match with the simulation results.

Next, we model the throughput reduction caused by a single neighbor of a node due to the propagation delay.

3.3.1 Throughput Reduction Caused by a Single Neighbor

If the propagation delay between two nodes is 0, throughput of node 1 is [98]

$$T_1(R_1, R_2, 0) = \frac{R_1}{1 + R_1 + R_2}. \quad (3.32)$$

To single out the effect of propagation delay, we decompose $T_1(R_1, R_2, d)$ into two parts:

$$T_1(R_1, R_2, d) = T_1(R_1, R_2, 0)g_1(R_1, R_2, d) \quad (3.33)$$

where g_1 represents the reduction in the throughput caused by the propagation delay due to a neighbor at distance d and it can be obtained by dividing the throughput found using the semi-Markov model to the zero-delay throughput. In order to obtain a simplification for g_1 , we first investigate how g_1 changes with respect to R_1 , R_2 and d using the proposed semi-Markov model. The dependence of g_1 on d is intuitive: $g_1(R_1, R_2, 0) = 1$ because there are no collisions, while g_1 decreases as d increases since larger propagation delay results in higher collision probability. However, the dependences of g_1 on R_1 and R_2 are more complicated. Fig. 3.7 shows how g_1 changes with respect to R_1 and R_2 for $d = 0.3$. The

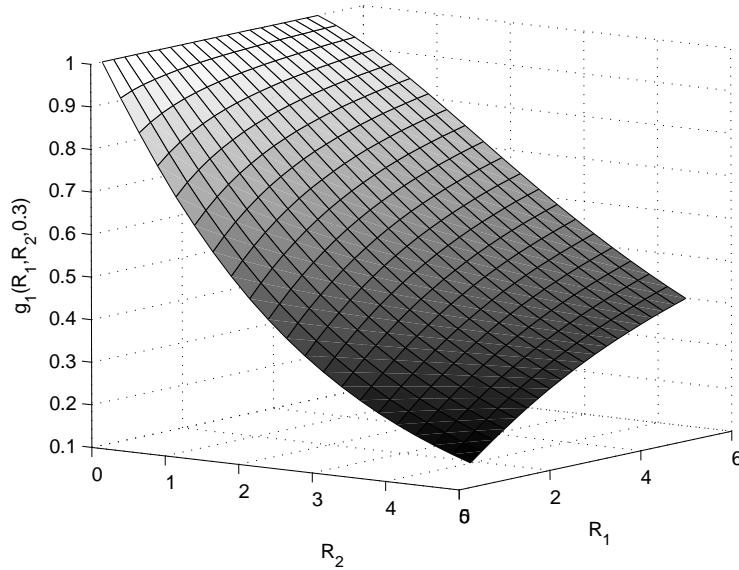


Figure 3.7: $g_1(R_1, R_2, d)$ with changing R_1 and R_2 .

following properties can be observed from this figure:

- If $R_2 = 0$, $g_1(R_1, 0, d) = 1$ independent of R_1 . Since there are no collisions if node 2 does not probe the channel, this result is expected.
- For a given $R_1 \neq 0$, g_1 decreases as R_2 increases since the ratio of collided transmissions of node 1 increases.
- For a given $R_2 \neq 0$, g_1 increases as R_1 increases. Although the number of collisions that node 1 experiences increases with its probing rate, the ratio of its successful transmissions to its attempted transmissions increases, resulting in an increase in g .

We propose the following functional form in order to approximate g_1 , which satisfies all of the above conditions

$$\tilde{g}_1(R_1, R_2, d) = \frac{1}{1 + k \frac{R_2^b d^c}{R_1^a}} \quad (3.34)$$

where a , b , c and k are positive parameters representing the effect of several variables on g_1 . We applied a least squares fit with integer values for a , b and c and obtained an approximate function which is given by

$$\tilde{g}_1(R_1, R_2, d) = \frac{1}{1 + k \frac{R_2^2 d}{R_1}} \quad (3.35)$$

where $k = 1.53$. So, an approximation to T_1 is given by

$$\tilde{T}_1(R_1, R_2, d) = \frac{R_1}{1 + R_1 + R_2} \frac{1}{1 + k \frac{R_2^2 d}{R_1}}. \quad (3.36)$$

The performance of this simplified function is given in Fig. 3.4. Although this simplification is not as accurate as the semi-Markov model, the maximum absolute error in the throughput is limited to 0.06. Using this model, we will now derive the asymptotic capacity and the optimum probing rate.

3.3.2 Derivation of the Asymptotic Capacity and Optimum Probing Rate

Let R represent the probing rate of all nodes. If there is no propagation delay in the channel, there are no collisions. Since all nodes probe the channel at exponentially distributed intervals, neighbors of a node behave as a single node. Hence, the throughput of a node is given by $T_1(R, (N-1)R, 0)$ where $(N-1)R$ represents the total probing rates of all other nodes. For the non-zero propagation delay case, we include the effect of each neighbor as if its effect in reducing the throughput of a node is independent from other nodes. We multiply the zero-collision throughput by the individual collision reductions $g_1(R, R, \bar{d})$ using the average distance for all nodes. Then, the total throughput of all nodes, $T^A(\cdot)$, can be written as

$$T^A(R, \bar{d}, N) = NT_1(R, (N-1)R, 0)[g_1(R, R, \bar{d})]^{N-1}. \quad (3.37)$$

where $g_1(R, R, \bar{d})$ is the throughput reduction of a node caused by another node if these two nodes were the only nodes sharing the channel. Using (3.35), the total throughput is approximated as

$$T^A(R, \bar{d}, N) \approx \tilde{T}^A(R, \bar{d}, N) \triangleq N \frac{R}{1 + NR} \left(\frac{1}{1 + kR\bar{d}} \right)^{N-1}. \quad (3.38)$$

The first derivative of the throughput function has a single positive root giving the optimum rate, R^* , which maximizes the throughput, \tilde{T}^A , as given by

$$R^*(\bar{d}, N) = \frac{2}{k\bar{d}(N-2) + \sqrt{k\bar{d}}\sqrt{k\bar{d}(N-2)^2 + 4(N-1)N}}. \quad (3.39)$$

Note that R^* decreases with $1/N$ as N goes to infinity. The limit of the total optimum network probing rate achieved by all nodes as N goes to infinity can be written as

$$R^A(\bar{d}) \triangleq \lim_{N \rightarrow \infty} NR^*(\bar{d}, N) = \frac{2}{k\bar{d} + \sqrt{k\bar{d}}(4 + k\bar{d})}. \quad (3.40)$$

$R^A(\bar{d})$ can be bounded from below and above as given by

$$\frac{1}{k\bar{d} + \sqrt{k\bar{d}}} \leq R^A(\bar{d}) \leq \frac{1}{k\bar{d}}. \quad (3.41)$$

According to (3.41), the total optimum network probing rate decreases faster than \bar{d}^{-1} for large N .

Maximum achievable throughput by a single node can be obtained by substituting (3.39) into (3.38). The limit of the total capacity achieved by all nodes as the number of nodes goes to infinity can be written as

$$c(\bar{d}) \triangleq \lim_{N \rightarrow \infty} \tilde{T}^A(R^*, \bar{d}, N) = \frac{2e^{-\frac{2k\bar{d}}{k\bar{d} + \sqrt{k\bar{d}(4+k\bar{d})}}}}{2 + k\bar{d} + \sqrt{k\bar{d}(4+k\bar{d})}} \quad (3.42)$$

and $c(\bar{d})$ can be upper and lower bounded as

$$\underline{c}(\bar{d}) \triangleq \frac{e^{-1}}{1 + k\bar{d} + \sqrt{k\bar{d}}} \leq c(\bar{d}) \leq \frac{e^{-\frac{1}{1 + \frac{1}{\sqrt{k\bar{d}}}}}}{1 + k\bar{d}} \triangleq \bar{c}(\bar{d}). \quad (3.43)$$

Since

$$\lim_{\bar{d} \rightarrow \infty} \frac{\bar{c}(\bar{d})}{\underline{c}(\bar{d})} = 1, \quad (3.44)$$

these bounds are asymptotically tight as $\bar{d} \rightarrow \infty$. Since the dominant term in both bounds is \bar{d}^{-1} , the model predicts that the total capacity decreases with \bar{d}^{-1} for large N . Fig. 3.8 depicts these bounds along with the total capacity as a function of \bar{d} for different number of nodes. As N increases, the total capacity curve falls between the upper and lower bounds.

We now evaluate the accuracies of the total optimum probing rate and the asymptotic capacity expressions given by (3.40) and (3.42), respectively. We performed simulations for $N = 10, 25, 50$ and 100 by uniformly distributing nodes over a circular area whose size is determined in order to satisfy the desired average delay, \bar{d} . For each N , we conducted simulations for $\bar{d} = 0.1, 0.2, 0.3, 0.4$ and 0.5 . For each N and \bar{d} combination, we simulated 10 different topologies and we reported the average of the results of these simulations. For each topology, we performed 50 simulations for total probing rates between 0 and 5 with a resolution of 0.1 to obtain the optimum probing rate which maximizes the total network throughput. We denote this maximum network throughput as the network capacity. For $N = 2$, we simulated a single topology with 2 nodes that are separated by \bar{d} for each value of the probing rate.

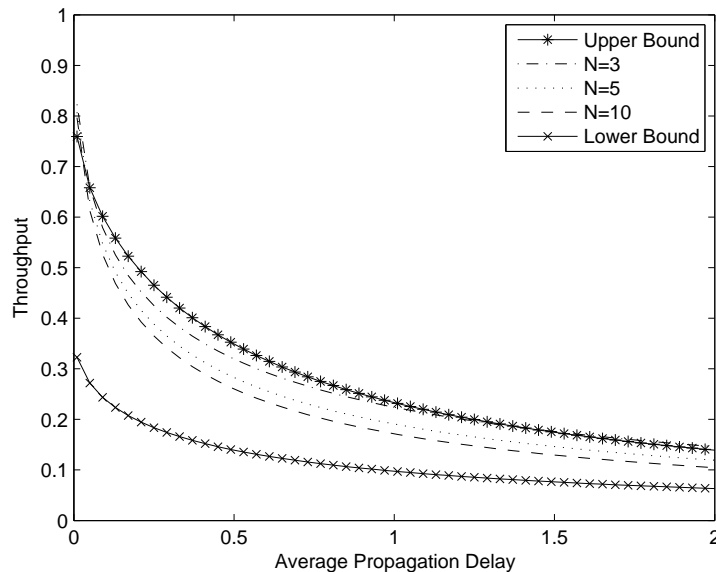


Figure 3.8: Comparison of the total network throughput as a function of \bar{d} for different values of N along with the lower and upper bounds.

The network capacity obtained by simulations for different N is plotted as \bar{d} increases in Fig. 3.9. The proposed asymptotic capacity expression given by (3.42) is also depicted. For large N , the capacity of the network approaches to the proposed asymptotic capacity. These results suggest that the capacity of the network does not degrade indefinitely as the number of nodes increases. Naturally, however, the individual throughputs of nodes degrade with $1/N$ as nodes join the network.

Fig. 3.10 presents the optimum total probing rate obtained by simulations for different values of N as \bar{d} increases. The asymptotic optimum total probing rate given by (3.40) is also depicted. Our analysis indicates that the optimum total probing rate converges to an asymptotic value for large N for a given \bar{d} . So, the nodes have to reduce their probing rates in proportion with $1/N$ as a node enters the network to keep the total probing rate in the network constant.

These results indicate that the proposed asymptotic optimum probing rate and the capacity expressions successfully match with the simulation results for large N . The independence assumption made in deriving these expressions does

not result in a significant inaccuracy.

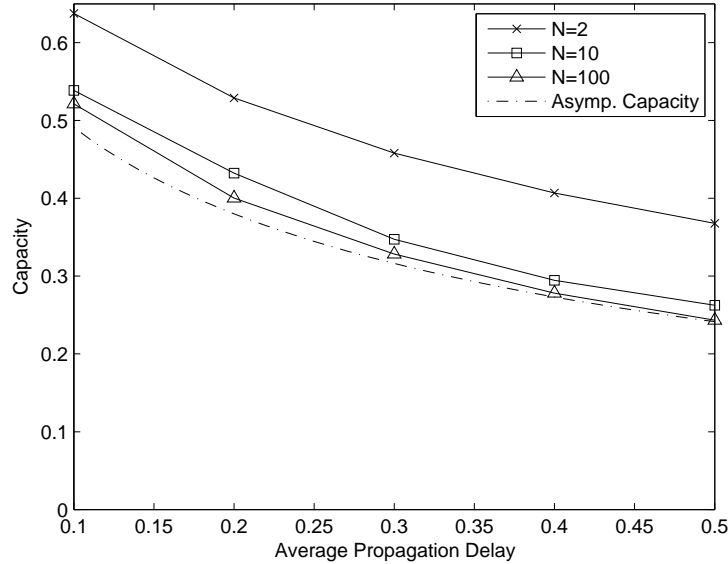


Figure 3.9: The capacity of the network as \bar{d} increases. The asymptotic capacity is plotted using (3.42).

3.4 Improving Short-term Fairness in a CSMA channel with non-negligible propagation delay

In a CSMA channel with non-negligible propagation delay, a node stays exposed to a completed transmission after the transmitting node finishes the transmission. For that reason, the transmitting node finds the channel idle for some extra duration after a completed transmission so this node can start a new successive transmission if it probes the channel within this interval, i.e., while the channel is in State 5 or in State 8 in the semi-Markov model presented in Section 3.2. This opportunity may impair the short-term fairness of the CSMA link by allowing a node to transmit successively several times. In this section, we investigate the extent of unfairness caused by successive transmissions and propose a method to reduce the short-term unfairness.

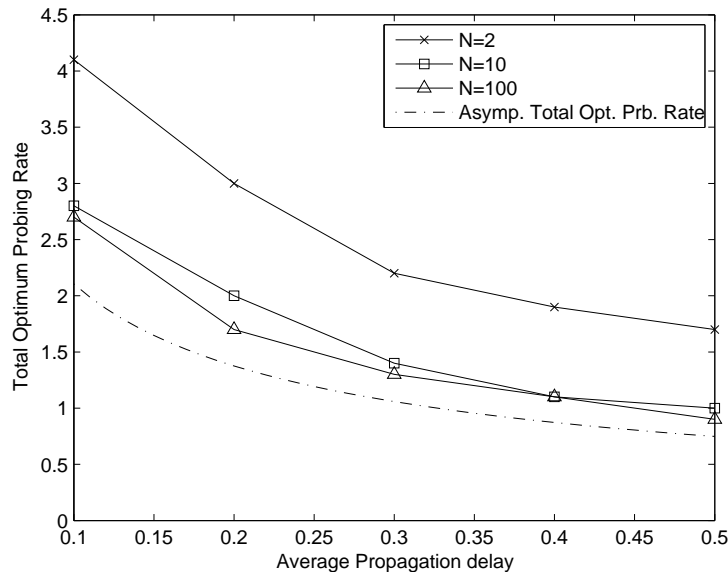


Figure 3.10: Total optimum probing rate in the network as \bar{d} increases. Asymptotic total optimum probing rate is plotted using (3.40).

In the proposed method, the probing rate of a transmitting node is reduced after a transmission, so that the transmitting station has a lower probability of capturing the channel. This back-off mechanism corresponds to reducing the probing rate of the node after completing a transmission when the node is in States 5 or 8 in the semi-Markov CSMA model. The reduction is performed both after a successful transmission and a collided transmission, since the node cannot immediately know whether the completed transmission is successful at the end of its transmission.

As the short-term fairness metric, we use the mean number of successive transmissions that a node makes when it captures the channel [72]. The throughput performance of the proposed method can be evaluated by making modifications on the analytical model presented in Section 3.2. However, we resort to simulations in this section since it is not possible to obtain the mean number of successive transmissions from the model due to its memoryless property.

We simulated N nodes sharing a CSMA channel with a propagation delay of d for $N = 2, 10$ and 100 . For $N = 2$, the two nodes are placed with a distance d

between them and, for $N = 10$ and 100 , they are distributed uniformly inside a circle so that the average distance between nodes is d . In the back-off mechanism, the probing rate of a node is reduced by b times ($b \geq 1$) after each transmission. The case $b = 1$ corresponds to the pure CSMA case where the transmitter does not reduce its probing rate. We obtained the maximum achievable throughput for each values of b , $b = 1, 2, 4, 10$, which maximizes over all possible values of the probing rate. The mean number of successive transmissions are reported at the maximum throughput. Note that the ideally fair mechanism is a TDMA-like channel sharing where the nodes take turns to transmit in which case the mean number of successive transmissions is one. Also note that the successive transmission probability of a node in a fair random access mechanism is $\frac{1}{N}$ which results in $\frac{N}{N-1}$ successive transmissions for a node on the average.

Figs. 3.11 and 3.12 plot the maximum throughput and the mean number of successive transmissions for different values of b and N as d increases. The short-term unfairness problem is more apparent for $N = 2$ as it becomes less significant for larger N since the mean number of successive transmissions approaches to one. For $N = 2$, the fairness improves as b increases. As b increases, the maximum achievable throughput slightly increases for small propagation delays while the throughput slightly reduces for larger propagation delays. For $N = 10$ and 100 , the short-term unfairness problem is insignificant because some of the randomly placed nodes are close to the transmitting node for large N and these nodes are exposed to the transmission of a node only for a short duration. Yet, the number of successive transmissions reduces as b increases without a degradation in the throughput. For all N , the fairness degrades as d increases because the duration that other nodes are exposed to a transmission increases and thus the probability that the transmitting node starts a successive transmission increases.

We have evaluated the fairness and throughput performance of the back-off mechanism under saturated traffic conditions and we observe that the back-off mechanism improves the short-term fairness without degrading throughput. The evaluation of the mechanism for a heterogeneous traffic load is a subject of future study. In this case, the performance of the back-off mechanism may not be as desirable as in the case of the saturated traffic. For example, when one of the

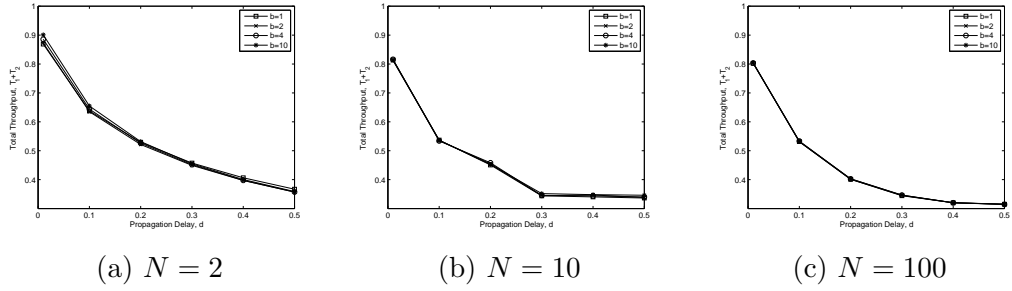


Figure 3.11: Maximum throughput achieved by the back-off scheme.

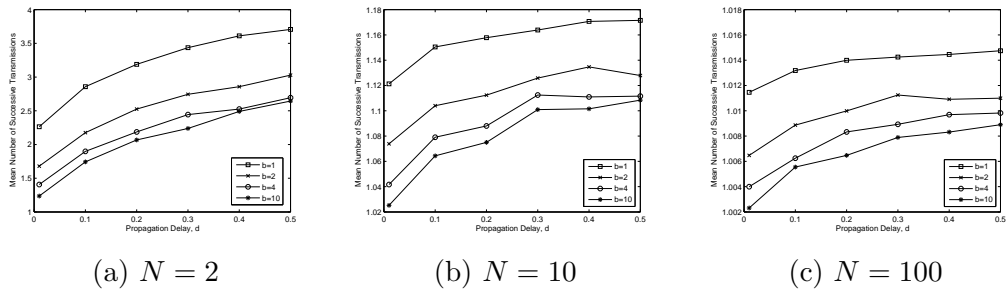


Figure 3.12: Mean number of successive transmission achieved by the back-off scheme.

nodes has traffic and the other nodes are idle, the back-off mechanism will cause an under-utilization of this node by reducing the probing rate of this node after each transmission.

3.5 Comparison of the proposed CSMA model with IEEE 802.11b channel access

In this section, we evaluate the performance of the CSMA/CA channel access scheme of the IEEE 802.11 protocol in terms of the capacity and the optimum probing rate using simulations. Although the CSMA/CA MAC scheme is different than the pure CSMA scheme modeled in this paper, we wanted to see whether conclusions similar to the ones drawn in earlier sections for the pure CSMA model can be obtained for the 802.11 channel access scheme. We simulated a network scenario where saturated bidirectional User Datagram Protocol (UDP) traffic

exists between two nodes that are connected via a 802.11b link with a distance d . We performed simulations using the ns-2 network simulator [99]. In order to make the comparison more compatible, we disabled the RTS/CTS mechanism of the 802.11 MAC in the simulations. We selected the packet length as 2300 bytes which is close to the maximum frame length in the 802.11 standard. The transmission power of the transmitters are selected sufficiently high so that packets are lost only due to contention. We adjusted the acknowledgement timeout value of the 802.11 standard according to the propagation delay to prevent premature timeouts.

In order to make an appropriate comparison, we calculated the throughput as the ratio of time spent for successful transmissions to total simulation time and we normalized the propagation delay with respect to the packet transmission time. Fig. 3.13 presents the throughput for the 802.11 protocol along with the optimum throughput obtained from the analytical model proposed for the pure CSMA as the propagation delay increases. Although the throughput of the 802.11 protocol changes in parallel with respect to the optimum throughput obtained for the pure CSMA model, it is below the optimum throughput because of the acknowledgement mechanism. Even when the propagation delay is negligible, the maximum achievable throughput of the CSMA/CA MAC scheme is 0.75 due to the dead period during the transmission of the acknowledgment frame and due to the minimum contention window size which limits the maximum probing rate of the 802.11 MAC.

We also compared the proposed optimum rate analysis against the back-off mechanism of the 802.11 protocol. In addition to the random back-off duration, the inter-transmission time between transmissions in the 802.11 protocol includes the waiting time for the acknowledgment and the DCF Interframe Space (DIFS) duration. Because of these fixed durations, the 802.11 random back-off duration is not exactly comparable with the random probing interval of the pure CSMA mechanism considered in this paper. We instead compared the total waiting time between the transmissions in the 802.11 protocol against the total waiting time between transmissions in the pure CSMA mechanism. Fig. 3.14 presents the normalized waiting time between transmissions for the 802.11 protocol and for the pure CSMA operating at the proposed optimum rate. Waiting time between

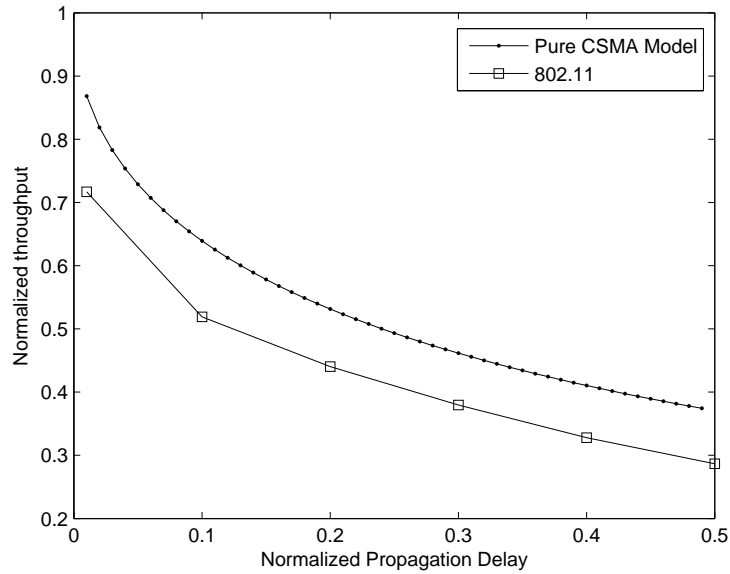


Figure 3.13: Throughput of the IEEE 802.11 MAC and the optimum throughput of the pure CSMA model.

transmissions are higher in the 802.11 protocol but it behaves in a parallel fashion to the optimum case. The fixed acknowledgment (ACK) timeout duration incorporated in the 802.11 protocol can be accounted for this difference.

It can be concluded that the 802.11 MAC protocol performs in a parallel manner with the proposed model for the pure CSMA in terms of the optimum probing rate and throughput as the propagation delay increases. Although the 802.11 standard adapts the probing rate using the collision information without the knowledge of the propagation delay, it performs considerably well for the simulated two-node scenario. In order to improve the performance of the 802.11 protocol under large propagation delays, the acknowledgment mechanism can be eliminated; but a new probing rate adaptation mechanism has to be developed in this case.

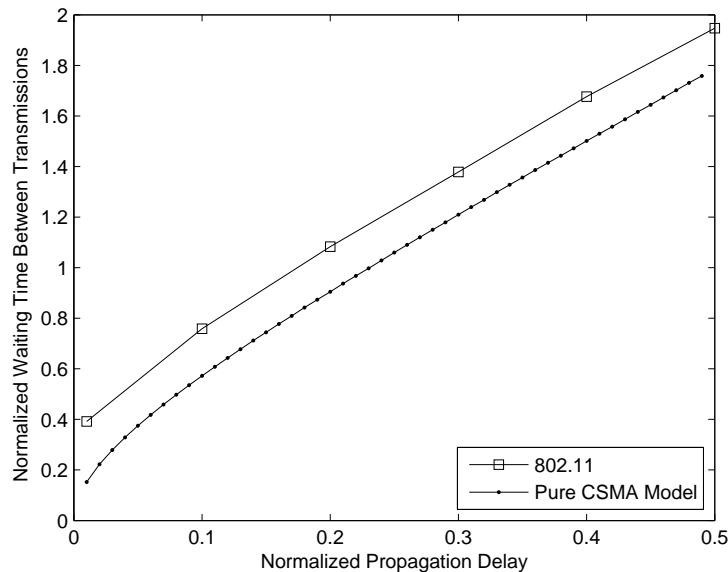


Figure 3.14: Mean waiting times between transmissions of the IEEE 802.11 MAC and the pure CSMA model operating at the optimum probing rate.

3.6 Conclusions

We modeled the capacity of a single-hop CSMA network when the propagation delays are comparable with the transmission delay. Although large propagation delays are not typical for local area networks, underwater acoustic networks and wireless regional area networks suffer from such propagation delays.

We presented a semi-Markov model for the 2-node case and we derived the capacity and the optimum probing rate expressions for a large number of nodes using this model. We examined how nodes should adapt their aggressiveness in such a CSMA channel. We derived the optimum symmetric rate expression as a function of the average propagation delay, \bar{d} , and the number of nodes, N . The optimum probing rate for each node decreases asymptotically with $1/N$ as N increases. On the other hand, the total optimum probing rate achieved by all nodes in the network decreases faster than \bar{d}^{-1} for large N .

We have also derived the asymptotic total channel capacity for large networks. According to the proposed model, the total capacity at the optimum rate is

asymptotically proportional to \bar{d}^{-1} as the number of nodes, N , increases. Despite the increasing number of collisions between nodes, the achieved capacity does not converge to 0 no matter how large the number of nodes in the network is if all nodes in the network probe the channel at the optimum rate.

We have also studied the fairness of the CSMA protocol under large propagation delays and analyzed a back-off mechanism which improves the short-term fairness of the CSMA protocol without a throughput penalty under saturated traffic conditions.

We have compared the proposed capacity and the optimum probing rate analytical model with the performance of the IEEE 802.11b channel access scheme using a simple two-node scenario. We observed that the 802.11b performs in a similar fashion with the proposed model for the pure CSMA as the propagation delay increases although 802.11 MAC utilizes an acknowledgment mechanism.

Chapter 4

Effect of Network Density and Size on the Short-term Fairness Performance of CSMA Systems

Along with the popularity of wireless devices, the density of wireless transmitters in our daily environment increases. This dense deployment results in increased interference between transmitters. Although each transmitter only interferes with its neighbors, interfering transmitters form a large-scale loosely interacting system of transmitters. We investigate the influence of the global system parameters on the performance of the individual transmitters using the insights from the statistical physics literature.

We are mainly interested in the short-term fairness performance of such a system. Short-term fairness is defined as the fairness of the throughput distribution of a system of transmitters when it is monitored for a short-time. This property is different from the more commonly used concept of long-term fairness where the average throughput distribution of nodes are evaluated. Short-term fairness is especially important for delay-sensitive applications such as multimedia communications because starvation of nodes even for a short duration may severely impact the quality of experience.

We assume the transmitters employ carrier sense multiple access (CSMA) protocol so a transmitter can capture the channel only if its neighboring transmitters are not transmitting. We evaluate how much the short-term fairness performance depends on the properties of the large scale system. We investigate if the system size, system topology and degree of the topology influences the system performance. Although the interactions between the nodes are local, we observe that some of the global parameters of the system affects the performance of individual nodes. We also aim to characterize a throughput limit under which the CSMA system is short-term fair.

Our main contributions are as follows:

- We claim that the short-term fairness among the interacting wireless transmitters is affected by the degree of the conflict graph of these transmitters if the conflict graph is a random regular graph where each vertex has the same number of neighbors. A denser deployment results in an increase in the number of contending neighbors of a network and our results suggest that the practically useful portion of the throughput region reduces as the number of neighboring networks increases.
- We demonstrate the implications of our study on a practical city-wide Wi-Fi deployment scenario. Our results indicate that short-term fairness has to be sacrificed to improve coverage in such a system. To improve coverage, the density of the deployment has to be increased which causes the nodal degree of the system to increase. This in turn reduces short-term fairness.
- We discuss if there is a reduction in the performance of interacting networks as the system size increases. Our results suggest that there is a weak dependence on the system size if the density of deployment is kept unchanged and the deployment has a random regular conflict graph. On the other hand, the performance of networks with a grid conflict graph may severely degrade with system size if all networks operate at high throughputs.
- We highlight the results from the statistical physics and theoretical computer science literatures on the long-range dependence in physical systems

and identify a relationship between CSMA systems and physical systems. Despite the discrepancies between the physical models and the practical networking scenarios, we point out similarities between the short-term fair capacity region and the phase transition thresholds of the physical models.

The rest of this chapter is organized as follows: Section 4.1 describes the system model. We explain the short-term fairness metrics that we use in Section 4.2. A mathematical analysis of the short-term fairness of the tree topology is given in Section 4.3. Section 4.4 presents a simulation-based analysis of the tree, grid and random topologies. Section 4.5 illustrates the trade-off between short-term fair capacity and coverage for a practical Wi-Fi deployment scenario. Several observations on the relationship between the phase transitions of the hard-core model and the CSMA network are presented in Section 4.6. A summary and discussion of results are given in Section 4.7.

4.1 System Model and Studied Topologies

4.1.1 System Model

We study a system of transmitters distributed over an area. The interference relationships between these transmitters are modeled using a *conflict graph* in which each node represents a transmitter and two nodes are connected with a link if their corresponding transmitters interfere with each other. We consider two transmitters as interfering if they are in the carrier sensing range of each other. From now on, we use the terms node, transmitter and access point interchangeably throughout the chapter.

We study the idealized CSMA model which is analyzed in [98, 55, 66]. In this model, it is assumed that carrier sensing is instantaneous and always successful, which leads to a zero-collision system. Since interfering transmitters cannot be in transmission concurrently in the idealized CSMA model, the set of transmitting nodes at a given time forms an independent set of the conflict graph.

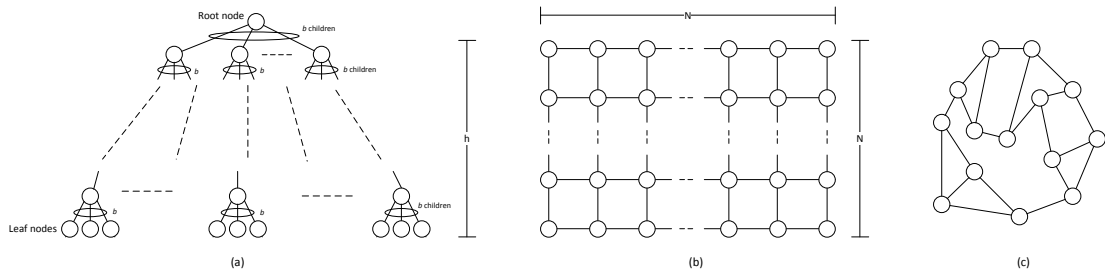


Figure 4.1: Studied Topologies. (a) The tree topology that we study. Each node has b children except leaf nodes. (b) The N by N grid. (c) A sample regular random topology with a degree of 3.

We assume that all transmitters in the system are saturated, that is, transmitters always have data to transmit. Each transmitter in the CSMA system probes the channel at random times according to a Poisson point process and starts transmission when it finds the channel idle. The mean waiting time between two consecutive probing instants, $1/\lambda$, determines the aggressiveness of a transmitter where λ is defined as the probing rate. The lengths of transmissions are exponentially distributed with mean 1.

4.1.2 Studied Conflict Graph Topologies

In this study, we analyze three different conflict graph topologies: tree, grid and random regular topologies. In urban areas, independently distributed Wi-Fi networks can be expected to form a fairly random conflict graph. However, in a large campus or corporate network, transmitters may be placed in a more structured manner which may result in a grid conflict graph topology. Although not common in practice, tree topology is suitable for mathematical analysis and it has been commonly used in deriving bounds in the statistical physics literature.

We study a tree in which every node except leaf nodes have b children as shown in Figure 4.1a. The degree of nodes in the tree is $d = b + 1$ except the leaf nodes and the root node. The height of the tree and the number of nodes in the tree are denoted by h and n , respectively. The grid topology we simulated is an N by N grid with $d = 4$ as shown in Figure 4.1b. We also generated connected random regular topologies, where each node has a degree of d , using the software

developed by Viger [100]. A random regular topology with $d = 3$ can be seen in Figure 4.1c. Short-term fairness analysis of irregular random topologies appears difficult because they typically fail to achieve long-term fairness when all nodes have the same access rate due to the inhomogeneity of the topology. Since long-term fairness is a prerequisite for evaluating the short-term fairness, we limited our study to random regular graph topologies where long-term fairness is always achieved since each node has the same degree.

We have also investigated the conflict graph of a mesh deployment of Wi-Fi access points. To cover an area with access points, it has been shown that a mesh deployment provides better coverage than a totally random deployment [101]. In such a deployment, number of conflicting neighbors of an access point is determined by the density of deployment. When the access points interfere with their nearest neighbors, the conflict graph becomes the grid topology described above. As the density increases, the conflict graph becomes a higher-degree graph. We investigate the effect of the density of deployment on short-term fairness and coverage in Section 4.5.

4.2 Short-term Fairness Metrics

4.2.1 Short-term Fairness Horizon

The first metric that we have used is the short-term fairness horizon which is explained in Section 2.3.2.1 but with a small modification. Short-term fairness horizon is originally measured in time units. However, if the probing rates of transmitters are too low, the network converges to equilibrium very slowly. This behavior results in artificially large values for the short-term fairness horizon at low probing rates. Instead of measuring time until fairness, counting the average number of transmissions per transmitter leads to a healthier comparison between different scenarios. This metric normalizes the effect of probing rate allowing a better comparison of the fairness performances at different probing rates. For that reason, we consider the number of transmissions per transmitter required to

achieve fairness as the short-term fairness horizon in this study.

4.2.2 Short-term Fair Capacity Region

For a given conflict graph, throughput of a node refers to the fraction of time that the node transmits, and the throughput region of the conflict graph refers to the collection of achievable per-node throughputs. In this study, we are mainly interested in how much of the throughput region can be achieved within the acceptable limits of short-term fairness. We define this subset of the throughput region as *short-term fair capacity region*. In order to quantify the short-term fair capacity, a short-term fairness horizon threshold has to be determined such that the network is considered short-term unfair when the short-term fairness horizon is beyond this threshold. In a study which is focused on developing a fair MAC protocol [102], the authors observed that it takes 80-140 packets per user for the IEEE 802.11 standard to become fair. Considering this result, we select 100 transmissions per node as a threshold for short-term fairness. We also used 50 transmissions per node as another threshold which corresponds to a stricter fairness requirement. However, these choices are not restrictive; the behavior of the capacity region does not significantly change with the selection of the threshold as it will be demonstrated in Section 4.4.

4.2.3 Number of successive transmissions

Another metric that can be used for measuring short-term fairness is to calculate the number of transmissions that a node makes successively as it captures the channel. This metric is closely related to the the probability of a node making a successive transmission before any of its neighbors has a chance to transmit. If this probability is high, it indicates that a node captures the channel for a long time and its neighbors starve during this period.

For a random access protocol, a successive transmission probability of $\frac{1}{d+1}$ indicates a perfectly short-term fair network where d is the number of neighbors

of the node. At the time a node finishes its transmission, it is certain that its neighbors are idle. Including the recently finished node, all of the $(d + 1)$ nodes will probe the channel after waiting for an exponentially distributed duration with mean $1/\lambda$. If the recently finished node probes the channel before all its neighbors, it is certain that it will find the channel idle and it can start another transmission. However, if one of the neighboring nodes probes the channel before the recently finished node, it may not find the channel idle because of its other neighbors. For that reason, the probability of a node to start a successive transmission is higher than the transmission probability of neighboring nodes.

Number of successive transmissions is a local measure of short-term fairness which can be computed using the statistics of a single node and its neighbors. Short-term fairness horizon, however, is a global metric which requires states of all nodes have to be taken into account. For that reason, number of successive transmissions appears to be a more tractable metric for mathematical analysis. We present an analysis of the short-term fairness of the tree conflict graph using this metric in the next section.

4.3 Mathematical Analysis for a Tree

In this section, we develop an approximate fairness model for a tree conflict graph using the successive transmission probability as the fairness metric.

We are interested in determining the probability that a node starts transmission before its neighbors after finishing its transmission. In order to evaluate the successive transmission probability of a node, we refer to Kelly's work [103] which gives the conditional probability of a node being in transmission when its parent is not transmitting as a function of probing rate. For the tree topology, let p be the probability of the child being idle given that its parent is idle. The value of this probability typically depends on the node, but for large trees nodes that are far from the leaves tend to have similar values due to symmetry. Kelly's analysis identifies a common value in the limit of an infinite tree, which serves

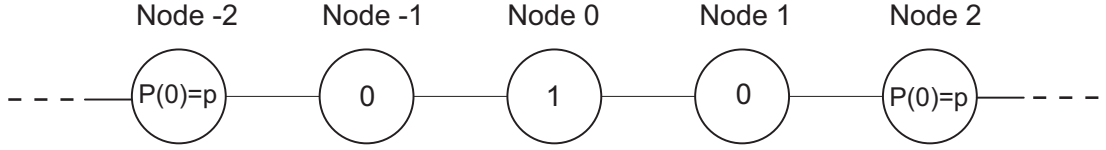


Figure 4.2: States of nodes in a line topology. Node 0 is transmitting, Node -1 and 1 are therefore idle and Node -2 and 2 are active with probability p .

as a convenient approximation for large finite trees. Namely, it is shown that p is the positive solution of $\lambda = \frac{1-p}{p^d}$ and the throughput of each node is $T = \frac{1-p}{2-p}$ when channel access rates of leaf nodes are normalized to compensate for their advantage. Although Kelly's analysis is carried out for the Cayley tree in which the root node has d children, it is extensible for the tree that we study whose root node has $d - 1$ children.

To illustrate our approach let us consider a special case of a tree with $d = 2$ which is an infinite line topology. Let Nodes -2 to 2 be adjacent nodes in this line as shown in Figure 4.2. Each node probes the channel at rate λ . Let Node 0 be at the end of its transmission. At this point, its neighbors (Nodes -1 and 1) are idle; and, Nodes -2 and 2 are idle with probability p . Node 0 has a higher chance of capturing the channel: Even if Node -1 or Node 1 probe the channel before Node 0, they may find the channel busy because Nodes -2 and 2 may be transmitting. Node 0 will probe the channel after a duration exponentially distributed with rate λ . Nodes -1 and 1 will also probe the channel after exponentially distributed durations with λ but they may find the channel busy because Nodes -2 and 2 may be in transmission with probability \tilde{p} . The probability \tilde{p} is the conditional probability of a grandchildren of a node is idle given that the node has performed a previous transmission. In this analysis, we assume $\tilde{p} = p$, so Nodes -1 and 1 have an effective probing rate of λp instead of λ . Then, the probability that Node 0 starts its transmission before Nodes -1 and 1 is given by

$$P_s = \frac{\lambda}{\lambda + 2\lambda p} = \frac{1}{1 + 2p}. \quad (4.1)$$

If we generalize this formula to a tree with a degree d , we get

$$P_s(p) = \frac{1}{1 + dp^{d-1}} \quad (4.2)$$

where p is the positive solution of

$$\lambda = \frac{1-p}{p^d}. \quad (4.3)$$

For $d > 3$, we cannot obtain p in closed form which prohibits obtaining a direct relationship between probing rate, λ , and successive transmission probability, P_s . However, it is possible to establish a relationship between throughput and successive transmission probability since $T = \frac{1-p}{2-p}$ [103]. It can be written that

$$P_s(T) = \frac{1}{1 + d\left(\frac{1-2T}{1-T}\right)^{d-1}} \quad (4.4)$$

where $0 < T < 0.5$.

At very low probing rates, the successive transmission probability of a node is independent of the global topology where it is solely determined by the degree of a node. Since all nodes have the same probing rate, the probability of a node to perform a successive transmission before its neighbor is given by

$$\lim_{T \rightarrow 0} P_s(T) = \frac{1}{d+1}. \quad (4.5)$$

At very high probing rates, however, successive transmission probability of a node converges to 1, i.e.,

$$\lim_{T \rightarrow 0.5} P_s(T) = 1. \quad (4.6)$$

$T = 0.5$ is the maximum achievable throughput by all nodes in the network because it is not possible for more than half of the nodes in the tree to be active concurrently. In this case, once a node has a chance to transmit, it tends to transmit repeatedly at successive probing instants, severely degrading short-term fairness.

The assumption of $\tilde{p} = p$ causes the proposed model to slightly deviate from simulation results which will be analyzed in Section 4.4.2.

4.4 Simulation Study

We now study the effects of several network attributes on short-term fairness. We investigate three different conflict graph topologies: tree, grid and random

regular.

4.4.1 Simulation Method

In this part, we use the short-term fairness horizon as the fairness metric. We also measure the successive transmission probability for the tree topology in order to evaluate the accuracy of proposed analysis.

We measure the short-term fairness horizon in our simulations using the following procedure: We keep a throughput counter for each node; this counter records the total throughput that the node has gained until the current time in the simulation. Using these throughput values, we repeatedly check for the Jain's index of the network as the simulation continues. If the network achieves a Jain's index of 0.95, we record the number of completed transmissions per node until that moment as the short-term fairness horizon. At this moment, we reset the counters and again wait for the network to reach a fairness index of 0.95. We sample the short-term fairness horizon 50 times by repeating this procedure and take the average of these values.

In order to measure the short-term fairness horizon, the network has to achieve a fairness index of 0.95 in the long run; that is, it must be long-term fair. To establish long-term fairness, probing rates of nodes have to be adjusted such that all nodes have the same long-term throughput. However, computing the probing rates that result in a fair equilibrium distribution is non-trivial [61]. Although there is a closed form expression for probing rates which equalizes throughputs for the tree topology [103], there is no such expression for N by N grids and random topologies.

In the simulations of grid and random topologies, we assign the same probing rate to each node and assume that they can achieve a fairness index of 0.95 in the long-run. This assumption is valid for our simulations because all simulations achieved a fairness index of 0.95. Simulating large random topologies is also of help because the effect of locally unfair throughput distributions can be balanced

in a large network.

In the tree topology, leaf nodes have an important advantage over the internal nodes; they have a single neighbor whereas internal nodes have d neighbors. For that reason, leaf nodes face less competition and they can gain higher throughputs than internal nodes. Since the leaf nodes form a large portion of nodes in the tree, the probing rates of leaf nodes have to be adjusted such that they have the same throughput with internal nodes. Using the analysis in [103], we select the probing rates such that the throughput distribution is long-term fair.

4.4.2 Tree Topology

Figure 4.3a depicts the short-term fairness horizon for tree topologies with different values of d as a function of λ . At the same probing rate, short-term fairness horizon of higher degree topologies is shorter than lower degree topologies. However, nodes in the higher-degree networks need to probe the channel at a higher rate than the nodes in the lower-degree networks in order to achieve the same throughput. For that reason, comparing the performance of topologies with different degrees at the same probing rate is not fair.

The relationship between fairness and throughput is more relevant for our purposes than the relationship between fairness and probing rate because we are interested in characterizing a practically useful throughput region. Figure 4.3b shows how short-term fairness horizon changes as a function of throughput. At low throughputs, short-term fairness horizon does not depend on d . As the throughput increases, there is a sharp increase in the short-term fairness horizon. The maximum value of the throughput where short-term fairness can be satisfied decreases as d increases. The reason behind this behavior is that the nodes are more dependent on each other in densely connected networks at high throughputs. When the average throughput in the network is low, transmission of a node is rarely prevented by its neighbors. So, nodes behave almost independently and short-term fairness does not depend on the global properties of the system such as the degree. As the probing rates increase, dependence between

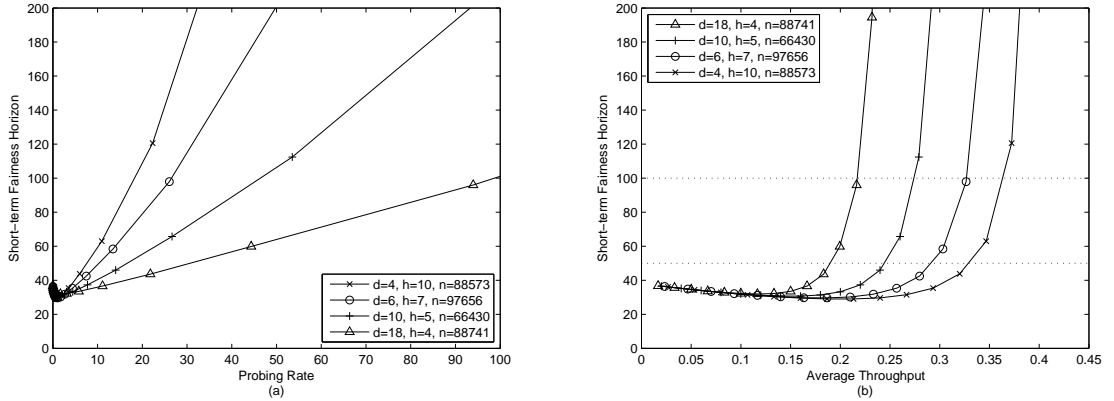


Figure 4.3: Short-term fairness horizon of the tree topology with different degrees. (a) as the probing rate increases (b) as the average throughput increases. Short-term fairness thresholds of $Th=50$ and 100 transmissions per node are also shown as horizontal dashed lines.

nodes increases. A node frequently finds the channel busy since at least one of its neighbors is already transmitting. This phenomenon is more apparent in higher degree networks because nodes are more densely connected. So, the nodes in higher-degree topologies starve for a long time at high probing rates that are required for achieving high throughputs.

This relationship between the fairness and the degree of the tree demonstrates an important limitation of random access networks working at high throughput. A centralized scheduler can provide a throughput of 0.5 to all nodes in the tree independent of the degree by alternating transmissions between nodes at even and odd distances to the root node. Since the transmissions are alternated between nodes at each time step, short-term fairness of this scheduler is optimum. On the other hand, fairness of the CSMA network significantly depends on the degree and average throughput of the network.

Since short-term fairness is significantly affected by the degree and throughput, it is natural to ask how much of the throughput region can be achieved within the acceptable limits of short-term fairness. We have previously defined this practically useful throughput limit as the *short-term fair capacity region*. The short-term fairness thresholds of 50 and 100 transmissions are depicted as horizontal lines in Figure 4.3b. Throughputs corresponding to these thresholds

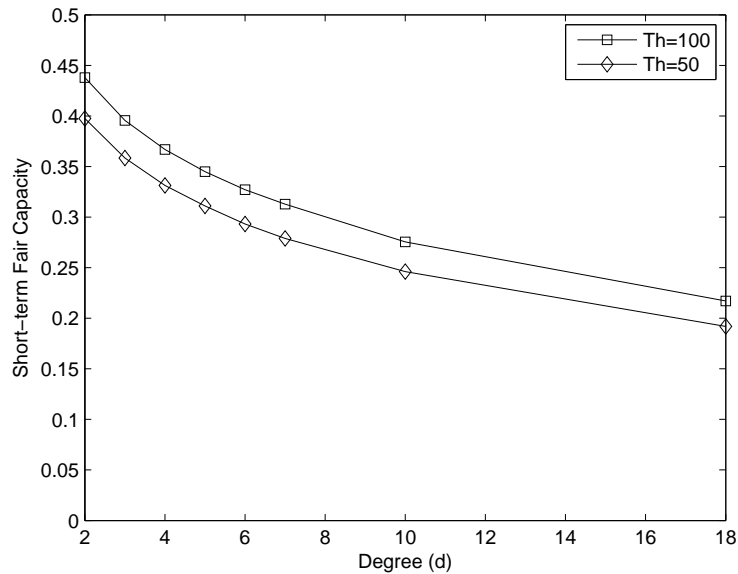


Figure 4.4: Short-term fair capacity of the tree topology as the degree increases.

are computed using interpolation and plotted in Figure 4.4 where the short-term fair capacity of a tree network under CSMA is plotted as d increases. In this plot, degrees omitted from Figure 4.3b are also included to give a better picture of the short-term fair capacity region. For $d = 2$, the network can achieve a throughput of 0.44 in a short-term fair manner for a threshold of 100. However, for $d = 18$, the maximum throughput which can be obtained under short-term constraints drops to 0.22.

Figure 4.5 presents simulation results for trees with different heights but with the same number of children, $b = 3$, i.e. $d = 4$ for internal nodes. The tree with $h = 1$ has a very good fairness performance since it consists of only 4 nodes. For very small networks consisting of a few nodes, the number of nearby nodes which influence the state of a node is very small. As extra nodes are added to the neighborhood of a node, the number of transmitters affecting the state of the transmitter increases. This increase results in a decrease in short-term fairness. However, as the network grows beyond the neighborhood, the influence of the newly added nodes declines gradually. For that reason, short-term fairness becomes almost independent of the network size for sufficiently large topologies, i.e., short-term fairness does not degrade further once the network size becomes

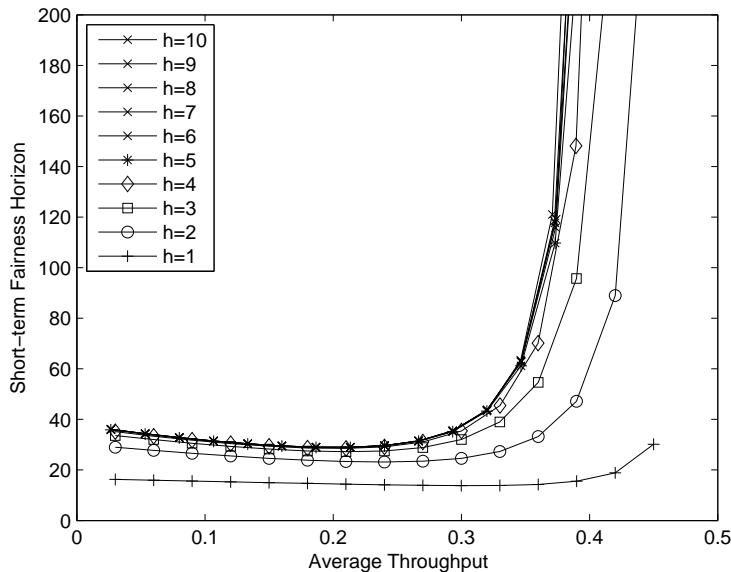


Figure 4.5: Short-term fairness horizon of the tree topology as the height of the tree increases. Internal nodes in all trees have $d = 4$

sufficiently large.

Number of Successive Transmissions

We now present the mean number of successive transmissions of a node and compare the results with the analysis given in Section 4.3. We collected transmission statistics of each node during the simulations presented in the previous part. Statistics of only internal nodes are used because leaf nodes have only a single neighbor resulting in different transmission statistics from internal nodes.

We compare fairness performances of tree topologies with different degrees using this new metric. Figure 4.6 plots the mean number of successive transmissions of a node as the throughput increases along with the mean number of transmissions computed using the proposed fairness model using a binomial assumption. The proposed model gives a closed-form relationship between the successive transmission probability and throughput as given by (4.4). The successive transmission probability is computed using the assumption that probability

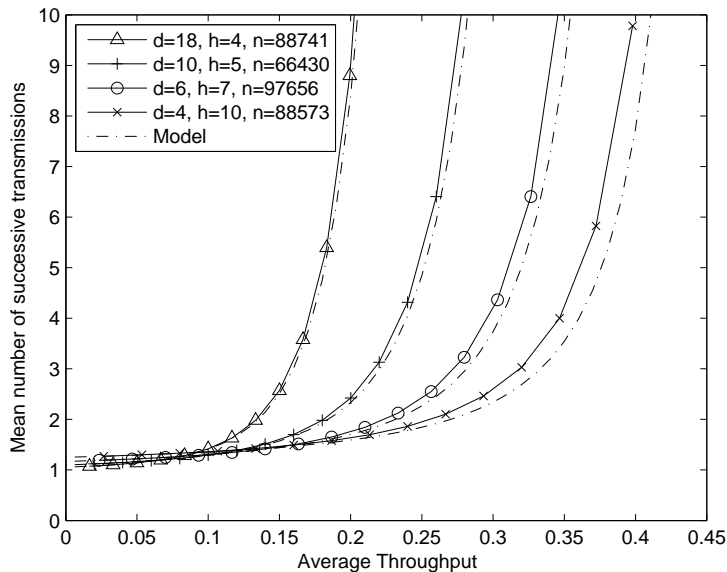


Figure 4.6: Mean number of successive transmissions as the average throughput increases. Dashed lines plot the results of the proposed model.

of the secondary neighbors of a node being idle is independent of the number of its previous transmissions. Since this assumption gets closer to reality as d increases, the model is very accurate especially for higher degree trees. At a very low throughput, the successive transmission probability of a node is lower for a higher degree graph as given by (4.5). However, as the throughput increases, the higher degree graphs show worse short-term fairness because of the increased dependence between nodes.

Figure 4.6 is very similar to Figure 4.3b which shows that both metrics, short-term fairness horizon and number of successive transmissions, characterize the short-term fairness behavior in a similar manner. Since behaviors of both metrics resemble, we do not present the successive transmission probability statistics in the rest of this paper.

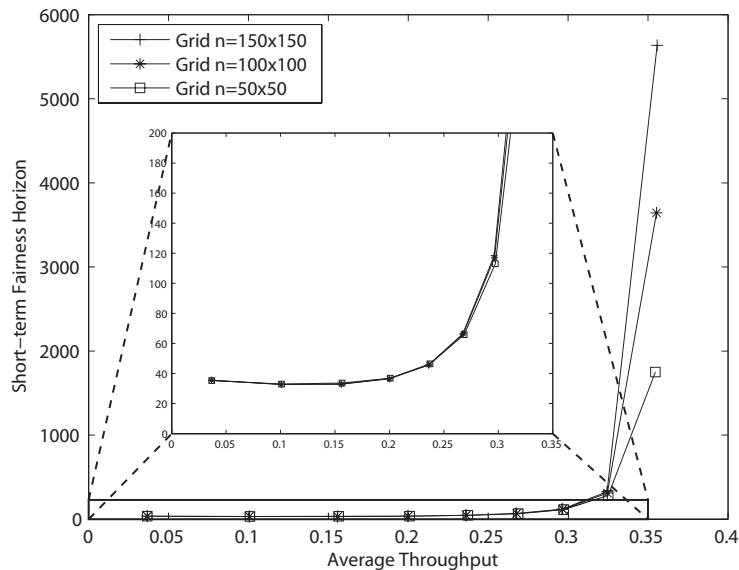


Figure 4.7: Short-term fairness horizon of the grid topology for three different dimensions.

4.4.3 Grid Topology

We now examine the short-term fairness properties of the grid topology. Since the degree of the grid topology is fixed at 4 for internal nodes, the only parameter that we investigate is the network size. We simulated the grid topology for $n=50 \times 50$, 100×100 and 150×150 .

Figure 4.7 shows how short-term fairness of the grid topology changes as the average throughput in the network increases. It may not be possible to operate the CSMA protocol under reasonable short-term fairness requirements above an average throughput of 0.35 because the short-term fairness horizon reaches extremely high values. At such high throughputs, short-term fairness of the grid topology also depends on the network size. At a throughput of 0.35, short-term fairness horizon of the 100×100 grid network is twice of the horizon of the 50×50 grid. At this throughput, short-term fairness horizon of all simulated topologies is larger than 1000 transmissions which can be considered unacceptable for practical purposes.

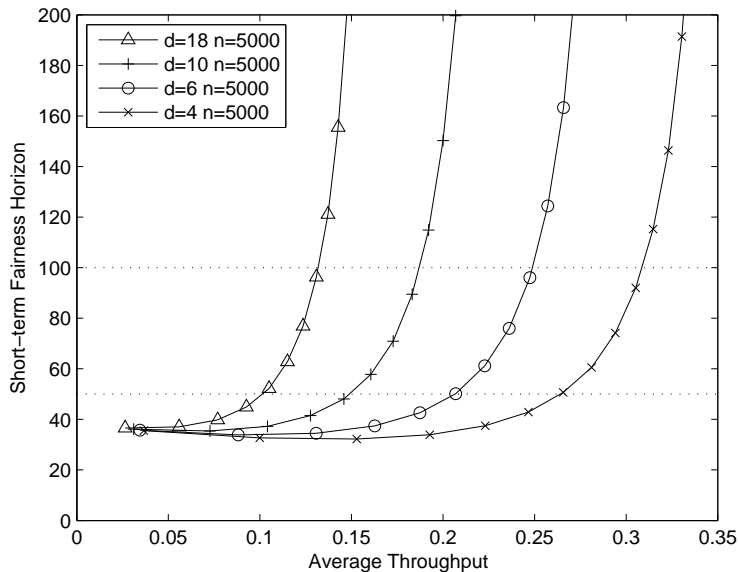


Figure 4.8: Average short-term fairness horizon of randomly generated topologies with different degrees as the average throughput increases. Short-term fairness thresholds of $Th=50$ and 100 transmissions per node are also shown as horizontal dashed lines.

Grid topology exhibits undesirable short-term fairness properties mainly because it has two maximal independent sets which correspond to the blacks and whites of the checkerboard pattern. The throughput distribution of the network favors either of these maximal independent sets at high probing rates. Since these maximal independent sets have no elements in common, transition from one to the other occurs rarely at high probing rates resulting in long starvation periods for some nodes.

4.4.4 Random Topology

We now investigate the short-term fairness properties of randomly generated contention graph topologies. For each d , 10 random topologies each having 5000 nodes are generated as described in Section 4.1.2. Short-term fairness horizon of these topologies are computed for increasing throughputs and averaged to obtain a short-term fairness horizon plot for each d .

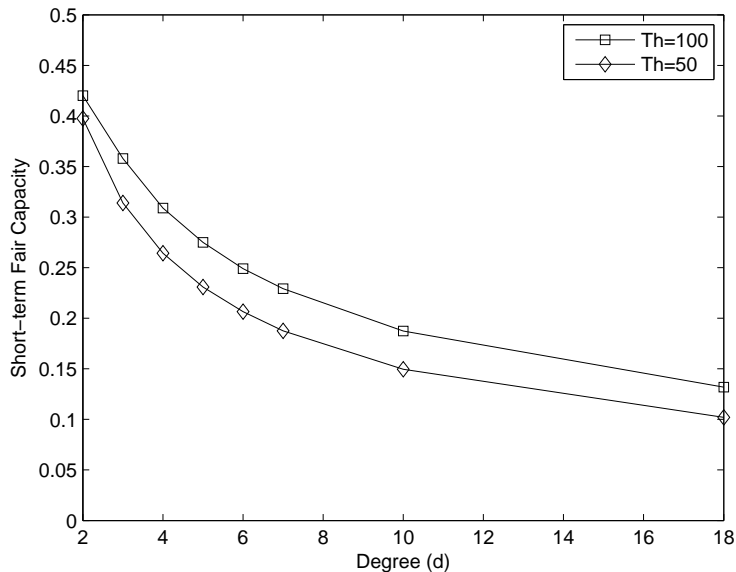


Figure 4.9: Short-term fair capacity of the randomly generated topologies as the degree increases with short-term fairness thresholds of Th=50 and 100.

Figure 4.8 shows how short-term fairness horizon changes as the throughput increases. It is very similar to the tree topology: at low throughputs, short-term fairness horizon weakly depends on d but high-degree topologies have substantially larger short-term fairness horizon than low-degree topologies at higher throughputs. Short-term fairness thresholds of 50 and 100 are also depicted as horizontal dashed lines. Throughputs obtained at these thresholds are plotted in Figure 4.9 where we observe that short-term fair capacity degrades as network degree increases. The reduction in the short-term fair capacity as the degree increases is more apparent in the random topology than the tree topology as will be compared later.

Figure 4.10 plots how short-term fairness horizon changes with the size of the random network. The plot is obtained by simulating randomly generated topologies with $d = 4, 6$ and 10 for $n = 1000, n = 5000$ and 20000 . It is observed that the short-term fairness of the random topology does not depend significantly on n for large networks.

These results imply that the performance of a system of randomly placed

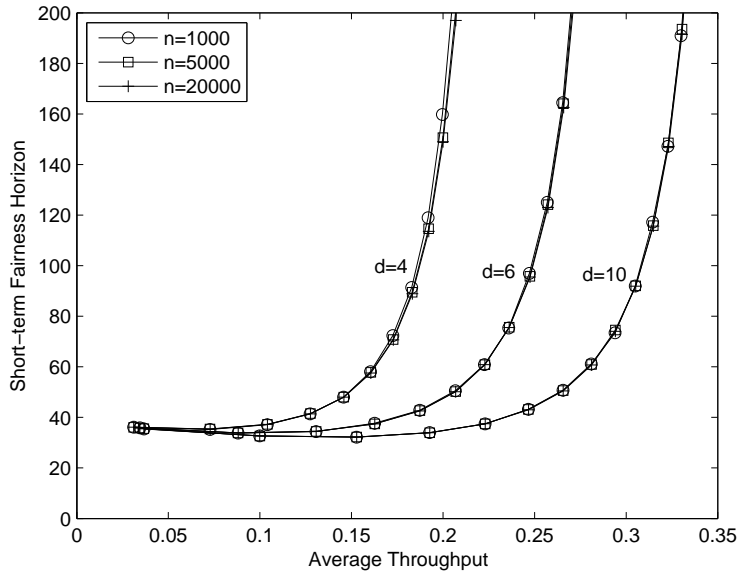


Figure 4.10: Average short-term fairness horizons for the randomly generated topologies with different network sizes.

networks does not degrade with the system size if the number of neighbors is kept fixed. However, as the density, along with d , increases, a performance reduction in the short-term fairness is observed.

4.4.5 Comparison of Different Topologies

Figure 4.11 compares fairness performances of tree, grid and random topologies all with $d = 4$. At low throughputs, short-term fairness is marginally affected by the network topology because nodes do not interact strongly with each other. However, as the throughput increases, nodes interact strongly and topological structure becomes more important. Among the topologies we consider, tree topology has the best short-term fairness performance mainly because interdependency between nodes in the tree topology is lower than any other topology: tree can be separated into two independent parts by removing a single node. Low interdependency results in good short-term fairness performance because network does not spend too much time around some transmission patterns.

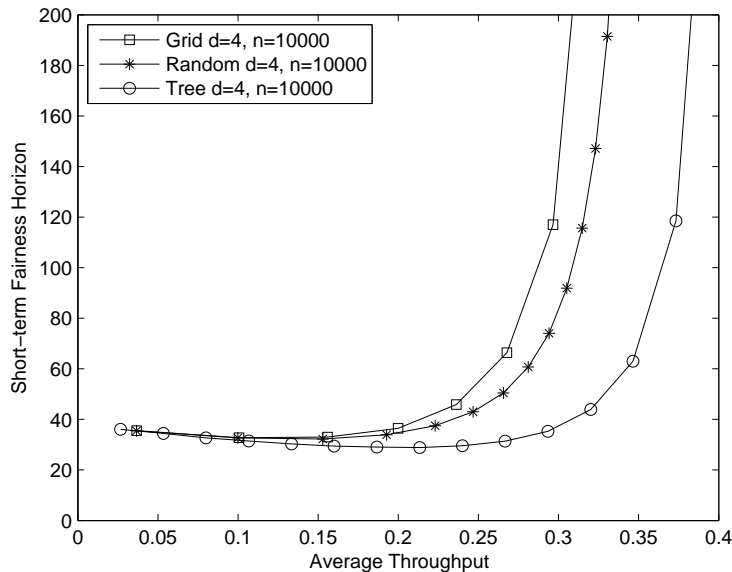


Figure 4.11: Short-term fairness horizons for the tree, grid and random topologies as the throughput increases. All three topologies have $d = 4$.

In contrast to the tree topology, grid topology exhibits high dependency between nodes which results in a poor fairness performance. The active nodes of the grid topology tend to be in one of the two maximal independent sets so that nodes which do not belong to the active transmission pattern wait for a long time to become active. Random topology lies between the tree and the grid topologies in terms of short-term fairness.

Figure 4.12 plots the short-term fair capacities of the tree and random topologies as d increases. A tree with $d = 2$ is a line topology; similarly, a connected random topology with $d = 2$ is also a line topology. So, both topologies have the same capacity at $d = 2$. As d increases, the difference between these two topologies increases. At $d = 18$, short-term fair capacity of the random topology is 53% of the tree topology.

This comparison demonstrates that although the network degree is the main determining factor for the short-term fairness, it is not the sole influencing factor. Other characteristics such as the structure of independent sets and network topology may also affect the short-term fairness performance. Also, it should

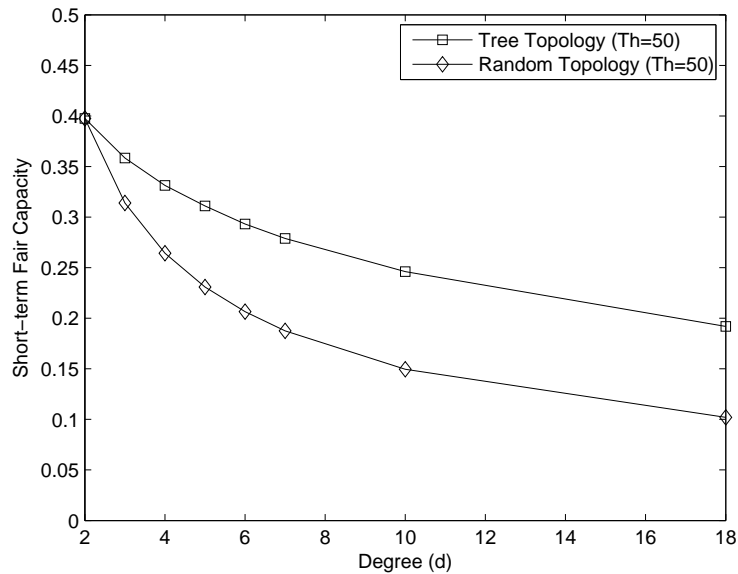


Figure 4.12: Short-term fair capacities for tree and random topologies as the degree increases with short-term fairness threshold $Th=50$.

be noted that we here present averages taken over a large number of topologies, however, short-term fairness of each individual topology may not monotonically degrade with d .

4.5 Practical Implications on the Deployment of Wi-Fi Networks

Municipal wireless networks become increasingly widespread to provide wireless connectivity for cities. For example, Oklahoma City provides wireless coverage for a 555-square-mile area using 1100 mesh nodes and 900 mobile nodes. As well as municipalities, private companies are also interested in providing urban wireless coverage. For instance, Google provides city-wide Wi-Fi access for Mountain View, California.

Our findings may have some implications on the performance of such city-wide networks regarding their deployment density. Densely deploying Wi-Fi access

points may be required to provide a better coverage of the mobile users. On the other hand, as the density of deployment increases, the number of interfering neighbors of an access point increases, which in turn increases the nodal density of the system. Our analysis indicates that nodal degree of the system inversely affects the short-term fairness of a system of wireless networks. For that reason, there may be a trade-off between the short-term fairness of the system and the deployment density to some extent.

To investigate this relationship, we simulated a 10km by 10km area covered by Wi-Fi access points. Previous studies showed that a regular deployment such as the mesh deployment provides better coverage than a totally random deployment [101]. We here investigate the relationship between the density of deployment and short-term fairness performance of networks.

The transmission range of each access point is selected to be 250m and carrier sensing range of access points is selected to be 550m which are the default values for ns-2 network simulator. We simulated for inter-nodal distances between 200m and 900m. For each inter-nodal distance, we formed the conflict graph by linking the access point with their neighbors within their carrier sensing ranges. Two sample conflict graphs corresponding to different deployment scenarios for $l = 300\text{m}$ and $l = 450\text{m}$ are depicted in Figure 4.13. As the inter-nodal degree reduces, the number of interfering neighbors of an access point increases, in turn increasing the degree of the conflict graph. We assumed that the access points have similar traffic requirements and each of them independently probes the channel at the same rate according to a Poisson point process. Similar to previous simulations, we measured the short-term fairness horizon of each topology corresponding to a given inter-nodal distance.

Short-term fairness of the network against the throughput of individual access points for different inter-nodal distances are plotted in Figure 4.14. As the deployment density increases, the short-term fairness horizon starts to increase rapidly at lower throughputs. For $l > 550$, there is no interaction between nodes. This low interference results in desirable short-term fairness performance: there is no degradation in short-term fairness with increasing throughput. For denser

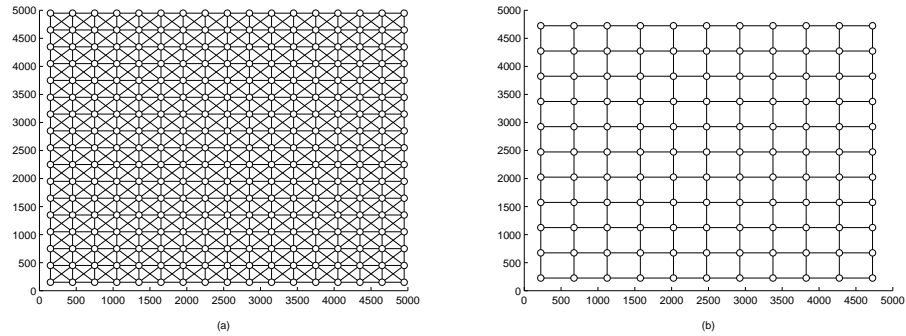


Figure 4.13: A 5 km by 5 km area is covered by Wi-Fi access points which are located in a mesh pattern where (a) $l = 300m$ and (b) $l = 450m$. The interference relationship between nodes are denoted by lines between interfering nodes.

deployments, however, short-term fairness horizon starts to degrade rapidly as throughputs increase.

Although a larger inter-nodal distance gives a good short-term fairness performance, coverage ratio decreases as the inter-nodal distance increases. Figure 4.15 presents the coverage of access points as the inter-nodal distance increases. In this plot, coverage is calculated by assuming that an access point can cover a circular area with a radius of its transmission range and total coverage is the union of these circular areas. Although the short-term fairness is very good, it is only possible to cover almost half of the area with an inter-nodal distance of 600m. From this plot, it can be said that a sacrifice from short-term fairness is needed to achieve a significant coverage of the area.

The results imply that there is a trade-off between the short-term fairness of the network and its coverage. Improving coverage may come at the expense of reducing short-term fairness which should be considered in designing Wi-Fi networks along with other factors such as cost, connectivity, etc.

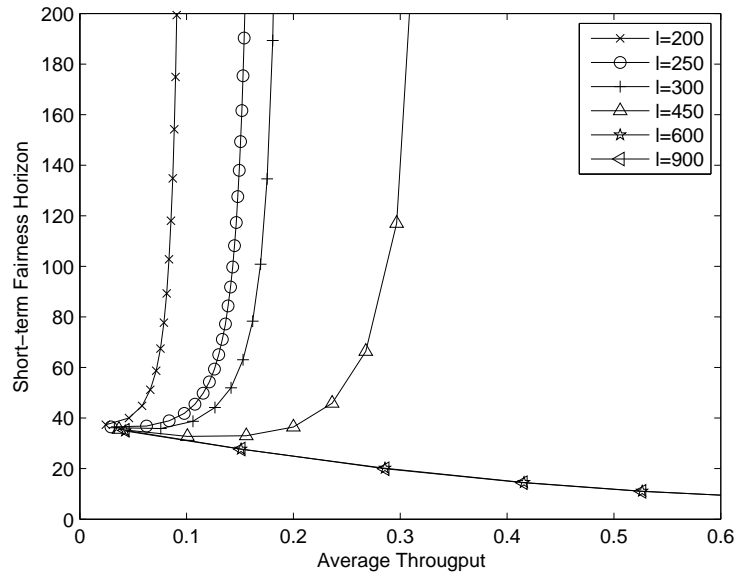


Figure 4.14: Short-term fairness horizon of the simulated Wi-Fi deployment for different internodal distances. Higher density of deployment results in higher short-term fairness horizon at the same throughput.

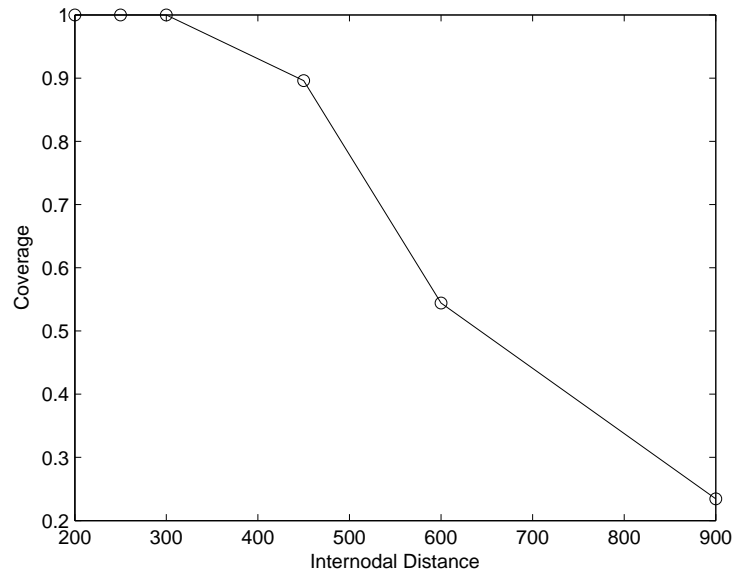


Figure 4.15: Coverage of the simulated Wi-Fi deployment for different internodal distances.

4.6 Analogy with the hard-core model

The idealized CSMA network model closely resembles a simple model of a material which is called as the hard-core model [104]. In this model, particles of the material can be found at the vertices of a lattice graph under the condition that two particles cannot be found at neighboring nodes. This model is equivalent to the ideal CSMA network where two neighboring nodes cannot be active at the same time. So, finding a particle at a given vertex is equivalent to finding a node transmitting in a CSMA network. Recently, the underlying dynamics of the hard-core model has been used to analyze the performance of ideal CSMA [68, 69, 81].

The equivalent of the probing rate in the CSMA network is the fugacity in the hard-core model. As the probing rate of a node increases in the CSMA network, the probability of finding it active increases. Similarly, probability of finding a particle at a given vertex is increased as the fugacity increases. The difference between the idealized CSMA model and the hard-core model is that the individual transmitters in the CSMA model can have different probing rates. In contrast, the fugacity in the hard-core model is a system-wide parameter. So, the equivalent of the hard-core gas model with a given fugacity is a CSMA network where the probing rate of all nodes is equal to the fugacity.

The long-range correlations of the hard-core model have been investigated in the statistical physics literature and the analogy between an idealized CSMA network and the hard-core model allows us to make use of some of these results. In this literature, however, the conditions of long-range correlations are characterized in terms of fugacity. On the other hand, we are interested in conditions in terms of throughput which does not have a direct analogue in the context of the hard-core model.

Since long-range correlations in a CSMA network causes transmission patterns to persist over long time scales, we here investigate if conditions creating long-range correlations have a relationship with the short-term fairness of a CSMA network. We explain two conditions from the literature which corresponds to two

different intensities of long range correlations and present simulation results which demonstrate the possible relation between these conditions and the short-term fair capacity.

The first condition which is indicative of long-range correlations in the model is the existence of multiple equilibrium distributions. The second condition which indicates a stronger correlation is the reconstruction condition under which long-range correlations enable the reconstruction of the state of the root node using the states of leaf nodes in the tree as the length of the tree approaches to infinity.

4.6.1 Uniqueness of a Gibbs Measure

Gibbs measure is the equilibrium distribution of a large number of locally interacting particles [105]. Since the interactions between particles are local, Gibbs measure has the Markov property where each node is conditionally independent of the rest of the network given the states of its neighbors. It is known that there exists at least one Gibbs measure satisfying the local conditional distributions. However, the system may also admit multiple measures in an infinite graph under some conditions which is called as phase transition.

The hard core model on the infinite square lattice, for example, may admit multiple equilibrium distributions. For small λ , there is a unique Gibbs measure on the square lattice. However, it is possible to find two equilibrium distributions for large λ , namely μ_{white} and μ_{black} . μ_{white} corresponds to the case where the whites of the checkerboard pattern have a higher probability than the blacks of the checkerboard pattern. μ_{black} corresponds to the opposite case where the blacks are favored over whites.

A phase transition typically manifests itself in the form of a unique equilibrium distribution that has multi-modal nature in a finite graph. That is, most of the probability measure is concentrated around several quasi-stable states. Transitions between such states become rare as the system size increases, leading to multiple distinct equilibrium distributions in the limit.

Dobrushin showed that when the fugacity is below a certain critical threshold, i.e., $\lambda < \lambda_c$, a system has a unique measure [106]. However, determination of this threshold is a difficult problem even for regular topologies. Kelly has obtained the uniqueness threshold for the tree topology with degree d [103]:

$$\lambda < \frac{1}{d-1} \left(\frac{d-1}{d-2} \right)^d. \quad (4.7)$$

Previous literature was interested in determining threshold fugacities but they did not consider the stationary probabilities, that is, throughputs that correspond to these thresholds. The uniqueness threshold for the tree topology corresponds to the case where the stationary probability of a node being active is $\frac{1}{d}$ which also follows from [103]. If the throughput of nodes in the tree is less than $\frac{1}{d}$, the system has a unique measure.

4.6.2 Reconstruction Threshold

A stronger condition that is indicative of long-range correlations between nodes is called the *reconstruction* condition. Reconstruction problem is interested in characterizing the conditions under which the state of the root can be reconstructed using the states of the leaf nodes as the height of the tree approaches to infinity. Reconstruction property is a stronger condition than having multiple equilibrium distributions.

Exact reconstruction threshold for the tree topology is not known but, recently, it is shown that the hard-core model on the tree has non-reconstruction if [107]:

$$\lambda < \frac{(\ln(2) - o(1)) \ln^2(d)}{2 \ln \ln(d)}. \quad (4.8)$$

4.6.3 Short-term Fairness and Mixing Time

The described conditions occur as a result of increased correlation between the particles in the material. Similarly, short-term fairness of a CSMA network reduces mainly because states of nodes become increasingly correlated which causes some nodes to starve for a long time reducing short-term fairness.

Short-term fairness is thought to be estimated by the mixing time of the underlying system dynamics [76] where mixing time is defined as the time required for the underlying Markov chain to converge to its equilibrium distribution. Convergence to equilibrium slows down if the network sticks to some transmission patterns during the convergence process. For that reason, slow mixing is considered to be an indicator of short-term unfairness.

Previous studies on the mixing time of the hard-core model investigate the conditions of fast mixing. A recent study shows that the fast mixing region extends beyond the uniqueness region and reaches to the reconstruction region for the tree topology [108]. Because of this relationship, we investigate here whether these two thresholds have any implications in determining the region beyond which short-term fairness of the CSMA network starts to deteriorate.

4.6.4 Simulations

The described uniqueness and reconstruction thresholds are for the tree topology and are in terms of fugacities. We obtain throughputs obtained at these fugacities by performing simulations and compare the results against the short-term fair horizon for the tree topology.

Figure 4.16 plots the short-term fairness horizon of the tree topologies for $d = 4, 10$ and 18 , along with the throughputs corresponding to the uniqueness threshold and the non-reconstruction bound. For $d = 4$, the uniqueness threshold and the non-reconstruction bound are close to each other corresponding to the point where short-term fairness starts to increase rapidly. However, for larger

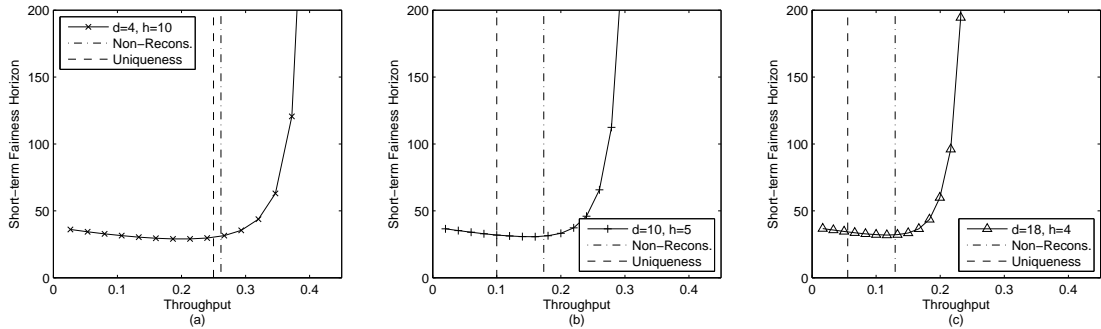


Figure 4.16: The uniqueness threshold, non-reconstruction bound and the short-term fairness horizon for tree topologies with (a) $d = 4$ (b) $d = 10$ (c) $d = 18$.

d , the uniqueness threshold underestimates this point of increase while the non-reconstruction bound consistently locates the point where the horizon starts to increase rapidly.

These simulations demonstrate a possible analogy between the phase transitions of the hard-core model and short-term fairness of the CSMA network. In light of the recent research results showing that the fast mixing threshold of the tree topology extends to the reconstruction threshold [108], this line of study suggests further research especially for other topologies.

4.7 Conclusions

This paper was aimed at characterizing the performance of a system of networks employing CSMA protocol under a short-term fairness constraint. Our main findings can be summarized as follows: 1) Short-term fairness significantly depends on the degree of the network: high-degree topologies have less short-term fair capacity than low-degree topologies. 2) Short-term fairness does not depend on network size for reasonably large fixed degree random networks.

Conflict graph topology is an important factor affecting the short-term fair capacity. The grid topology is inherently unfair at high throughputs. When the Wi-Fi transmitters form a grid conflict graph the network may become severely unfair at high throughputs. However, in random conflict graphs, such behavior

is not observed so that randomly placed transmitters are unlikely to experience this degradation in short-term fairness.

Dependence of short-term fairness on the degree of the network has implications for deployment of large area Wi-Fi networks. Deploying a dense network improves coverage; however, it reduces short-term fair capacity by increasing the average degree.

We have also presented simulation results which suggest a correlation between the phase transitions of the hard-core model from statistical physics literature to the short-term fairness of the CSMA network. Our results suggest that the reconstruction threshold can be used as a good indicator of the short-term fair capacity region for the tree topology which is in accordance with the recent results on the mixing time.

Our study focuses on fixed-rate CSMA systems where the nodes do not adaptively change their probing rates. Whether a similar short-term unfairness phenomenon will be observed in adaptive CSMA systems is a subject of future study. We conjecture that the short-term unfairness problem may also be observed in adaptive CSMA systems at high loads because the nodes need to probe the channel very frequently resembling a fixed rate system at high loads. Similarly, the extent of short-term unfairness in CSMA based MAC protocols, such as the 802.11 protocol, has to be investigated.

In addition to further analysis of adaptive CSMA, methods to resolve the short-term fairness problems have to be devised. As our results show, only a portion of the capacity region can be achieved under short-term fairness constraints, so a sacrifice from throughput may be needed to alleviate the short-term unfairness problem in a distributed fashion.

Chapter 5

Energy-optimum Carrier Sensing Rate and Throughput in CSMA-based Wireless Networks

To improve the battery lifetimes of wireless devices and due to environmental considerations, the energy efficiency of wireless communication protocols has to be improved. There are many wireless communications protocols that employ a variant of the carrier sense multiple access protocol (CSMA) due to its simple and distributed nature (e.g., the IEEE 802.11 for WLANs, IEEE 802.15.4 for WPANs and B-MAC for sensor networks [3]). We here find the optimum carrier-sensing rate and throughput which maximizes the number of transmitted bits in a wireless CSMA network for a fixed energy budget.

Recently, carrier-sensing rate adaptation algorithms have been devised to achieve throughput-optimality in a CSMA network [109]. In these algorithms, each node senses the channel at a rate which increases with its packet queue length (or virtual queue length). As packet queues grow, the nodes may sense the channel at arbitrarily high rates. However, the increased energy consumption due to such increased carrier-sensing rate has not been investigated to the best of our knowledge. We here aim to quantify the relationship between sensing rate,

throughput and energy consumption in a CSMA network.

We consider a saturated CSMA network where all nodes always have a packet to send and employ non-persistent CSMA [12]: If the channel is busy when a node senses the channel, it waits for an exponentially distributed duration with mean λ^{-1} and attempt to transmit again. During the waiting time between transmission attempts, the node can be either in the idle listening state or in the sleeping state. For the rest of the paper, we will refer to the waiting time between transmission attempts as *sleeping* since the sleeping state is the most energy saving state. However, the proposed analysis is still applicable even when nodes perform idle listening between transmission attempts.

We are interested in the following question: What is the optimum value of λ which maximizes the number of transmitted bits for the lifetime of the node which is limited by its energy budget. If λ is selected too small, the nodes will rarely transmit a packet and spend most of their lifetimes in the sleep mode. In this case, a node consumes its energy budget mostly in the sleeping state albeit sleeping has minor energy consumption. A very low λ can improve the duration of service but it will not improve the number of bits that it can transmit during its lifetime.

If λ is selected too large, the nodes will frequently wake-up and sense the channel to transmit a packet. Although it is usually omitted in the literature, each time a node senses the channel and finds it busy, a small amount of energy is spent without making a transmission. So, a very high λ will also result in energy inefficiency.

We find the energy-optimum carrier-sensing rate, λ^* , which minimizes the energy consumption per transmitted bit. The energy-optimum rate exploits the trade-off between the energy consumed for sleeping and energy consumed for carrier sensing. The energy-optimum rate leads to an energy-optimum throughput, σ^* , which gives the energy-optimum operating load for the network. To maximize the number of transmitted bits for a given energy budget, the network has to operate at a throughput of σ^* .

We first provide an analytical model for the energy consumption of a single-hop CSMA network, and then extend the analysis to a multi-hop network with a random regular conflict graph. For both scenarios, we analyze the energy consumed in various states such as sleeping and carrier-sensing. We derive the energy-optimum carrier sensing rate and the corresponding energy-optimum throughput which minimize the energy consumption per transmitted bit. The energy-optimum throughput exploits a balance between the energy consumed in the states of sleeping and carrier sensing per transmitted bit.

For the single-hop network, we show that the energy-optimum throughput is higher for larger networks because sleeping costs increase dramatically at a low throughput with the number of nodes. Also, the energy-optimum throughput increases as the power required for carrier-sensing reduces in proportion to the power required for sleeping. As sensing becomes less expensive, the nodes should attempt to transmit packets more frequently to minimize the energy consumed per bit.

For the multi-hop case, we show that the energy-optimum throughput depends on the degree of the conflict of graph of the network and on the power consumption of carrier sensing. We find that the energy-optimum throughput reduces as the degree of the conflict graph increases, i.e., as the interference increases. Similar to the single-hop case, the energy-optimum carrier sensing rate and the energy-optimum throughput increase as the power required for carrier sensing reduces.

The energy consumption analyses for single-hop and multi-hop networks are given in Sections 5.1 and 5.2, respectively. We derived bounds for the energy-optimum throughput and maximum throughput for the multi-hop case in Section 5.3. The numerical evaluation of the proposed analysis is given in Section 5.4. Section 5.5 presents the conclusions and discussion.

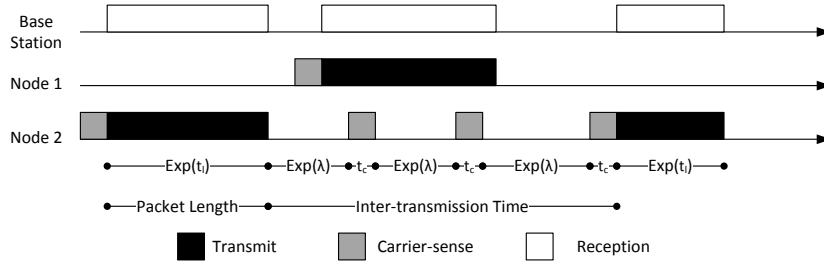


Figure 5.1: A sample timeline of two nodes in a single-hop scenario.

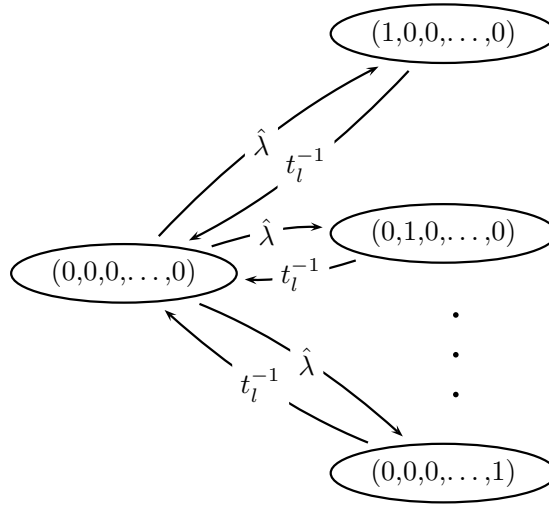


Figure 5.2: Markov chain for the single-hop case. The stationary probabilities of the states except the initial state gives the throughput of each node.

5.1 Single-hop Network

We first consider a single-hop network scenario where the nodes transmit to a central base station. A timeline of the transmissions of a node in such a single-hop network can be seen in Fig. 5.1. The probability distributions of durations are also shown in the timeline. In the figure, node 2 transmits its second packet after two unsuccessful carrier sensing attempts. In this section, we analyze the energy consumption of such a network and obtain the energy-optimum throughput and carrier-sensing rate.

5.1.1 System Model

In the analysis of the single-hop CSMA, we use the Markov chain model of CSMA which is proposed in [98]. This model has been frequently used in the study of optimal CSMA recently [109, 66, 68]. Based on this model, the Markov chain for a single hop scenario can be constructed as in Fig. 5.2 for a mean packet duration of t_l . For example, in the figure, the state $(0, 0, 0, \dots, 0)$ corresponds to the state where none of the nodes are transmitting and state $(0, 1, 0, \dots, 0)$ corresponds to the case where only the second node is transmitting. This model assumes instantaneous carrier-sensing, so the collisions are avoided.

Instantaneous sensing assumption allows arbitrarily large sensing rates to be handled by this model. However, in reality, carrier-sensing takes a non-negligible time which prevents the nodes to access the channel at high rates. To incorporate the sensing duration into the carrier sensing frequency while preserving the zero-collision assumption, we obtain a normalized sensing rate, $\hat{\lambda}$, by adding the sensing duration, t_c , to the mean of the carrier sensing period, $1/\lambda$:

$$\hat{\lambda} = \frac{1}{\frac{1}{\lambda} + t_c}. \quad (5.1)$$

This implies that the carrier-sensing duration is also assumed to be exponentially distributed. Although the sensing duration is deterministic in reality, this assumption does not lead to an inaccuracy in the analysis as will be shown in Sec. 5.4. So, as λ approaches to infinity, $\hat{\lambda}$ approaches to t_c^{-1} which means that the maximum sensing frequency is limited by the sensing duration.

We define the throughput of a node, σ , as the ratio of the time spent to transmit a packet to the total time. So, the throughput of nodes 1 to N corresponds to the stationary probability of states $(1, 0, 0, \dots, 0)$ to $(0, 0, 0, \dots, 1)$ in Fig. 5.2. Then, the throughput of a node in terms of $\hat{\lambda}$ and λ is given by

$$\sigma = \frac{\hat{\lambda}}{\frac{1}{t_l} + \hat{\lambda}N} = \frac{\lambda}{\frac{1}{t_l} + \lambda(N + \frac{t_c}{t_l})} \quad (5.2)$$

and the total throughput of the network can be written as

$$\sigma_{tot} = N\sigma. \quad (5.3)$$

The maximum throughput per node can be obtained as λ approaches to infinity:

$$\sigma_{\max} = \lim_{\lambda \rightarrow \infty} \sigma = \frac{1}{N + \frac{t_c}{t_l}}. \quad (5.4)$$

The maximum throughput of a node is dependent on the number of nodes sharing the channel and the ratio of sensing duration to the packet duration.

The inverse relationship between the throughput and the carrier-sensing frequency can be obtained by taking the inverse function of (5.2):

$$\lambda = \frac{\sigma}{t_l(1 - N\sigma) - t_c\sigma}. \quad (5.5)$$

for $\sigma \leq \sigma_{\max}$.

5.1.2 Energy Consumption Model

We are interested in determining the energy spent for transmission, sleeping and carrier sensing per transmitted bit. The duration between the transmissions of two successive packets consists of time spent for carrier sensing and time spent while sleeping. Since throughput equals to the ratio of the average packet duration to the sum of the average packet duration with the mean inter-transmission duration, it is possible to obtain the mean inter-transmission duration in terms of throughput by solving

$$\frac{t_l}{t_l + E[T_i]} = \sigma \quad (5.6)$$

which gives the solution as

$$E[T_i] = \frac{t_l(1 - \sigma)}{\sigma}. \quad (5.7)$$

The inter-transmission duration includes several carrier-sensing periods which consists of a sleeping period and a carrier-sensing operation. If the carrier-sensing operation is unsuccessful, the sensing period is repeated. Since the mean of sleeping duration between carrier sensing attempts is $\frac{1}{\lambda}$ and the mean carrier sensing duration is t_c , it is possible to compute the share of sleeping and carrier sensing in the inter-transmission duration. The mean time spent for carrier sensing per

packet can be found using (5.5) as

$$E[T_c] = \frac{t_l(1-\sigma)}{\sigma} \frac{t_c}{\frac{1}{\lambda} + t_c} = \frac{t_c(1-\sigma)}{1-N\sigma} \quad (5.8)$$

and mean time spent for sleeping per packet is given by

$$E[T_s] = \frac{t_l(1-\sigma)}{\sigma} \frac{\frac{1}{\lambda}}{\frac{1}{\lambda} + t_c} = \frac{(1-\sigma)(t_l(1-N\sigma) - t_c\sigma)}{\sigma(1-N\sigma)}. \quad (5.9)$$

Since the mean packet duration is t_l , i.e., $E[T_t] = t_l$, total energy consumption per packet is given by

$$E[E_p] = \frac{t_c(1-\sigma)}{1-N\sigma} P_c + \frac{(1-\sigma)(t_l(1-N\sigma) - t_c\sigma)}{\sigma(1-N\sigma)} P_s + t_l P_t. \quad (5.10)$$

where P_c , P_s and P_t correspond to the power consumed while carrier sensing, sleeping and transmission, respectively. Then, energy per transmitted bit is given by

$$E[E_b] = \frac{E[E_p]}{t_l R} \quad (5.11)$$

where R is the data transmission rate. Energy per bit has a single minimum for $\sigma \leq \sigma_{\max}$, so the energy minimizing σ can be found by solving $\frac{\partial E[E_b]}{\partial \sigma} = 0$ as

$$\sigma^* = \frac{1}{\sqrt{\frac{P_c - P_s}{P_s} \frac{t_c}{t_l} (N-1) + N}} \quad (5.12)$$

and the corresponding energy-optimum carrier-sensing rate can be found by substituting (5.12) into (5.2) as

$$\lambda^* = \frac{1}{\sqrt{\frac{P_c - P_s}{P_s} t_c t_l (N-1) - t_c}} \quad (5.13)$$

for $\sigma^* \leq \sigma_{\max}$.

Then, the total energy-optimum network throughput is given by

$$\sigma_{tot}^* = N\sigma^* = \frac{N}{\sqrt{\frac{P_c - P_s}{P_s} t_c t_l (N-1) - t_c}}. \quad (5.14)$$

The total energy-optimum throughput decreases as P_c gets larger in comparison to P_s which means that σ_{tot}^* reduces as the carrier sensing gets more expensive. Also, as N increases, σ_{tot}^* increases because the sleeping costs increase faster than the carrier sensing costs as N increases. In the limit as $N \rightarrow \infty$, $\sigma_{tot}^* \rightarrow 1$. A detailed discussion of the properties of σ_{tot}^* is presented in Section 5.4.1.

5.2 Multi-hop Network

We now study a multi-hop network where nodes both transmit and receive packets unlike the single hop scenario where the nodes only transmit to a base station. Similar to the single-hop case, each node always has a packet to send and wakes up after exponentially distributed periods with mean λ^{-1} and senses the channel. If the channel is idle, the node transmits the packet to one of its neighbors. If a node is not transmitting or receiving a packet, it sleeps to conserve energy. In our model, we assume that the sender and receiver of a packet are perfectly synchronized, both wake-up at the same time to complete the transmission. If the channel is busy when the sender wakes up, it sleeps again and wake-up after an exponentially distributed period with mean λ^{-1} . We are interested in the energy-optimum value of λ which minimizes the energy consumption per transmitted bit, hence maximizes the number of bits that a node can transmit during its lifetime.

5.2.1 System Model

We perform our analysis on the conflict graph of links in the network. A conflict graph represents the interference relationships among links between wireless nodes in the network as shown in Fig. 5.3. A directed link in the network is represented by a vertex in the conflict graph and there is an edge between vertices in the conflict graph if the corresponding links are interfering with each other. In such a model, there are no hidden terminals and the propagation delays between nodes are negligible, so collisions are avoided. This model has recently been used in the design of throughput-optimal CSMA [68, 110].

For the sake of analysis, we consider a random regular conflict graph, i.e., each vertex in the conflict graph has the same number of neighbors, d . We assume that the transmission and reception links of a node in the wireless network correspond to a neighboring node pair in the contention graph. The nodes have saturated traffic and each node senses the channel at independent and exponentially distributed intervals with rate λ . If a node senses that there are no conflicting

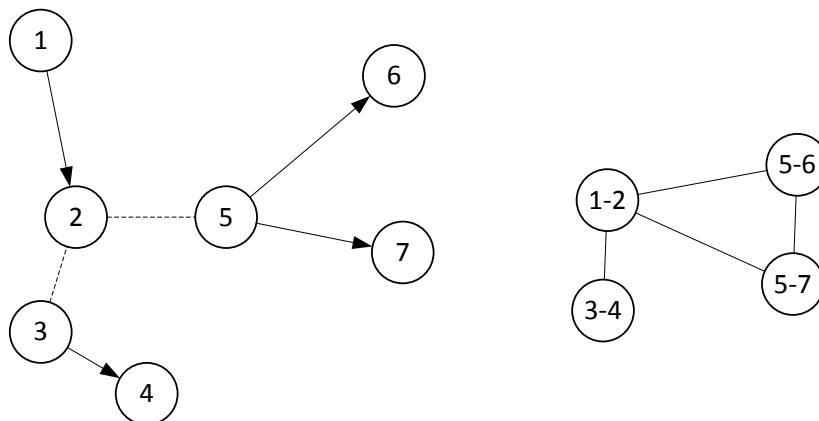


Figure 5.3: A wireless network topology and the conflict graph of its links. Lines with arrows indicate the links in the network topology and dashed lines indicate that two nodes are within the interference range of each other without having a link between them.

transmissions, it starts a transmission for an exponentially distributed duration with mean t_l .

5.2.2 Energy Consumption Model

In order to quantify the energy consumption per bit, we first have to obtain a relationship between the carrier-sensing rate and throughput. For the single-hop case, the throughputs can be easily obtained by solving the Markov chain given in Fig. 5.2. Although a similar Markov chain can be constructed for a multi-hop network, it requires enumeration of independent sets of the conflict graph which is computationally difficult. Besides, a different Markov chain has to be constructed for each topology. For that reason, we here focus on random regular conflict graphs which have a surprisingly similar throughput-sensing rate relationship with a special type of graphs known as the Cayley tree. In a Cayley tree, each node except the leaf nodes have the same number of neighbors, d . The relationship between throughput and carrier sensing rate in a Cayley tree graph is investigated in the context of loss networks by Kelly [103].

In this analysis, all non-leaf nodes have the same channel sensing rate whereas the channel sensing rates of leaf nodes are adjusted so that they have the same

throughput with internal nodes. The relationship between the throughputs of nodes, σ , and the channel sensing rate of internal nodes, λ , is obtained using a fixed point equation. We here only present the results and omit the details of the analysis, but the readers may refer to [103, 111] for more details. According to this analysis, the stationary probability of a node being active, i.e. the throughput of a node, is given by

$$\sigma = \frac{1 - a}{2 - a} \quad (5.15)$$

where a is the solution of

$$f(a) = \nu a^d + a - 1 = 0. \quad (5.16)$$

and ν is the call arrival rate for calls with unit mean duration. In our case, the packet lengths are not equal to one so $\nu = \hat{\lambda} t_l$ where $\hat{\lambda}$ is the normalized sensing rate and t_l is the packet duration. Equation (5.16) has a unique solution since $f(0) = -1$, $f(1) = \nu > 0$ and $f'(a) > 0$.

If the solution of (5.15) is substituted into (5.16), the normalized carrier-sensing rate corresponding to a given throughput can be obtained as

$$\hat{\lambda} = \frac{(1 - 2\sigma)^{-d}(1 - \sigma)^{d-1}\sigma}{t_l} \quad (5.17)$$

which leads to the following relationship between throughput and the carrier-sensing rate considering (5.1):

$$\lambda = \frac{\sigma}{-t_c\sigma + t_l(1 - 2\sigma)^d(1 - \sigma)^{1-d}}. \quad (5.18)$$

To have $\lambda > 0$, the following condition has to be satisfied

$$\frac{(1 - 2\sigma)^d(1 - \sigma)^{1-d}}{\sigma} > \frac{t_c}{t_l} \quad (5.19)$$

which poses an upper bound on σ :

$$\sigma \leq \sigma_d^{\max}. \quad (5.20)$$

Rewriting (5.19), σ_d^{\max} is the solution to the equation:

$$\left(\frac{1 - 2\sigma_d^{\max}}{1 - \sigma_d^{\max}} \right)^d = \frac{t_c}{t_l} \frac{\sigma_d^{\max}}{1 - \sigma_d^{\max}}. \quad (5.21)$$

For $d = 2$, the maximum throughput, σ_2^{\max} , is given by

$$\sigma_2^{\max} = \frac{1}{2} - \frac{1}{2\sqrt{4\frac{t_l}{t_c} + 1}}. \quad (5.22)$$

For $d > 2$, we obtain lower and upper bounds on σ_d^{\max} , which are presented in Sec. 5.3.

Similar to the single-hop case, it is possible to obtain the mean duration between two successive transmissions by solving

$$\frac{t_l}{t_l + E[T_i]} = \sigma \quad (5.23)$$

which gives the solution:

$$E[T_i] = \frac{t_l(1 - \sigma)}{\sigma}. \quad (5.24)$$

During inter-transmission time, a node can be in three different states: It can be sleeping, carrier-sensing or receiving a packet. In the random regular network, a node receives one packet on the average during the inter-transmission time:

$$E[T_r] = t_l. \quad (5.25)$$

Remaining time of the inter-transmission duration is shared between the time spent for carrier-sensing and time spent for sleeping. Time spent for sleeping can be written as

$$E[T_s] = (E[T_i] - E[T_r])\frac{\frac{1}{\lambda}}{\frac{1}{\lambda} + t_c} = \frac{t_l(1 - 2\sigma)}{\sigma} \frac{\frac{1}{\lambda}}{\frac{1}{\lambda} + t_c}. \quad (5.26)$$

Using the relationship between λ and σ given by (5.18), $E[T_s]$ can be obtained only in terms of σ as

$$E[T_s] = \frac{t_l - 3t_l\sigma - t_c(1 - 2\sigma)^{1-d}(1 - \sigma)^d\sigma + 2t_l\sigma^2}{\sigma - \sigma^2}. \quad (5.27)$$

Time spent for carrier-sensing can similarly be written as

$$E[T_c] = (E[T_i] - E[T_r])\frac{t_c}{\frac{1}{\lambda} + t_c} = t_c(1 - 2\sigma)^{1-d}(1 - \sigma)^{d-1}. \quad (5.28)$$

Then, total energy consumption per packet is given by

$$E[E_p] = E[T_s]P_s + E[T_c]P_c + E[T_i]P_t + E[T_r]P_r \quad (5.29)$$

$$= t_l \left(P_r + P_t + P_s \left(-2 + \frac{1}{\sigma} \right) \right) + \quad (5.30)$$

$$(P_c - P_s)t_c(1 - 2\sigma)^{1-d}(1 - \sigma)^{-1+d} \quad (5.31)$$

and the energy per transmitted bit is given by

$$E[E_b] = \frac{E[E_p]}{t_l R}. \quad (5.32)$$

The energy-optimum throughput, σ_d^* , which minimizes $E[E_b]$ can be found algebraically by solving $\frac{\partial E[E_b]}{\partial \sigma} = 0$ as given by

$$(d-1)(P_c - P_s)t_c(1-2\sigma)^{-d}(1-\sigma)^{d-2} - \frac{P_s t_l}{\sigma^2} = 0 \quad (5.33)$$

The solution for $d = 2$ can be found as

$$\sigma_2^* = \frac{1}{2 + \sqrt{\frac{(P_c - P_s)t_c}{P_s t_l}}}. \quad (5.34)$$

For $d = 3$ and $d = 4$, it is also possible to obtain a close form expression for σ_d^* but we do not present these results here due to space constraints. For $d \geq 5$, a numerical solution has to be obtained but we provide several bounds for the optimum throughput in the next section. The corresponding energy-optimum carrier-sensing rate for $d = 2$ can be found by substituting (5.34) into (5.18) as:

$$\lambda_2^* = \frac{t_l + \sqrt{\left(\frac{P_c}{P_s} - 1\right)t_c t_l}}{t_c \left(t_l \left(\frac{P_c}{P_s} - 2\right) - \sqrt{t_c t_l \left(\frac{P_c}{P_s} - 1\right)}\right)} \quad (5.35)$$

for $\sigma_2^* \leq \sigma_2^{\max}$.

5.3 Bounds on the energy-optimum throughput and maximum throughput

The exact solution of the maximum throughput and the energy-optimum throughput are presented only for the $d = 2$ case. In this part, we obtain lower and upper bounds on the maximum throughput, σ_d^{\max} , and the energy-optimum throughput, σ_d^* where σ_d^{\max} is the solution to (5.21) and σ_d^* is the solution to (5.33).

5.3.1 Lower bounds on the maximum throughput, σ_d^{\max}

Since $\sigma_d^{\max} < \frac{1}{2}$, right hand side of (5.21) can be bounded as

$$\left(\frac{1 - 2\sigma_d^{\max}}{1 - \sigma_d^{\max}}\right)^d = \frac{t_c}{t_l} \frac{\sigma_d^{\max}}{1 - \sigma_d^{\max}} \leq \frac{t_c}{t_l} \quad (5.36)$$

giving the following lower bound:

$$\sigma_d^{\max} \geq \frac{1 - \left(\frac{t_c}{t_l}\right)^{1/d}}{2 - \left(\frac{t_c}{t_l}\right)^{1/d}} \triangleq \underline{\sigma}_d^{\max,1} \quad (5.37)$$

Another lower bound can be found by rewriting (5.21) as

$$(1 - 2\sigma_d^{\max}) = f(\sigma_d^{\max}, d) \left(\frac{t_c}{t_l}\right)^{1/d} \quad (5.38)$$

where

$$f(\sigma_d^{\max}, d) = (1 - \sigma_d^{\max}) \left(\frac{\sigma_d^{\max}}{1 - \sigma_d^{\max}}\right)^{1/d}. \quad (5.39)$$

For $0 < \sigma_d^{\max} < 1$, $f(\sigma_d^{\max}, d)$ has a single maximum at $\sigma_d^{\max} = \frac{1}{d}$ since $f' > 0$ if $\sigma_d^{\max} < \frac{1}{d}$ and $f' < 0$ if $\sigma_d^{\max} > \frac{1}{d}$. Hence,

$$(1 - 2\sigma_d^{\max}) \leq \left(1 - \frac{1}{d}\right) \left(\frac{\frac{1}{d}}{1 - \frac{1}{d}}\right)^{1/d} \left(\frac{t_c}{t_l}\right)^{1/d} \quad (5.40)$$

which gives the following lower bound:

$$\sigma_d^{\max} \geq \frac{1}{2} - \frac{(d-1)^{(1-\frac{1}{d})}}{2d} \left(\frac{t_c}{t_l}\right)^{1/d} \triangleq \underline{\sigma}_d^{\max,2}. \quad (5.41)$$

5.3.2 Upper bound on the maximum throughput, σ_d^{\max}

An upper bound on σ_d^{\max} can be found using an approximation of (5.21) as $\frac{t_c}{t_l} \rightarrow 0$:

$$\left(\frac{1 - 2\sigma_d^{\max}}{1 - \sigma_d^{\max}}\right)^d = \frac{t_c}{t_l} \frac{\sigma_d^{\max}}{1 - \sigma_d^{\max}} \approx \frac{t_c}{t_l} \quad (5.42)$$

which can be written as

$$1 - 2\sigma_d^{\max} \approx (1 - \sigma_d^{\max}) \left(\frac{t_c}{t_l}\right)^{\frac{1}{d}}. \quad (5.43)$$

Since $(1 - \sigma_d^{\max}) > \frac{1}{2}$, an approximate upper bound on σ_d^{\max} is given by

$$\sigma_d^{\max} \lesssim \frac{1}{2} - \frac{1}{4} \left(\frac{t_c}{t_l} \right)^{\frac{1}{d}} \triangleq \bar{\sigma}_d^{\max}. \quad (5.44)$$

5.3.3 Lower bound on the energy-optimum throughput, σ_d^*

(5.33) can be rewritten as

$$1 - 2\sigma_d^* = g(\sigma_d^*, d) \left(\frac{(P_c - P_s)t_c(d-1)}{P_s t_l} \right)^{1/d} \quad (5.45)$$

where

$$g(\sigma_d^*, d) = \left(\frac{\sigma_d^*}{1 - \sigma_d^*} \right)^{2/d} (1 - \sigma_d^*). \quad (5.46)$$

Since $g' > 0$ if $\sigma_d^* < \frac{2}{d}$ and $g' < 0$ if $\sigma_d^* > \frac{2}{d}$ for $0 < \sigma_d^* < 1$, g has a single maximum at $\sigma_d^* = \frac{2}{d}$. Then, an inequality can be written as

$$1 - 2\sigma_d^* \leq \left(\frac{\frac{2}{d}}{1 - \frac{2}{d}} \right)^{2/d} \left(1 - \frac{2}{d} \right) \left(\frac{(P_c - P_s)t_c(d-1)}{P_s t_l} \right)^{1/d} \quad (5.47)$$

which gives the following lower bound:

$$\sigma_d^* \geq \frac{1}{2} - \frac{(d-2)^{(1-\frac{2}{d})} \left(\frac{(d-1)(P_c - P_s)t_c}{P_s t_l} \right)^{\frac{1}{d}}}{d(2^{1-\frac{2}{d}})} \triangleq \underline{\sigma}_d^*. \quad (5.48)$$

5.3.4 Upper bound on the energy-optimum throughput, σ_d^*

It is possible to write (5.33) as a fixed point equation:

$$\sigma = h(\sigma) = \left(\frac{1 - 2\sigma}{1 - \sigma} \right)^{\frac{d}{2}} (1 - \sigma) \frac{1}{\sqrt{\alpha(d-1)}} \quad (5.49)$$

where

$$\alpha = \frac{(P_c - P_s)t_c}{P_s t_l}. \quad (5.50)$$

The solution to the fixed-point equation $\sigma = h(\sigma)$ is σ_d^* . We define another function $m(\sigma) = h(\sigma)\sigma$ whose maximum point, σ_1 , satisfies $\sigma_1 > \sigma_d^*$ under certain conditions $\alpha > \alpha^*$ and $d < d^*$.

The function $m(\sigma)$ has a single maximum for $0 < \sigma < \frac{1}{2}$ at

$$\sigma_1 = \frac{1}{16} \left(d - \sqrt{d(d+16)} + 8 \right). \quad (5.51)$$

Since $h'(\sigma) < 0$ for $0 < \sigma < \frac{1}{2}$, $h(\sigma)$ is decreasing in σ . For that reason, $\sigma_1 > h(\sigma_1)$ implies $\sigma_1 > \sigma_d^*$.

At σ_1 , the following equation is satisfied

$$m'(\sigma_1) = h'(\sigma_1)\sigma_1 + h(\sigma_1) = 0 \quad (5.52)$$

which results in $h(\sigma_1) = -h'(\sigma_1)\sigma_1$. So, the condition $\sigma_1 > h(\sigma_1)$ can be written as $h'(\sigma_1) > -1$, implying that $\bar{\sigma}_d^* = \sigma_1$ defined in (5.51) is an upper bound for the energy-optimum throughput under this condition, which is satisfied by the following set of parameters:

$$\frac{(P_c - P_s)t_c}{P_s t_l} > 4 \quad \text{for } 2 \leq d \leq 94. \quad (5.53)$$

If this condition is not satisfied for $2 < d < 94$, the function $\bar{\sigma}_d^*$ falls below σ_d^* .

5.3.5 Lower bound on $\sigma_d^*/\sigma_d^{\max}$

A lower bound on the ratio $\sigma_d^*/\sigma_d^{\max}$ can be obtained by dividing the lower bound for σ_d^* by the upper bound for σ_d^{\max} :

$$\frac{\sigma_d^*}{\sigma_d^{\max}} \gtrsim \frac{\underline{\sigma}_d^*}{\bar{\sigma}_d^{\max}} = \frac{2 \left(d - 4^{\frac{1}{d}} (d-2)^{1-\frac{2}{d}} \left(\frac{(d-1)t_c(P_c - P_s)}{P_s t_l} \right)^{1/d} \right)}{\left(2 - \left(\frac{t_c}{t_l} \right)^{1/d} \right) d}. \quad (5.54)$$

5.3.6 Upper bound on $\sigma_d^*/\sigma_d^{\max}$

Dividing $\bar{\sigma}_d^*$ by $\underline{\sigma}_d^{\max,1}$, an upper bound on the ratio $\sigma_d^*/\sigma_d^{\max}$ can be obtained as:

$$\begin{aligned} \frac{\sigma_d^*}{\sigma_d^{\max}} &\leq \frac{\bar{\sigma}_d^*}{\underline{\sigma}_d^{\max,1}} \\ &= \frac{1}{16} \left(d - \sqrt{d(d+16)} + 8 \right) \frac{2 - \left(\frac{t_c}{t_l} \right)^{1/d}}{1 - \left(\frac{t_c}{t_l} \right)^{1/d}}. \end{aligned} \quad (5.55)$$

Similarly, dividing $\bar{\sigma}_d^*$ to $\underline{\sigma}_d^{\max,2}$ gives another upper bound:

$$\frac{\sigma_d^*}{\sigma_d^{\max}} \leq \frac{\bar{\sigma}_d^*}{\underline{\sigma}_d^{\max,2}} = \frac{\frac{1}{16} \left(d - \sqrt{d(d+16)} + 8 \right)}{\frac{1}{2} - \frac{(d-1)^{(1-\frac{1}{d})}}{2d} \left(\frac{t_c}{t_l} \right)^{1/d}}. \quad (5.56)$$

5.4 Numerical Results

5.4.1 Single-hop Network

We first investigate the accuracy of the proposed energy consumption analysis for the single-hop case. We performed simulations for $N = 5, 10$ and 100 . Simulation parameters are based on the measurements from the Mica2 mote reported in [3]: $P_t = 60mW$, $P_c = P_r = 45mW$, $P_s = 0.09mW$, $t_l = 15ms$, $t_c = 0.35ms$ and $R = 19.23Kb/s$. For each N , we performed simulations by increasing λ and we recorded the corresponding throughput and energy consumption in the network.

Fig. 5.4a presents the total energy consumption as the total throughput in the network increases. Figure also depicts (5.11) versus $N\sigma$ which matches with the simulation results. The two components of energy consumption, energy consumed while sleeping and carrier-sensing, are plotted in Figs. 5.4b and 5.4c, respectively. The high accuracy of the match between simulation and analytical results shows that the assumption of exponentially distributed carrier-sensing durations does not affect the accuracy of the analysis.

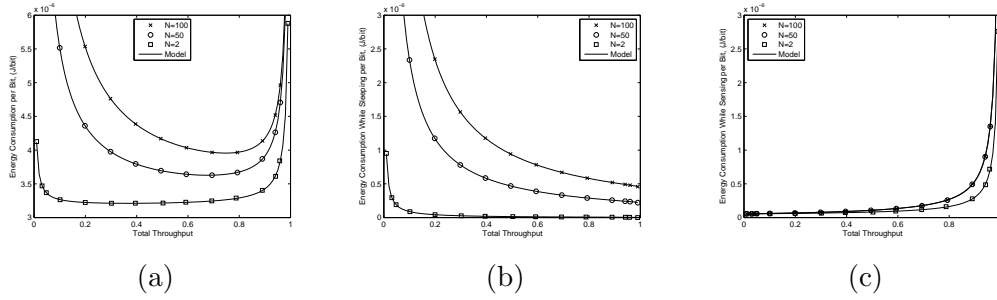


Figure 5.4: Energy consumption per node in the single-hop network. (a) Total energy consumption (b) Energy consumed while sleeping (c) Energy consumed while carrier sensing

It can be observed that the energy consumption per bit is higher for networks with a larger number of nodes. The main reason of this increase is associated with the increased sleeping costs with N as it can be seen in Fig. 5.4b. In a single-hop network, only a single node can transmit at a time so the rest of the nodes are sleeping. This results in an approximately linear increase in the sleeping costs with N so total energy consumption increases with N .

It can also be observed that the energy-optimum total throughput increases as N increases. Fig. 5.5 plots the energy-optimum total throughput as the number of nodes increases along with the proposed optimum throughput given by (5.14). The reason behind this increase is the different behaviors of energy consumed while sleeping and carrier-sensing as the number of nodes increases. The energy consumed while sleeping increases approximately linearly with the number of nodes. On the other hand, the energy consumed for carrier-sensing does not increase significantly with the number of nodes as it can be observed from Fig. 5.4c. So, the trade-off throughput tends to increase as N increases since the sleeping costs are lower at high throughputs.

Fig. 5.6 plots the optimum carrier-sensing frequency per node as the number of nodes increases. The figure also depicts (5.13) obtained from the analytical model. The model predicts the optimum carrier-sensing rate per node very accurately. To achieve energy minimization per bit, the nodes should reduce their carrier-sensing frequency approximately in proportional to $1/\sqrt{N}$ as it can be deduced from (5.13).

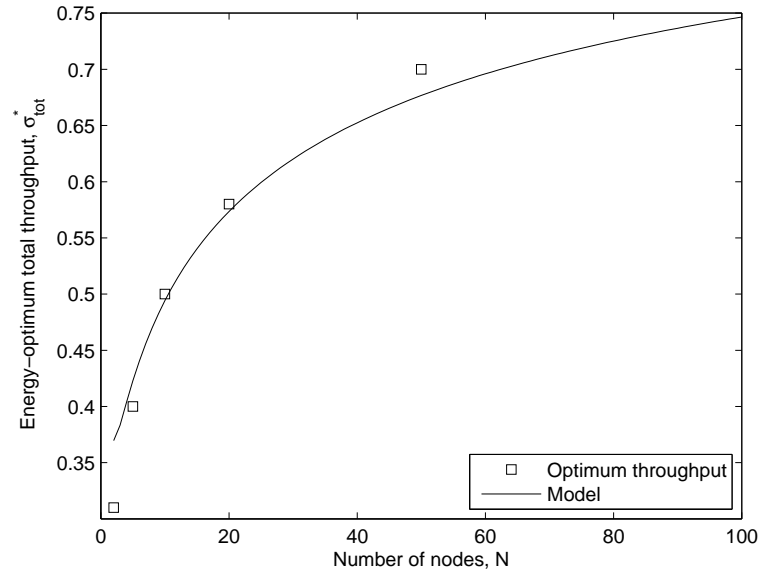


Figure 5.5: Change of energy-optimum total throughput as the number of nodes increases for the single-hop network.

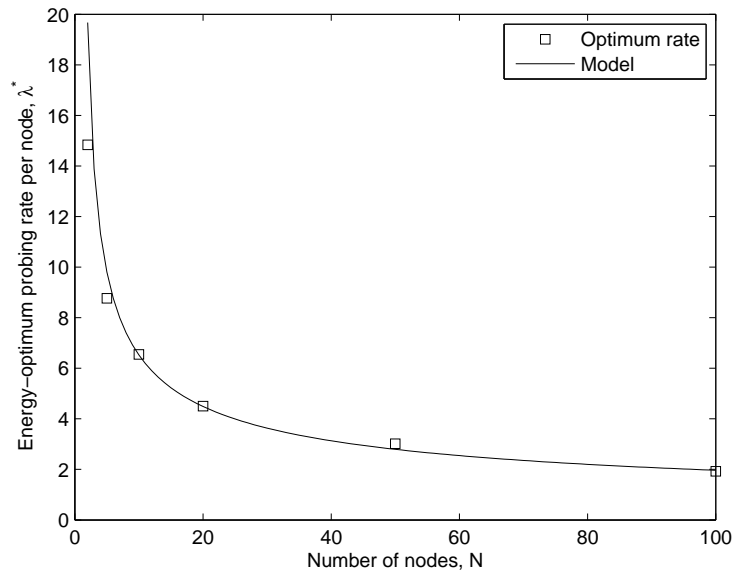


Figure 5.6: Energy-optimum carrier-sensing rate per node as the number of nodes increases for the single-hop network.

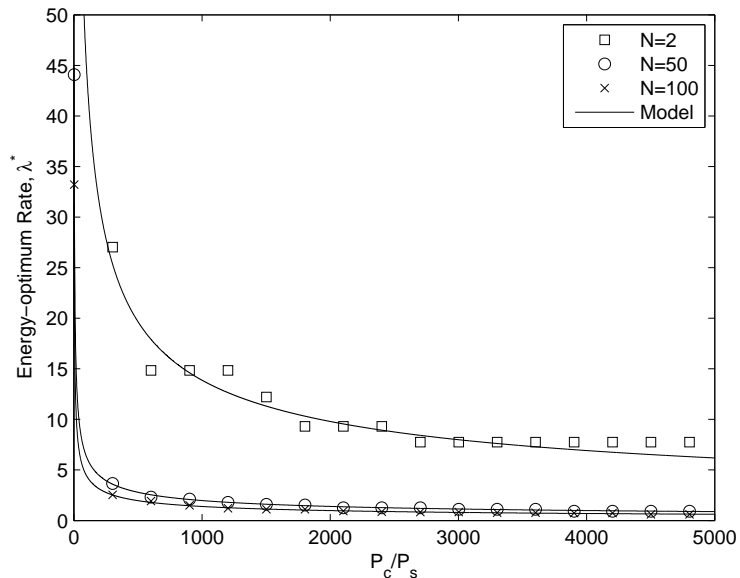


Figure 5.7: Energy-optimum carrier-sensing rate per node as P_c/P_s increases for the single-hop network.

Figs. 5.7 and 5.8 depict the energy-optimum carrier-sensing rate and energy-optimum throughput as the ratio of P_c/P_s changes, respectively. As the cost of carrier-sensing increases with respect to sleeping, the nodes need to sense the channel less frequently to minimize energy consumption per bit, so the energy-optimum rate and throughput reduces.

5.4.2 Multi-hop Network

To evaluate our analytical model for multi-hop networks, we performed simulations for random regular conflict graphs with $d = 2, 3$ and 10, which are created by the topology generation algorithm proposed by Viger [100]. Each simulated conflict graph consists of 1000 nodes.

We first investigate the accuracy of the relationship between the carrier sensing rate and the throughput given by (5.15) and (5.16) for random regular conflict graphs. Although the analysis is for a Cayley tree conflict graph where each internal node has a degree of d , we performed simulations for both the tree

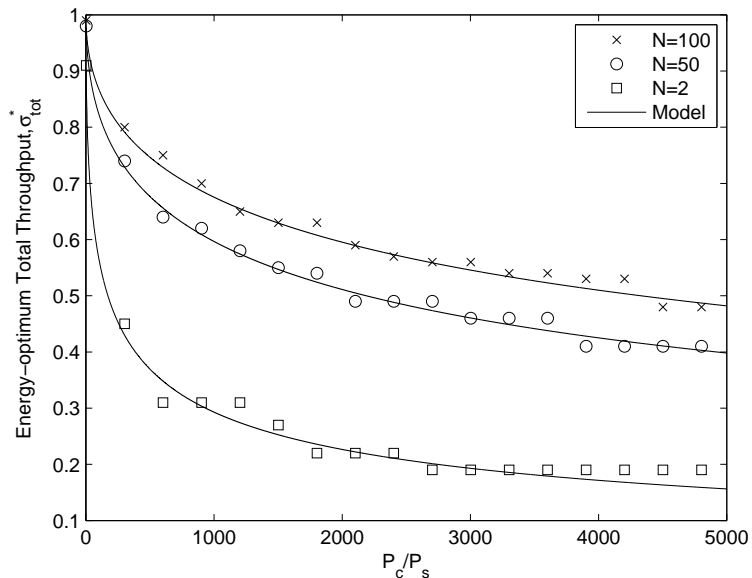


Figure 5.8: Energy-optimum total throughput as P_c/P_s increases for the single-hop network.

conflict graph and the random regular conflict graphs where each node has a degree of d for a unit packet length. As it can be seen from Fig. 5.9, the analysis is highly accurate for random regular conflict graphs as well as the Cayley-tree conflict graph. This result suggests that the relationship between the throughput and the carrier sensing rate mainly depends on the degree of the conflict graph.

We now investigate the energy consumption of the multi-hop network with the same parameters as the single-hop case as given in Sec. 5.4.1. The average energy consumption of the network per transmitted bit and the components of the energy consumption are shown in Fig. 5.10 for $d = 2, 3$ and 10 along with the values obtained from the proposed analytical model as given by (5.32). At low throughputs, sleeping increases the energy consumption per transmitted bit, and at high throughputs, the energy spent for carrier sensing dominates. As d increases, the energy spent for carrier sensing becomes significant because the probability that a carrier sensing attempt fails increases due to higher interference.

Fig. 5.11 plots how the energy-optimum carrier sensing rate changes as a function of P_c/P_s . As the energy consumption for carrier sensing increases, the

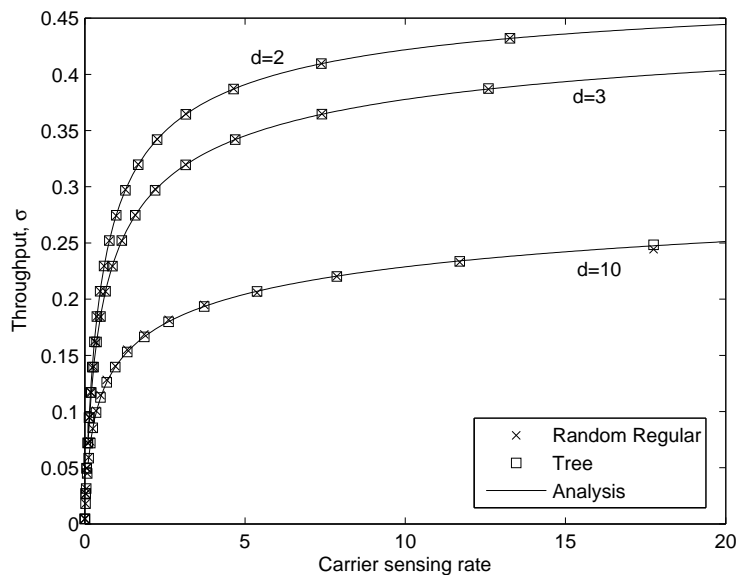


Figure 5.9: Relationship between the throughput and the carrier sensing rate for tree conflict graphs and random regular conflict graphs with $d = 2, 3$ and 4 .

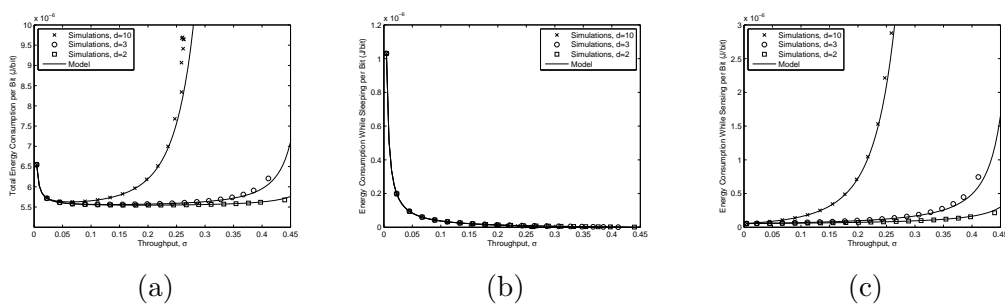


Figure 5.10: Energy consumption per node in the multi-hop network. (a) Total energy consumption (b) Energy consumed while sleeping (c) Energy consumed while carrier sensing

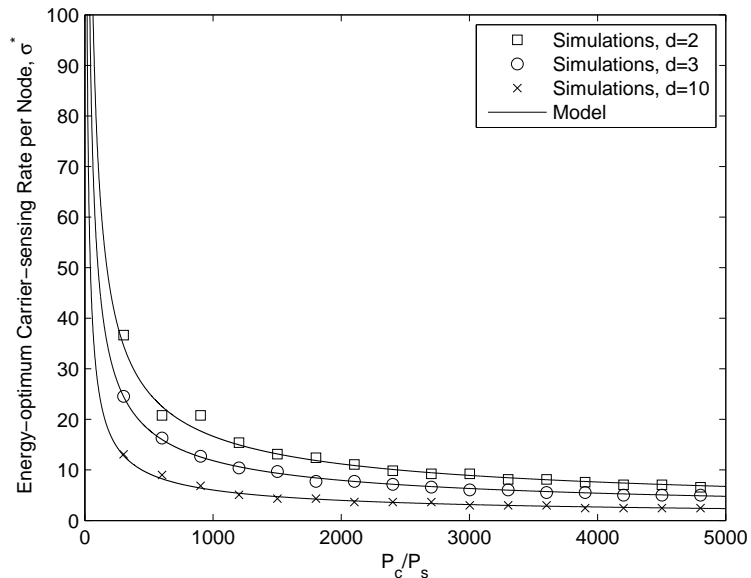


Figure 5.11: The energy-optimum carrier sensing rate as a function of $\frac{P_c}{P_s}$ for the multi-hop network.

energy-optimum carrier sensing rate reduces. Each failed carrier sensing attempt wastes energy—if carrier sensing is very expensive, nodes need to be less aggressive in order to reduce the probability of finding the channel busy. Fig. 5.12 plots the corresponding energy-optimum throughput obtained. For $d = 2$, (5.35) and (5.34) closely match with the energy-optimum carrier sensing rate and the energy-optimum throughput. For $d = 3$ and $d = 10$, the numerical solution of (5.33) is used to obtain the energy-optimum throughput and the result is substituted into (5.18) to obtain the energy-optimum carrier-sensing rate.

5.4.3 Bounds on the σ_d^{max} and σ_d^* for the multi-hop network.

In this part, we demonstrate the change in the σ_d^* and σ_d^{max} with d and evaluate the performance of the proposed bounds. Fig. 5.13 plots σ_d^{max} as d increases for $\frac{t_c}{t_l} \approx 0.02$ which corresponds to the simulation parameters used in this section and for $\frac{t_c}{t_l} = 0.001$ which is the case where carrier-sensing takes a shorter time in comparison to the packet duration. In this figure, the lower and upper bounds on

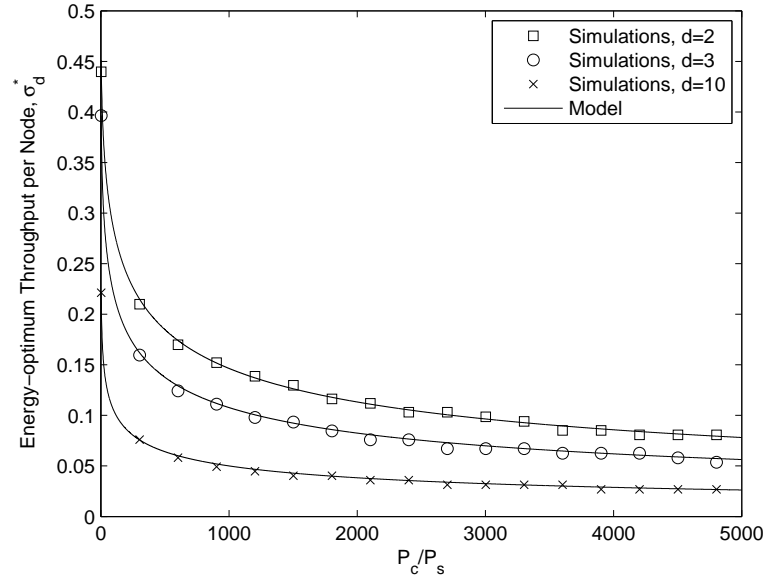
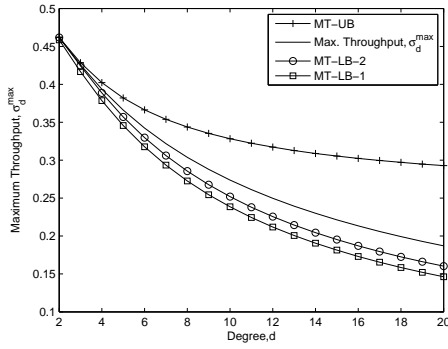


Figure 5.12: The energy-optimum throughput as a function of $\frac{P_c}{P_s}$ for the multi-hop network.

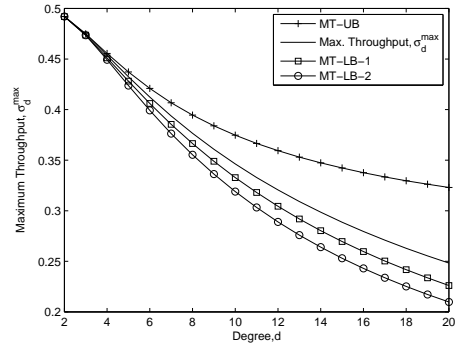
σ_d^{max} derived in Sec. 5.3.1 and Sec. 5.3.2 are also depicted. At low degrees, $\underline{\sigma}_d^{max,2}$ provides a better lower bound but $\underline{\sigma}_d^{max,1}$ performs better at higher degrees. On the other hand, the upper bound $\bar{\sigma}_d^{max}$ is close for small values of d but it becomes looser as d increases.

Fig. 5.14 plots the energy-optimum throughput, σ_d^* , along with its lower and upper bounds. For $\frac{t_c}{t_l} \approx 0.02$, $\underline{\sigma}_d^*$ results in negative values for $d < 8$ but its tightness improves as d increases. For $\frac{t_c}{t_l} = 0.001$, $\underline{\sigma}_d^*$ provides a very tight bound by differing less than 0.1% from σ_d^* at $d = 20$. The upper bound $\bar{\sigma}_d^*$ is not valid for $\frac{t_c}{t_l} = 0.001$ since the conditions of upper bound given by (5.53) is not satisfied. However, for $\frac{t_c}{t_l} = 0.02$, it provides an upper bound which changes nearly parallel to σ_d^* for the considered range of d values.

The ratio of the energy-optimum throughput to the maximum throughput is plotted in Fig. 5.15 along with the lower and upper bounds $\frac{\sigma_d^*}{\bar{\sigma}_d^{max}}$, $\frac{\bar{\sigma}_d^*}{\underline{\sigma}_d^{max,1}}$ and $\frac{\bar{\sigma}_d^*}{\underline{\sigma}_d^{max,2}}$. It is observed that the ratio $\frac{\sigma_d^*}{\bar{\sigma}_d^{max}}$ decreases as d increases. For $\frac{t_c}{t_l} = 0.001$, the upper bounds are not valid. However, for $\frac{t_c}{t_l} \approx 0.02$, the upper bounds demonstrate that the ratio of energy-optimum throughput cannot exceed half of

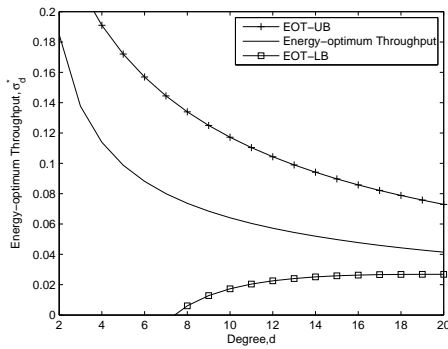


(a)

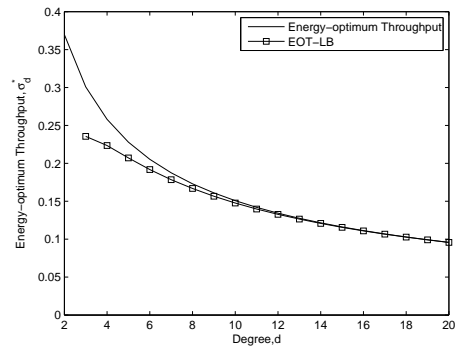


(b)

Figure 5.13: Maximum throughput as a function of d for the multi-hop network for a) $\frac{t_c}{t_l} \approx 0.02$ b) $\frac{t_c}{t_l} = 0.001$



(a)



(b)

Figure 5.14: Energy-optimum throughput as a function of d for the multi-hop network for a) $\frac{t_c}{t_l} \approx 0.02$ b) $\frac{t_c}{t_l} = 0.001$

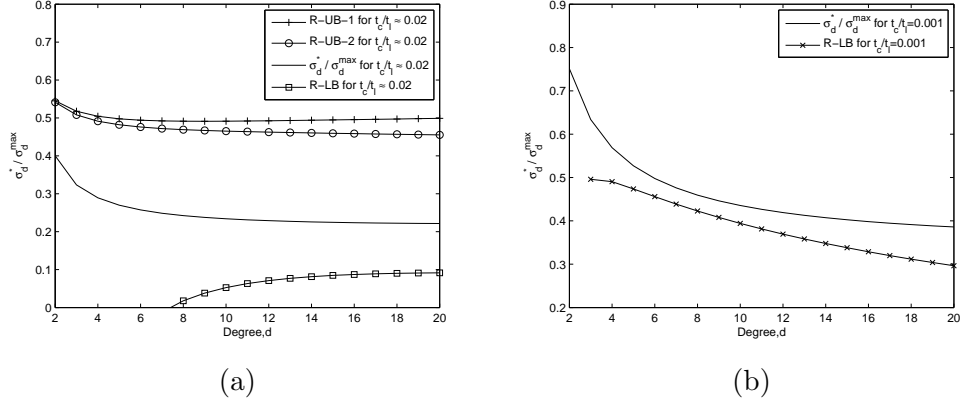


Figure 5.15: Ratio of energy-optimum throughput to maximum throughput as a function of d for the multi-hop network for a) $\frac{t_c}{t_l} \approx 0.02$ b) $\frac{t_c}{t_l} = 0.001$

the maximum throughput for $d \geq 4$.

5.5 Conclusions

We proposed an energy consumption model of a node in a CSMA network. The proposed model shows that the number of failed carrier sensing attempts significantly increases at high throughputs causing energy waste. On the contrary, at low throughputs, nodes sleep during most of their lifetimes which also results in energy waste as far as the energy per transmitted bit is considered. We derived the energy-optimum carrier sensing rate and the corresponding energy-optimum throughput for both a single-hop network and a multi-hop network.

For single-hop networks, we observe that the energy-optimum throughput increases with the number of nodes sharing the channel. On the other hand, the energy-optimum throughput reduces with the degree of the conflict graph for multi-hop networks. For both the single-hop and multi-hop case, our results suggest that as the power required for carrier sensing increases, the energy-optimum sensing rate and throughput reduce. By proposing several bounds, we show that the energy-optimum throughput cannot exceed approximately half of the maximum throughput for the simulation parameters which are taken from the previous

literature.

Our results have implications for the design of adaptive optimal-CSMA algorithms. We observe a dramatic increase in the carrier-sensing rates as the throughput limits reached, as a result, the energy consumption also increases significantly. The trade-off between the energy consumption and throughput has to be considered in the design of adaptive MAC algorithms.

Table 5.1: List of Notations

Symbol	Definition
σ	Throughput per node
σ_{tot}	Total throughput in the network
σ^*	Energy-optimum throughput per node
σ_{tot}^*	Energy-optimum total throughput in the network
σ^{\max}	Maximum throughput per node
λ	Carrier-sensing rate
$\hat{\lambda}$	Normalized carrier-sensing rate
λ^*	Energy-optimum carrier-sensing rate
t_l	Packet duration
t_c	Carrier-sensing duration
N	Number of nodes
P_t	Transmit power
P_r	Receive power
P_c	Power spent during carrier-sensing
P_s	Power spent during sleeping
T_i	Inter-transmission duration
T_t	Time spent for transmission per packet
T_r	Time spent for reception per packet
T_c	Time spent for carrier sensing per packet
T_s	Time spent for sleeping per packet
R	Data transmission rate
E_p	Energy consumed per transmitted packet
E_b	Energy consumed per transmitted bit

Chapter 6

Conclusions

We here focused on the CSMA protocol which forms the basis of the many existing wireless networking protocols. We investigated the performance of the CSMA protocol in several newly encountered wireless communications scenarios.

The first issue was the performance of the CSMA protocol for channels with large propagation delay. Main application area of this study is underwater acoustic networks where the acoustic waves have a very low propagation speed. Lack of a central coordinator and the difficulty of synchronization in underwater networks make random access techniques a viable option and CSMA is one of the candidates to be used in the underwater setting. However, main problem of using CSMA in large propagation delay channels is the collisions caused by propagation delay.

In such a channel, we investigated how the throughput of a CSMA channel behaves as a function of the carrier sensing rate of nodes under saturated traffic load. At very low carrier sensing rates, the collision probability is very low but the channel utilization is also very limited. At very high channel sensing rates, on the other hand, the channel is mostly busy but the throughput may still be low because of increased number of collisions due to propagation delay. We obtained the optimum carrier sensing rate which maximizes the throughput of a CSMA channel using the throughput model we proposed. We showed how the optimum

propagation delay and the maximum throughput changes with the number of nodes and with the average propagation delay in the network.

The main contribution of this study is that we showed how the carrier sensing rates of nodes should adapt according to the propagation delay and to the addition of a new node. The proposed model can be used in assessing the performance of existing MAC protocols. For example, we have compared the 802.11 scheme with our proposed model for a simple two-node scenario. In addition, the proposed model provides rules of thumb on the design of the new protocols for high-latency channels.

In this study, we have not proposed a specific method which adapts probing rates according to the model we proposed. To realize such a mechanism, a method which can deduce the propagation delay and the number of nodes has to be proposed. Design of such a MAC protocol is a subject of future study.

The second problem that we investigated is the short-term fairness of large-scale CSMA networks. In the CSMA protocol, a node can capture the channel if its neighbors are not transmitting. This condition creates an interaction between a node and its neighbors. Considering that the neighbors of a node also interact with their neighbors, a node also loosely interacts with further away nodes. We investigated the implications of this interaction on the short-term fairness of a CSMA network.

We investigated if the global parameters of a CSMA system have an effect on the short-term fairness performance of the individual nodes. We showed that the network degree has an important effect on the short-term fairness as higher degree networks are less short-term fair than low degree networks. We also demonstrated the system size has negligible effect for random regular network topologies. We also highlighted some of the results from the statistical physics literature on the long-range correlations in a locally interacting system of nodes. Since the short-term fairness of a CSMA network depends also on the long-range correlations, we investigated some of the conditions of long-range correlations.

Methods should be designed to reduce the short-term fairness problem of

large-scale CSMA systems. There is a consensus in the community that the short-term fairness cannot be attained while achieving the limits of the capacity region by a distributed protocol. Still, methods which provide a satisfactory short-term fairness performance while achieving a fraction of the capacity region have to be designed and this subject is a future line of study.

The third issue that we covered is the energy efficiency of the CSMA protocol. Energy efficiency has become a crucial factor for wireless networks because of the increase in the battery powered wireless devices and due to environmental considerations. Although energy consumption analyses of specific standards are available, a general framework relating the throughput of a network to its energy consumption was lacking. We proposed an energy consumption model which provides the energy consumption as a function of throughput. This model includes the energy consumed for carrier sensing and energy consumed while sleeping which are usually neglected in previous studies.

Using this model, we obtain the energy-optimum throughput at which a CSMA network should operate to minimize energy consumption. We also obtain the carrier-sensing rate which leads to this energy-optimum throughput. We obtain these results as a function of specific hardware parameters such as power required for carrier-sensing and sleeping, packet duration and carrier-sensing duration. So, given the parameters of the specific application, the energy-optimum operating load which minimizes energy consumption can be obtained using the proposed model.

Similar to the two previous topics, there is a need for designing a MAC protocol which implements the insights gained from the proposed analysis. For example, a MAC protocol which can adapt the bursty traffic load in the network to the energy-optimum operating load to conserve energy can be designed.

In summary, we have investigated the performance of the CSMA protocol from three different perspectives. This thesis, by providing mathematical models and simulation results, sheds light on the performance of CSMA protocol for several wireless scenarios which will become more widespread in the near future.

Bibliography

- [1] N. Abramson, “THE ALOHA SYSTEM: another alternative for computer communications,” in *Proceedings of the AFIPS*, 1970.
- [2] F. A. Tobagi, *Random Access Techniques for Data Transmission over Packet Switched Radio Networks*. PhD thesis, CALIFORNIA UNIV LOS ANGELES SCHOOL OF ENGINEERING AND APPLIED SCIENCE, 1974.
- [3] J. Polastre, J. Hill, and D. Culler, “Versatile low power media access for wireless sensor networks,” in *Proceedings of the 2nd International Conference on Embedded Networked Sensor Systems*, 2004.
- [4] J. Heidemann, W. Ye, J. Wills, A. Syed, and Y. Li, “Research challenges and applications for underwater sensor networking,” in *IEEE Wireless Communications and Networking Conference*, vol. 1, pp. 228–235, Apr. 2006.
- [5] C. Stevenson, G. Chouinard, Z. Lei, W. Hu, S. Shellhammer, and W. Caldwell, “IEEE 802.22: The first cognitive radio wireless regional area network standard,” *IEEE Communications Magazine*, vol. 47, pp. 130–138, Jan. 2009.
- [6] D. Bertsekas and R. Gallager, *Data networks (2nd ed.)*. Upper Saddle River, NJ, USA: Prentice-Hall, Inc., 1992.
- [7] R. Rom and M. Sidi, “Multiple access protocols: performance and analysis,” 1990.

- [8] L. G. Roberts, "Aloha packet system with and without slots and capture," *SIGCOMM Comput. Commun. Rev.*, vol. 5, pp. 28–42, 1975.
- [9] F. A. Tobagi and V. B. Hunt, "Performance analysis of carrier sense multiple access with collision detection," *Computer Networks*, vol. 4, pp. 245–259, 1980.
- [10] P. Karn, "MACA—a new channel access method for packet radio," in *ARRL/CRRL Amateur Radio 9th, Computer Networking Conference*, 1990.
- [11] V. Bharghavan, A. Demers, S. Shenker, and L. Zhang, "MACAW: a media access protocol for wireless LAN's," in *SIGCOMM '94: Proceedings of the conference on Communications architectures, protocols and applications*, (New York, NY, USA), pp. 212–225, ACM, 1994.
- [12] L. Kleinrock and F. Tobagi, "Packet switching in radio channels: Part I—carrier sense multiple-access modes and their throughput-delay characteristics," *IEEE Transactions on Communications*, vol. 23, pp. 1400–1416, Dec. 1975.
- [13] H. Takagi and L. Kleinrock, "Throughput analysis for persistent CSMA systems," *IEEE Transactions on Communications*, vol. 33, pp. 627–638, Jul. 1985.
- [14] C. Steger, P. Radosavljevic, and J. Frantz, "Performance of IEEE 802.11b wireless LAN in an emulated mobile channel," in *The 57th IEEE Semianual Vehicular Technology Conference*, vol. 2, pp. 1479–1483, Apr. 2003.
- [15] M. Clark, K. Leung, B. McNair, and Z. Kostic, "Outdoor IEEE 802.11 cellular networks: radio link performance," in *IEEE International Conference on Communications*, vol. 1, pp. 512–516, 2002.
- [16] K. Leung, B. McNair, J. Cimini, L.J., and J. Winters, "Outdoor IEEE 802.11 cellular networks: MAC protocol design and performance," in *IEEE International Conference on Communications*, vol. 1, pp. 595–599, Apr. 2002.

- [17] P. Bhagwat, B. Raman, and D. Sanghi, “Turning 802.11 inside-out,” *SIGCOMM Comput. Commun. Rev.*, vol. 34, pp. 33–38, Jan. 2004.
- [18] K. Chebrolu, B. Raman, and S. Sen, “Long-distance 802.11b links: Performance measurements and experience,” vol. 2006, pp. 74–85, 2006.
- [19] A. Sheth, S. Nedeveschi, R. Patra, S. Surana, E. Brewer, and L. Subramanian, “Packet loss characterization in WiFi-based long distance networks,” pp. 312–320, 2007.
- [20] R. Patra, S. Nedeveschi, S. Surana, A. Sheth, L. Subramanian, and E. Brewer, “WiLDNet: Design and implementation of high performance WiFi based long distance networks,” in *Proceedings of the 4th USENIX conference on networked systems design and implementation*, Apr. 2007.
- [21] G. Bianchi, “Performance analysis of the IEEE 802.11 distributed coordination function,” *IEEE Journal on Selected Areas in Communications*, vol. 18, no. 3, pp. 535–547, 2000.
- [22] E. Lopez-Aguilera, J. Casademont, and J. Cotrina, “Propagation delay influence in IEEE 802.11 outdoor networks,” *Wireless Networks*, vol. 16, pp. 1123–1142, May. 2010.
- [23] M. Tanaka, D. Umehara, M. Morikura, N. Otsuki, and T. Sugiyama, “New throughput analysis of long-distance IEEE 802.11 wireless communication system for smart grid,” in *IEEE International Conference on Smart Grid Communications*, pp. 90–95, Oct. 2011.
- [24] J. Simo Reigadas, A. Martinez-Fernandez, J. Ramos-Lopez, and J. Seoane-Pascual, “Modeling and optimizing IEEE 802.11 DCF for long-distance links,” *IEEE Transactions on Mobile Computing*, vol. 9, pp. 881–896, Jun. 2010.
- [25] J. Partan, J. Kurose, and B. N. Levine, “A survey of practical issues in underwater networks,” in *1st ACM International Workshop on Underwater Networks (WUWNet)*, pp. 17–24, Sep. 2006.

- [26] H. Matsuno, H. Ishinaka, and T. Shigeyasu, “Effect of propagation delay and RTS packet recognition time on MACA,” *Electronics and Communications in Japan (Part I Communications)*, vol. 88, pp. 21–31, Jan. 2005.
- [27] P. Xie and J.-H. Cui, “Exploring random access and handshaking techniques in large-scale underwater wireless acoustic sensor networks,” in *OCEANS*, pp. 1–6, Sep. 2006.
- [28] X. Guo, M. Frater, and M. Ryan, “A propagation-delay-tolerant collision avoidance protocol for underwater acoustic sensor networks,” in *OCEANS*, pp. 1–6, May 2006.
- [29] X. Guo, M. Frater, and M. Ryan, “Design of a propagation-delay-tolerant mac protocol for underwater acoustic sensor networks,” *IEEE Journal of Oceanic Engineering*, vol. 34, pp. 170–180, april 2009.
- [30] B. Peleato and M. Stojanovic, “Distance aware collision avoidance protocol for ad-hoc underwater acoustic sensor networks,” *IEEE Communications Letters*, vol. 11, pp. 1025–1027, Dec. 2007.
- [31] L. Vieira, J. Kong, U. Lee, and M. Gerla, “Analysis of ALOHA protocols for underwater acoustic sensor networks,” in *1st ACM International Workshop on Underwater Networks (WUWNet)*, Sep. 2006.
- [32] J. Ahn, A. Syed, B. Krishnamachari, and J. Heidemann, “Design and analysis of a propagation delay tolerant ALOHA protocol for underwater networks,” *Ad Hoc Networks*, vol. 9, pp. 752–766, Jul. 2011.
- [33] A. A. Syed, W. Ye, J. Heidemann, and B. Krishnamachari, “Understanding spatio-temporal uncertainty in medium access with ALOHA protocols,” in *2nd ACM International Workshop on Underwater networks (WUWNet)*, pp. 41–48, Sep. 2007.
- [34] S. De, P. Mandal, and S. S. Chakraborty, “On the characterization of Aloha in underwater wireless networks,” *Mathematical and Computer Modelling*, vol. 53, pp. 2093–2107, Jun. 2011.

- [35] Y. Zhou, K. Chen, J. He, and H. Guan, “Enhanced slotted Aloha protocols for underwater sensor networks with large propagation delay,” in *IEEE Vehicular Technology Conference (VTC Spring)*, pp. 1–5, May. 2011.
- [36] Y. Xiao, Y. Zhang, J. Gibson, and G. Xie, “Performance analysis of p-persistent Aloha for multi-hop underwater acoustic sensor networks,” in *International Conference on Embedded Software and Systems*, pp. 305–311, May 2009.
- [37] Z. Naor and H. Levy, “A centralized dynamic access probability protocol for next generation wireless networks,” in *IEEE INFOCOM*, vol. 2, pp. 767–775, 2001.
- [38] N. Chirdchoo, W.-S. Soh, and K. C. Chua, “Aloha-based MAC protocols with collision avoidance for underwater acoustic networks,” in *IEEE INFOCOM*, pp. 2271–2275, May 2007.
- [39] Y. Noh, P. Wang, U. Lee, D. Torres, and M. Gerla, “DOTS: A propagation delay-aware opportunistic MAC protocol for underwater sensor networks,” in *18th IEEE International Conference on Network Protocols (ICNP)*, Oct. 2010.
- [40] N. Chirdchoo, W.-S. Soh, and K. Chua, “RIPT: A receiver-initiated reservation-based protocol for underwater acoustic networks,” *IEEE Journal on Selected Areas in Communications*, vol. 26, pp. 1744–1753, Dec. 2008.
- [41] Y.-J. Chen and H.-L. Wang, “Ordered CSMA: a collision-free MAC protocol for underwater acoustic networks,” in *OCEANS*, pp. 1–6, Oct. 2007.
- [42] P. Xie and J.-H. Cui, “R-MAC: An energy-efficient MAC protocol for underwater sensor networks,” in *International Conference on Wireless Algorithms, Systems and Applications*, pp. 187–198, Aug. 2007.
- [43] M. Molins and M. Stojanovic, “Slotted FAMA: a MAC protocol for underwater acoustic networks,” in *OCEANS*, pp. 1–7, May. 2006.

- [44] A. Syed, W. Ye, and J. Heidemann, “T-Lohi: A new class of MAC protocols for underwater acoustic sensor networks,” in *IEEE INFOCOM*, pp. 231–235, Apr. 2008.
- [45] C. Petrioli, R. Petroccia, and J. Potter, “Performance evaluation of underwater MAC protocols: From simulation to at-sea testing,” in *IEEE OCEANS*, pp. 1–10, Jun. 2011.
- [46] R. Jain, D. Chiu, and W. Hawe, “A quantitative measure of fairness and discrimination for resource allocation in shared computer systems,” *ArXiv Computer Science e-prints*, 1998.
- [47] M. Mehrjoo, M. Dianati, X. S. Shen, and K. Naik, “Opportunistic fair scheduling for the downlink of IEEE 802.16 wireless metropolitan area networks,” in *Proceedings of the 3rd international conference on Quality of service in heterogeneous wired/wireless networks*, QShine ’06, (New York, NY, USA), ACM, 2006.
- [48] M. Garetto, T. Salonidis, and E. Knightly, “Modeling per-flow throughput and capturing starvation in CSMA multi-hop wireless networks,” *IEEE/ACM Transactions on Networking*, vol. 16, pp. 864–877, 2008.
- [49] M. Dianati, X. Shen, and S. Naik, “A new fairness index for radio resource allocation in wireless networks,” in *IEEE Wireless Communications and Networking Conference*, vol. 2, pp. 712–717, Mar. 2005.
- [50] J. Deng, Y. Han, and B. Liang, “Fairness index based on variational distance,” in *IEEE GLOBECOM*, pp. 1–6, Dec. 2009.
- [51] T. Lan and M. Chiang, “Measuring fairness: Axioms and applications,” in *Communication, Control, and Computing (Allerton), 2011 49th Annual Allerton Conference on*, pp. 156–163, Sep. 2011.
- [52] P. Gupta, R. Gray, and P. R. Kumar, “An experimental scaling law for ad hoc networks,” 2001.

- [53] S. Xu and T. Saadawi, “Does the IEEE 802.11 MAC protocol work well in multihop wireless ad hoc networks?,” *IEEE Communications Magazine*, vol. 39, pp. 130–137, Jun. 2001.
- [54] C. Chaudet, D. Dhoutaut, and I. Lassous, “Experiments of some performance issues with IEEE 802.11b in ad hoc networks,” in *Second Annual Conference on Wireless On-demand Network Systems and Services*, pp. 158–163, Jan. 2005.
- [55] X. Wang and K. Kar, “Throughput modelling and fairness issues in CSMA/CA based ad-hoc networks,” in *IEEE INFOCOM*, vol. 1, pp. 23–34, 2005.
- [56] M. Garetto, J. Shi, and E. W. Knightly, “Modeling media access in embedded two-flow topologies of multi-hop wireless networks,” in *Proceedings of the 11th annual international conference on Mobile computing and networking, MobiCom ’05*, (New York, NY, USA), pp. 200–214, ACM, 2005.
- [57] K. Medepalli and F. A. Tobagi, “Towards performance modeling of IEEE 802.11 based wireless networks: A unified framework and its applications,” in *IEEE INFOCOM*, pp. 1–12, Apr. 2006.
- [58] J. Shi, T. Salonidis, and E. W. Knightly, “Starvation mitigation through multi-channel coordination in CSMA multi-hop wireless networks,” in *Proceedings of the 7th ACM international symposium on Mobile ad hoc networking and computing, MobiHoc ’06*, (New York, NY, USA), pp. 214–225, ACM, 2006.
- [59] M. Durvy, O. Dousse, and P. Thiran, “Self-organization properties of CSMA/CA systems and their consequences on fairness,” *IEEE Transactions on Information Theory*, vol. 55, no. 3, pp. 931–943, 2009.
- [60] M. Durvy, O. Dousse, and P. Thiran, “On the fairness of large CSMA networks,” *IEEE Journal on Selected Areas in Communications*, vol. 27, no. 7, pp. 1093–1104, 2009.

- [61] P. M. van de Ven, S. C. Borst, D. Denteneer, A. J. Janssen, and J. S. van Leeuwaarden, “Equalizing throughputs in random-access networks,” *SIGMETRICS Perform. Eval. Rev.*, vol. 38, pp. 39–41, 2010.
- [62] P. van de Ven, J. van Leeuwaarden, D. Denteneer, and A. Janssen, “Spatial fairness in linear random-access networks,” *Performance Evaluation*, vol. 69, no. 34, pp. 121–134, 2012.
- [63] P. van de Ven, A. Janssen, J. van Leeuwaarden, and S. Borst, “Achieving target throughputs in random-access networks,” *Performance Evaluation*, vol. 68, no. 11, pp. 1103–1117, 2011.
- [64] E. Pinsky and Y. Yemini, “The asymptotic analysis of some packet radio networks,” *IEEE Journal on Selected Areas in Communications*, vol. 4, pp. 938–945, Sep. 1986.
- [65] S. C. Liew, C. H. Kai, H. C. Leung, and P. Wong, “Back-of-the-envelope computation of throughput distributions in CSMA wireless networks,” *IEEE Transactions on Mobile Computing*, vol. 9, pp. 1319–1331, Sep. 2010.
- [66] L. Jiang and J. Walrand, “A distributed CSMA algorithm for throughput and utility maximization in wireless networks,” in *46th Annual Allerton Conference on Communication, Control, and Computing*, pp. 1511–1519, Sep. 2008.
- [67] S. Rajagopalan and D. Shah, “Distributed algorithm and reversible network,” in *42nd Annual Conference on Information Sciences and Systems*, pp. 498–502, 2008.
- [68] S. Rajagopalan, D. Shah, and J. Shin, “Network adiabatic theorem: An efficient randomized protocol for contention resolution,” in *SIGMETRICS '09*, (New York, NY, USA), pp. 133–144, ACM, 2009.
- [69] L. Jiang, D. Shah, J. Shin, and J. Walrand, “Distributed random access algorithm: Scheduling and congestion control,” *IEEE Transactions on Information Theory*, vol. 56, no. 12, pp. 6182–6207, 2010.

- [70] C. E. Koksal, H. Kassab, and H. Balakrishnan, “An analysis of short-term fairness in wireless media access protocols (poster session),” in *ACM SIGMETRICS International Conference on Measurement and Modeling of Computer Systems*, pp. 118–119, 2000.
- [71] G. Berger-Sabbatel, A. Duda, O. Gaudoin, M. Heusse, and F. Rousseau, “Fairness and its impact on delay in 802.11 networks,” in *IEEE Global Telecommunications Conference*, vol. 5, pp. 2967 – 2973, 2004.
- [72] Z. Li, S. Nandi, and A. Gupta, “Modeling the short-term unfairness of IEEE 802.11 in presence of hidden terminals,” *Performance Evaluation*, vol. 63, pp. 441–462, May. 2006.
- [73] C. Barrett, M. Marathe, D. Engelhart, and A. Sivasubramaniam, “Analyzing the short-term fairness of IEEE 802.11 in wireless multi-hop radio networks,” in *10th IEEE International Symposium on Modeling, Analysis and Simulation of Computer and Telecommunications Systems*, pp. 137–144, 2002.
- [74] C. H. Kai and S. C. Liew, “Temporal starvation in CSMA wireless networks,” in *IEEE International Conference on Communications (ICC)*, pp. 1–6, 2011.
- [75] J. Liu, Y. Yi, A. Proutiere, M. Chiang, and H. V. Poor, “Towards utility-optimal random access without message passing,” *Wireless Communications and Mobile Computing*, vol. 10, pp. 115–128, Jan. 2010.
- [76] L. Jiang, M. Leconte, J. Ni, R. Srikant, and J. Walrand, “Fast mixing of parallel glauber dynamics and low-delay csma scheduling,” in *IEEE INFOCOM*, pp. 371–375, 2011.
- [77] N. Bouman, S. Borst, and J. van Leeuwen, “Achievable delay performance in CSMA networks,” in *49th Annual Allerton Conference on Communication, Control, and Computing (Allerton)*, pp. 384–391, 2011.
- [78] D. Shah, D. Tse, and J. Tsitsiklis, “Hardness of low delay network scheduling,” *IEEE Transactions on Information Theory*, vol. 57, no. 12, pp. 7810–7817, 2011.

- [79] L. Jiang, J. Ni, R. Srikant, and J. Walrand, “Performance bounds of distributed CSMA scheduling,” in *Information Theory and Applications Workshop (ITA)*, pp. 1–6, 2010.
- [80] V. Subramanian and M. Alanyali, “Delay performance of CSMA in networks with bounded degree conflict graphs,” in *IEEE International Symposium on Information Theory*, 2011.
- [81] M. Lotfinezhad and P. Marbach, “Throughput-optimal random access with order-optimal delay,” in *IEEE INFOCOM*, pp. 2867–2875, 2011.
- [82] D. Shah and J. Shin, “Delay optimal queue-based CSMA,” *SIGMETRICS Perform. Eval. Rev.*, vol. 38, no. 1, pp. 373–374, 2010.
- [83] J. Ni, B. Tan, and R. Srikant, “Q-CSMA: Queue-length based CSMA/CA algorithms for achieving maximum throughput and low delay in wireless networks,” in *IEEE INFOCOM*, pp. 1–5, Mar. 2010.
- [84] J. Ghaderi and R. Srikant, “On the design of efficient CSMA algorithms for wireless networks,” in *49th IEEE Conference on Decision and Control (CDC)*, pp. 954–959, 2010.
- [85] N. Bouman, S. C. Borst, and J. S. van Leeuwen, “Delay performance of backlog based random access,” *SIGMETRICS Perform. Eval. Rev.*, vol. 39, no. 2, pp. 32–34, 2011.
- [86] N. Bouman, S. Borst, J. van Leeuwen, and A. Proutiere, “Backlog-based random access in wireless networks: Fluid limits and delay issues,” in *23rd International Teletraffic Congress (ITC)*, pp. 39–46, 2011.
- [87] K. Langendoen and G. Halkes, “Energy-efficient medium access control,” in *Embedded Systems Handbook*, CRC press, 2005.
- [88] M. Miller and N. Vaidya, “Minimizing energy consumption in sensor networks using a wakeup radio,” in *IEEE Wireless Communications and Networking Conference*, 2004.
- [89] W. Ye, J. Heidemann, and D. Estrin, “An energy-efficient MAC protocol for wireless sensor networks,” in *IEEE INFOCOM*, 2002.

- [90] G. Halkes and K. Langendoen, “Crankshaft: An energy-efficient MAC-Protocol for dense wireless sensor networks,” in *Wireless Sensor Networks* (K. Langendoen and T. Voigt, eds.), vol. 4373 of *Lecture Notes in Computer Science*, pp. 228–244, Springer Berlin Heidelberg, 2007.
- [91] J. Hill and D. Culler, “Mica: a wireless platform for deeply embedded networks,” *IEEE Micro*, vol. 22, no. 6, pp. 12–24, 2002.
- [92] A. El-Hoiydi, “Aloha with preamble sampling for sporadic traffic in ad hoc wireless sensor networks,” in *IEEE International Conference on Communications*, vol. 5, pp. 3418–3423, 2002.
- [93] M. Buettner, G. V. Yee, E. Anderson, and R. Han, “X-MAC: a short preamble MAC protocol for duty-cycled wireless sensor networks,” in *Proceedings of the 4th International Conference on Embedded Networked Sensor Systems*, 2006.
- [94] A. El-Hoiydi, J.-D. Decotignie, C. Enz, and E. Le Roux, “Poster abstract: wiseMAC, an ultra low power MAC protocol for the wiseNET wireless sensor network,” in *Proceedings of the 1st international conference on embedded networked sensor systems*, SenSys '03, (New York, NY, USA), pp. 302–303, ACM, 2003.
- [95] Y. Sun, O. Gurewitz, and D. B. Johnson, “RI-MAC: a receiver-initiated asynchronous duty cycle MAC protocol for dynamic traffic loads in wireless sensor networks,” in *Proceedings of the 6th ACM Conference on Embedded Network Sensor Systems*, 2008.
- [96] L. Tang, Y. Sun, O. Gurewitz, and D. Johnson, “PW-MAC: An energy-efficient predictive-wakeup MAC protocol for wireless sensor networks,” in *IEEE INFOCOM*, 2011.
- [97] F. Cali, M. Conti, and E. Gregori, “Dynamic tuning of the IEEE 802.11 protocol to achieve a theoretical throughput limit,” *IEEE/ACM Transactions on Networking*, vol. 8, pp. 785–799, Dec. 2000.

- [98] R. Boorstyn, A. Kershenbaum, B. Maglaris, and V. Sahin, “Throughput analysis in multihop CSMA packet radio networks,” *IEEE Transactions on Communications*, vol. 35, pp. 267–274, Mar. 1987.
- [99] “Network simulator 2 (ns2).” <http://www.isi.edu/nsnam/ns/>.
- [100] F. Viger and M. Latapy, “Efficient and simple generation of random simple connected graphs with prescribed degree sequence,” in *Computing and Combinatorics*, Lecture Notes in Computer Science, Springer Berlin / Heidelberg, 2005.
- [101] J. Robinson and E. Knightly, “A performance study of deployment factors in wireless mesh networks,” in *IEEE INFOCOM*, pp. 2054–2062, 2007.
- [102] C. Cetinkaya and F. Orsun, “Cooperative medium access protocol for dense wireless networks,” in *The Third Annual Mediterranean Ad Hoc Networking Workshop - Med Hoc Net*, 2004.
- [103] F. P. Kelly, “Stochastic models of computer communication systems,” *Journal of the Royal Statistical Society. Series B (Methodological)*, vol. 47, pp. 379–395, 1985.
- [104] J. van den Berg and J. E. Steif, “Percolation and the hard-core lattice gas model,” *Stochastic Processes and their Applications*, vol. 49, no. 2, pp. 179 – 197, 1994.
- [105] H.-O. Georgii, *Gibbs Measures and Phase Transitions*. Walter de Gruyter & Co, 1988.
- [106] R. L. Dobrushin, “The problem of uniqueness of a Gibbsian random field and the problem of phase transitions,” *Functional Analysis and Its Applications*, vol. 2, pp. 302–312, 1968.
- [107] N. Bhatnagar, A. Sly, and P. Tetali, “Reconstruction threshold for the hard-core model,” in *Approximation, Randomization, and Combinatorial Optimization. Algorithms and Techniques* (M. Serna, R. Shaltiel, K. Jansen, and J. Rolim, eds.), vol. 6302 of *Lecture Notes in Computer Science*, pp. 434–447, Springer Berlin / Heidelberg, 2010.

- [108] R. Restrepo, D. Stefankovic, J. C. Vera, E. Vigoda, and L. Yang, “Phase transition for Glauber dynamics for independent sets on regular trees,” in *22nd Annual ACM-SIAM Symposium on Discrete Algorithms*, pp. 945–956, 2011.
- [109] S.-Y. Yun, Y. Yi, J. Shin, and D. Y. Eun, “Optimal CSMA: A survey,” in *IEEE International Conference on Communication Systems (ICCS)*, pp. 199–204, Nov. 2012.
- [110] L. Jiang and J. Walrand, “A distributed CSMA algorithm for throughput and utility maximization in wireless networks,” *IEEE/ACM Transactions on Networking*, vol. 18, pp. 960–972, June 2010.
- [111] F. P. Kelly, “Loss networks,” *The Annals of Applied Probability*, vol. 1, no. 3, pp. 319–378, 1991.